Multiwavelength and Multimessenger emission from Active Galactic Nuclei

Contents

1 Topics

- High energy gamma-rays from active galactic nuclei
- High energy neutrinos from blazars
- High energy emission from gamma-ray bursts

1.1 ICRANet participants

- Sahakyan Narek
- Gasparyan Sargis

1.2 Students

- Harutyunyan Gevorg
- Israyelyan Davit
- Khachatryan Mher
- Mari Harutyunyan
- Vazgen Vardanyan

1.3 Ongoing collaborations

- Razmik Mirzoyan (Max Planck Institute for Physics, Munich, Germany)
- Paolo Giommi (ASI Science Data Center)
- Damien Begue (Bar Ilan University, Israel)

- Ulisses Barres de Almeida (Centro Brasileiro de Pesquisas Fisicas - CBPF/MCT)
- Bernardo Fraga (Centro Brasileiro de Pesquisas Fisicas - CBPF)
- Karlica Mile (Nova Gorica)

2 Brief description

The main scientific activities of our group are in the field of X- and gamma-ray Astrophysics and Astroparticle physics. The results from the data analysis of Swift UVOT/XRT, NuStar, Chandra and Fermi LAT telescopes are used to investigate the particle acceleration and emission processes in the different classes of active galactic nuclei. The analysis of available data allows to investigate the emission processes and relativistic outflows in the most extreme regimes (keV-TeV).
Below we present several abstracts from the papers published in 2021, also with MAGIC collaboration.

- The strange case of the transient HBL blazar 4FGL J1544.3-0649

We present a multifrequency study of the transient γ-ray source 4FGL J1544.3-0649, a blazar that exhibited a remarkable behaviour raising from the state of an anonymous mid-intensity radio source, never detected at high energies, to that of one of the brightest extreme blazars in the X-ray and γ-ray sky. Our analysis shows that the averaged γ-ray spectrum is well described by a powerlaw with a photon index of 1.87 ± 0.04, while the flux above 100 MeV is $(8.0 \pm 0.9) \times 10^{-9}\, photon\, cm^{-2}\, s^{-1}$, which increases during the active state of the source. The X-ray flux and spectral slope are both highly variable, with the highest 2-10 keV flux reaching $(1.28 \pm 0.05) \times 10^{-10}\, erg\, cm^{-2}\, s^{-1}$. On several observations the X-ray spectrum hardened to the point implying as SED peak moving to energies larger than 10 keV. As in many extreme blazars the broadband spectral energy distribution can be described by a homogeneous one-zone synchrotron-self-Compton leptonic model. We briefly discuss the potential implications for high-energy multi-messenger astrophysics in case the dual behaviour shown by 4FGL J1544.3-0649 does not represent an isolated case, but rather a manifestation of a so far unnoticed relatively common phenomenon.

- Modelling the broad-band emission of 3C 454.3

The results of a long-term multiwavelength study of the powerful flat spectrum radio quasar 3C 454.3 using Fermi-LAT and Swift XRT/UVOT data are reported. In the γ-ray band, Fermi-LAT observations show several major flares when the source flux was $> 10^{-5}\ photon\ cm^{-2}\ s^{-1}$; the peak γ-ray flux above 141.6 MeV, $(9.22 \pm 1.96) \times 10^{-5}\ photon\ cm^{-2}\ s^{-1}$ observed on MJD 55519.33, corresponds to $2.15 \times 10^{50}\ erg\ s^{-1}$ isotropic γ-ray luminosity. The analysis of Swift XRT and UVOT data revealed a flux increase, although with smaller amplitudes, also in the X-ray and optical/UV bands. The X-ray emission of 3C 454.3 is with a hard spectral index of $\Gamma_X = 1.16 - 1.75$, and the flux in the flaring states increased up to $(1.80 \pm 0.18) \times 10^{-10} erg\ cm^{-2}\ s^{-1}$. Through combining the analyzed data, it was possible to assemble 362 high-quality and quasi-simultaneous spectral energy distributions of 3C 454.3 in 2008-2018 which all were modeled within a one-zone leptonic scenario assuming the emission region is within the broad line region, involving synchrotron, synchrotron self-Compton and external Compton mechanisms. Such an extensive modeling is the key for constraining the underlying emission mechanisms in the 3C 454.3 jet and allows to derive the physical parameters of the jet and investigate their evolution in time. The modeling suggests that during the flares, along with the variation of emitting electron parameters, the Doppler boosting factor increased substantially implying that the emission in these periods has most likely originated in a faster moving region.

- X-ray spectra, light curves and SEDs of blazars frequently observed by Swift

Blazars research is one of the hot topics of contemporary extragalactic astrophysics. That is because these sources are the most abundant type of extragalactic γ-ray, sources and are suspected to play a central role in multi-messenger astrophysics. We have used swift_xrtproc, a tool to carry out an accurate spectral and photometric analysis of the Swift-XRT data of all blazars observed by Swift at least 50 times between December 2004 and the end of 2020. We present a database of X-ray spectra, best-fit parameter values, count-rates and flux estimations in several energy bands of over 31,000 X-ray observations and single snapshots of 65 blazars. The results of the X-ray analysis have been combined with other multi-frequency archival data to assemble the broad-band Spectral Energy Distributions (SEDs) and the long-term lightcurves of all sources in the sample. Our study shows that large X-ray luminosity variability on different timescales is present in all objects. Spectral changes are also frequently observed with a "harder-when-brighter" or

"softer-when-brighter" behaviour depending on the SED type of the blazars. The peak energy of the synchrotron component (ν_{peak}) in the SED of HBL blazars, estimated from the log-parabolic shape of their X-ray spectra, also exhibits very large changes in the same source, spanning a range of over two orders of magnitude in Mrk421 and Mrk501, the objects with the best data sets in our sample.

- Investigation of the correlation patterns and the Compton dominance variability of Mrk 421 in 2017

A detailed characterisation and theoretical interpretation of the broadband emission of the paradigmatic TeV blazar Mrk 421, with special focus on the multi-band flux correlations. The dataset has been collected through an extensive multiwavelength campaign organised between 2016 December and 2017 June. The instruments involved are MAGIC, FACT, *Fermi*-LAT, *Swift*, GASP-WEBT, OVRO, Medicina and Metsähovi. Additionally, four deep exposures (several hours long) with simultaneous MAGIC and *NuSTAR* observations allowed a precise measurement of the falling segments of the two spectral components. The very-high-energy (VHE; $E > 100\,\mathrm{GeV}$) gamma rays and X-rays are positively correlated at zero time lag, but the strength and characteristics of the correlation change substantially across the various energy bands probed. The VHE versus X-ray fluxes follow different patterns, partly due to substantial changes in the Compton dominance during a few days without a simultaneous increase in the X-ray flux (i.e. orphan gamma-ray activity). Studying the broadband spectral energy distribution (SED) during the days including *NuSTAR* observations, we show that these changes can be explained within a one-zone leptonic model with a blob that increases its size over time. The peak frequency of the synchrotron bump varies by 2 orders of magnitude throughout the campaign. Our multi-band correlation study also hints at an anti-correlation between UV/optical and X-ray at a significance higher than 3σ. A VHE flare observed on MJD 57788 (2017 February 4) shows gamma-ray variability on multi-hour timescales, with a factor 10 increase in the TeV flux but only a moderate increase in the keV flux. The related broadband SED is better described by a two-zone leptonic scenario rather than by a one-zone scenario. We find that the flare can be produced by the appearance of a compact second blob populated by high energetic electrons spanning a narrow range of Lorentz factors, from $\gamma'_{min} = 2 \times 10^4$ to $\gamma'_{max} = 6 \times 10^5$.

- First detection of VHE gamma-ray emission from TXS 1515–273, study of its X-ray variability and spectral energy distribution

We report here on the first multi-wavelength (MWL) campaign on the blazar 3C 454.3, undertaken in 2019 and extending from radio to very-high-energy gamma rays (VHE). Up until now, this blazar had not been the subject of any detailed MWL observations. It has a rather hard photon index at GeV energies and was considered a candidate extreme high-synchrotron-peaked source. MAGIC observations resulted in the first-time detection of the source in VHE with a statistical significance of 7.6σ. The average integral VHE flux of the source is $6 \pm 1\%$ of the Crab nebula flux above 400 GeV. X-ray coverage was provided by *Swift*-XRT, , and . The long continuous X-ray observations were separated by $\sim$9 h, both showing clear hour scale flares. In the data, both the rise and decay timescales are longer in the soft X-ray than in the hard X-ray band, indicating the presence of a particle cooling regime. The X-ray variability timescales were used to constrain the size of the emission region and the strength of the magnetic field. The data allowed us to determine the synchrotron peak frequency and classify the source as a flaring high, but not extreme, synchrotron peaked object. Considering the constraints and variability patterns from the X-ray data, we model the broad-band spectral energy distribution. We applied a simple one-zone model, which could not reproduce the radio emission and the shape of the optical emission, and a two-component leptonic model with two interacting components, enabling us to reproduce the emission from radio to VHE band.

- Multiwavelength variability and correlation studies of Mrk 421 during historically low X-ray and -ray activity in 20152016

We report a characterization of the multi-band flux variability and correlations of the nearby (z=0.031) blazar Markarian 421 (Mrk 421) using data from Metsähovi, Swift, Fermi-LAT, MAGIC, FACT and other collaborations and instruments from November 2014 till June 2016. Mrk 421 did not show any prominent flaring activity, but exhibited periods of historically low activity above 1 TeV ($F_{>1\mathrm{TeV}} < 1.7\times10^{-12}\,\mathrm{ph\,cm^{-2}\,s^{-1}}$) and in the 2-10 keV (X-ray) band ($F_{2-10\,\mathrm{keV}} < 3.6\times10^{-11}\,\mathrm{erg\,cm^{-2}\,s^{-1}}$), during which the Swift-BAT data suggests an additional spectral component beyond the regular synchrotron emission.The highest flux variability occurs in X-rays and very-high-energy

(E>0.1 TeV) γ-rays, which, despite the low activity, show a significant positive correlation with no time lag. The HR_{keV} and HR_{TeV} show the *harder-when-brighter* trend observed in many blazars, but the trend flattens at the highest fluxes, which suggests a change in the processes dominating the blazar variability. Enlarging our data set with data from years 2007 to 2014, we measured a positive correlation between the optical and the GeV emission over a range of about 60 days centered at time lag zero, and a positive correlation between the optical/GeV and the radio emission over a range of about 60 days centered at a time lag of 43^{+9}_{-6} days.This observation is consistent with the radio-bright zone being located about 0.2 parsec downstream from the optical/GeV emission regions of the jet. The flux distributions are better described with a LogNormal function in most of the energy bands probed, indicating that the variability in Mrk 421 is likely produced by a multiplicative process.

- VHE gamma-ray detection of FSRQ QSO B1420+326 and modeling of its enhanced broadband state in 2020

QSO B1420+326 is a blazar classified as a Flat Spectrum Radio Quasar (FSRQ). In the beginning of 2020 it underwent an enhanced flux state. An extensive multiwavelength campaign allowed us to trace the evolution of the flare. We search for VHE gamma-ray emission from QSO B1420+326 during this flaring state. We aim to characterize and model the broadband emission of the source over different phases of the flare. The source was observed with a number of instruments in radio, near infrared, optical (including polarimetry and spectroscopy), ultraviolet, X-ray and gamma-ray bands. We use dedicated optical spectroscopy results to estimate the accretion disk and the dust torus luminosity. We perform spectral energy distribution modeling in the framework of combined Synchrotron-Self-Compton and External Compton scenario in which the electron energy distribution is partially determined from acceleration and cooling processes. During the enhanced state the flux of both SED components drastically increased and the peaks were shifted to higher energies. Follow up observations with the MAGIC telescopes led to the detection of very-high-energy gamma-ray emission from this source, making it one of only a handful of FSRQs known in this energy range. Modeling allows us to constrain the evolution of the magnetic field and electron energy distribution in the emission region. The gamma-ray flare was accompanied by a rotation of the optical polarization vector during a low polarization state. Also, a new,

superluminal radio knot contemporaneously appeared in the radio image of the jet. The optical spectroscopy shows a prominent FeII bump with flux evolving together with the continuum emission and a MgII line with varying equivalent width.

- Observation of the gamma-ray binary HESS J0632+057 with the H.E.S.S., MAGIC, and VERITAS telescopes

The results of gamma-ray observations of the binary system collected during 450 hours over 15 years, between 2004 and 2019, are presented. Data taken with the atmospheric Cherenkov telescopes H.E.S.S., MAGIC, and VERITAS at energies above 350 GeV were used together with observations at X-ray energies obtained with *Swift*-XRT, Chandra, *XMM*-Newton, NuSTAR, and Suzaku. Some of these observations were accompanied by measurements of the Hα emission line. A significant detection of the modulation of the VHE gamma-ray fluxes with a period of 316.7 ± 4.4 days is reported, consistent with the period of 317.3 ± 0.7 days obtained with a refined analysis of X-ray data. The analysis of data of four orbital cycles with dense observational coverage reveals short timescale variability, with flux-decay timescales of less than 20 days at very high energies. Flux variations observed over the time scale of several years indicate orbit-to-orbit variability. The analysis confirms the previously reported correlation of X-ray and gamma-ray emission from the system at very high significance, but can not find any correlation of optical Hα parameters with X-ray or gamma-ray energy fluxes in simultaneous observations. The key finding is that the emission of in the X-ray and gamma-ray energy bands is highly variable on different time scales. The ratio of gamma-ray to X-ray flux shows the equality or even dominance of the gamma-ray energy range. This wealth of new data is interpreted taking into account the insufficient knowledge of the ephemeris of the system, and discussed in the context of results reported on other gamma-ray binary systems.

3 Publications-2020

- Sahakyan, N., Modelling the broad-band emission of 3C 454.3, Monthly Notices of the Royal Astronomical Society, Volume 504, Issue 4, 2021, pp.5074-5086.
- Sahakyan, N. and Giommi, P., The strange case of the transient HBL blazar 4FGL J1544.3-0649, Monthly Notices of the Royal Astronomical Society, Volume 502, Issue 1, 2021, pp.836-844.
- Giommi, P.....sahakyan, N....., X-ray spectra, light curves and SEDs of blazars frequently observed by Swift, Monthly Notices of the Royal Astronomical Society, Volume 507, Issue 4, 2021, pp.5690-5702.
- Ruffini, R..... Sahakyan, N....., The morphology of the X-ray afterglows and of the jetted GeV emission in long GRBs, Monthly Notices of the Royal Astronomical Society, Volume 504, Issue 4, 2021, pp.5301-5326.
- MAGIC Collaboration, Adams, C.....Sahakyan, N....., Observation of the Gamma-Ray Binary HESS J0632+057 with the H.E.S.S., MAGIC, and VERITAS Telescopes, The Astrophysical Journal, Volume 923, Issue 2, id.241, 2021, 30 pp.
- MAGIC Collaboration, Acciari V., Ansoldi S.,.... Gasparyan, S.,...Sahakyan N.,.... Search for Very High-energy Emission from the Millisecond Pulsar PSR J0218+4232, The Astrophysical Journal, Volume 922, Issue 2, id.251, 2021, 14 pp.
- MAGIC Collaboration, Acciari V., Ansoldi S.,.... Gasparyan, S.,...Sahakyan N.,.... Investigation of the correlation patterns and the Compton dominance variability of Mrk 421 in 2017, Astronomy Astrophysics, Volume 655, id.A89, 2021, 36 pp.
- MAGIC Collaboration, Acciari V., Ansoldi S.,.... Gasparyan, S.,...Sahakyan N.,.... First detection of VHE gamma-ray emission from TXS 1515-273,

study of its X-ray variability and spectral energy distribution, Monthly Notices of the Royal Astronomical Society, Volume 507, Issue 1, 2021, pp.1528-1545.

- MAGIC Collaboration, Acciari V., Ansoldi S.,.... Gasparyan, S.,...Sahakyan N.,.... Multiwavelength variability and correlation studies of Mrk 421 during historically low X-ray and -ray activity in 2015-2016, Monthly Notices of the Royal Astronomical Society, Volume 504, Issue 1, 2021, pp.1427-1451.

- MAGIC Collaboration, Algaba J., Anczarski J.,.... Gasparyan, S.,...Sahakyan N.,.... Broadband Multi-wavelength Properties of M87 during the 2017 Event Horizon Telescope Campaign, The Astrophysical Journal Letters, Volume 911, Issue 1, id.L11, 2021, 43 pp.

- Abdalla H., Adam R.,.... Gasparyan, S.,...Sahakyan N.,.... H.E.S.S. and MAGIC observations of a sudden cessation of a very-high-energy -ray flare in PKS 1510089 in May 2016, Astronomy Astrophysics, Volume 648, id.A23, 2021, 22 pp.

- MAGIC Collaboration, Acciari V., Ansoldi S.,.... Gasparyan, S.,...Sahakyan N.,...., VHE gamma-ray detection of FSRQ QSO B1420+326 and modeling of its enhanced broadband state in 2020, Astronomy Astrophysics, Volume 647, id.A163, 2021, 19 pp.

- MAGIC Collaboration, Acciari V., Ansoldi S.,.... Gasparyan, S.,...Sahakyan N.,...., MAGIC Observations of the Nearby Short Gamma-Ray Burst GRB 160821B, The Astrophysical Journal, Volume 908, Issue 1, id.90, 2021, 11 pp.

3.1 Publications-2012-2020

- Sahakyan N., Israyelyan D., Harutyunyan G., Khachatryan M., Gasparyan S., Multiwavelength study of high-redshift blazars, Monthly Notices of the Royal Astronomical Society, olume 498, Issue 2, 2020, p.2594-2613.

- Sahakyan N., Broad-band study of high-synchrotron-peaked BL Lac object 1ES 1218+304, Monthly Notices of the Royal Astronomical Society, Volume 496, Issue 4, 2020, pp.5518-5527

- Sahakyan, N., Investigation of the -ray spectrum of CTA 102 during the exceptional flaring state in 2016-2017, Astronomy and Astrophysics, Volume 635, id.A25, 2020, 10 pp.

- Sahakyan N., Israyelyan D., Harutyunyan G., A Multiwavelength Study of Distant Blazar PKS 0537-286, Astrophysics, volume 63, 2020, p. 459–469

- Sahakyan N., Harutyunyan G., Israelyan D., Khachatryan M., Exploring the Origin of Multiwavelength Emission from High-Redshift Blazar B3 1343 + 451, Astrophysics, Volume 63, Issue 3, 2020, p.334-348

- Giommi P., Chang Y., Turriziani S., Glauch T., Leto C., Verrecchia F., Padovani P., Penacchioni A., Arneodo F., Barres de Almeida U., Brandt C., Capalbi M., Civitarese O., D; Elia V., Di Giovanni A., De Angelis M., Del Rio Vera J., Di Pippo S., Middei R., Perri M., Pollock A., Puccetti S., Ricard N., Ruffini R., Sahakyan N., Open Universe survey of Swift-XRT GRB fields: Flux-limited sample of HBL blazars, Astronomy and Astrophysics, Volume 642, id.A141, 2020, 9 pp.

- Sahakyan N., High Energy -ray variability of NGC 1275 and 3C 120, Proceedings of the International Astronomical Union, Volume 342, 2020, pp. 172-175

- MAGIC Collaboration, VERITAS Collaboration, Abeysekara, A., Benbow, W.,.... Gasparyan, S.,...Sahakyan N.,.... Villata, M., The Great Markarian 421 Flare of 2010 February: Multiwavelength Variability and Correlation Studies, The Astrophysical Journal, Volume 890, Issue 2, id.97, 2020, 21 pp.

- MAGIC Collaboration, Acciari V., Ansoldi S.,.... Gasparyan, S.,...Sahakyan N.,.... Lien, A., Multiwavelength variability and correlation studies of Mrk 421 during historically low X-ray and -ray activity in 2015-2016, Monthly Notices of the Royal Astronomical Society, DOI: 10.1093/mnras/staa3727

- MAGIC Collaboration, Acciari V., Ansoldi S.,.... Gasparyan, S.,...Sahakyan N.,.... Zarić, D., The Great Markarian 421 Flare of 2010 February: Multi-wavelength Variability and Correlation Studies, Astronomy and Astrophysics, Volume 635, id.A158, 2020, 10 pp.

- MAGIC Collaboration, Acciari V., Ansoldi S.,.... Gasparyan, S.,...Sahakyan N.,.... Lohfink A., New Hard-TeV Extreme Blazars Detected with the MAGIC Telescopes, The Astrophysical Journal Supplement Series, Volume 247, Issue 1, id.16, 2020, 24 p.

- MAGIC Collaboration, Acciari V., Ansoldi S.,.... Gasparyan, S.,...Sahakyan N.,.... Walker R., Monitoring of the radio galaxy M 87 during a low-emission state from 2012 to 2015 with MAGIC, Monthly Notices of the Royal Astronomical Society, Volume 492, Issue 4, 2020, p.5354-5365

- MAGIC Collaboration, Acciari V., Ansoldi S.,.... Gasparyan, S.,...Sahakyan N.,.... Tammi J., Study of the variable broadband emission of Markarian 501 during the most extreme Swift X-ray activity, Astronomy and Astrophysics, Volume 637, id.A86, 2020, 27 pp.

- MAGIC Collaboration, Acciari V., Ansoldi S.,.... Gasparyan, S.,...Sahakyan N.,.... Zarić, D., A search for dark matter in Triangulum II with the MAGIC telescopes, Physics of the Dark Universe, Volume 28, article id. 100529, 2020.

- MAGIC Collaboration, Acciari V., Ansoldi S.,.... Gasparyan, S.,...Sahakyan N.,.... Zarić, D., Broadband characterisation of the very intense TeV flares of the blazar 1ES 1959+650 in 2016, Astronomy and Astrophysics, Volume 638, id.A14, 2020, 16 pp.

- MAGIC Collaboration, Acciari V., Ansoldi S.,.... Gasparyan, S.,...Sahakyan N.,.... Reinthal R., Unraveling the Complex Behavior of Mrk 421 with Simultaneous X-Ray and VHE Observations during an Extreme Flaring Activity in 2013 April, The Astrophysical Journal Supplement Series, Volume 248, Issue 2, 2020, id.29

- MAGIC Collaboration, Acciari V., Ansoldi S.,.... Gasparyan, S.,...Sahakyan N.,.... Zheng W., An intermittent extreme BL Lac: MWL study of 1ES 2344+514 in an enhanced state, Monthly Notices of the Royal Astronomical Society, Volume 496, Issue 3, 2020, pp.3912-3928

- MAGIC Collaboration, Acciari V., Ansoldi S.,.... Gasparyan, S.,...Sahakyan N.,.... Zarić, D., Studying the nature of the unidentified gamma-ray source HESS J1841-055 with the MAGIC telescopes, Monthly Notices of the Royal Astronomical Society, Volume 497, Issue 3, 2020, p. 3734-3745

- MAGIC Collaboration, Acciari V., Ansoldi S.,.... Gasparyan, S.,...Sahakyan N.,.... Zarić, D., Bounds on Lorentz Invariance Violation from MAGIC Observation of GRB 190114C, Physical Review Letters, Volume 125, Issue 2, 2020, article id.021301

- MAGIC Collaboration, Acciari V., Ansoldi S.,.... Gasparyan, S.,...Sahakyan N.,.... Kehusmaa P., Testing two-component models on very high-energy gamma-ray-emitting BL Lac objects, Astronomy and Astrophysics, Volume 640, id.A132, 2020, 29 pp.

- MAGIC Collaboration, Acciari V., Ansoldi S.,.... Gasparyan, S.,...Sahakyan N.,.... Zarić, D., MAGIC observations of the diffuse -ray emission in the vicinity of the Galactic center, Astronomy and Astrophysics, Volume 642, id.A190, 2020, 9 pp.

- MAGIC Collaboration, Acciari V., Ansoldi S.,.... Gasparyan, S.,...Sahakyan N.,.... Parkinson P., Detection of the Geminga pulsar with MAGIC hints at a power-law tail emission beyond 15 GeV, Astronomy and Astrophysics, Volume 643, id.L14, 2020, 6 p.

- V. Acciari,.....S. Gasparyan...N. Sahakyan, ... D. Zaric, "Testing emission models on the extreme blazar 2WHSP J073326.7+515354 detected at very high energies with the MAGIC telescopes", Monthly Notices of the Royal Astronomical Society, Volume 490, Issue 2, p.2284-2299, 2019.

- R. Ruffini, R. Moradi, J. Rueda, L. Becerra, C. Bianco, C. Cherubini, S. Filippi, Y. Chen, M. Karlica, N. Sahakyan, Y. Wang, S. Xue, "On the GeV Emission of the Type I BdHN GRB 130427A", The Astrophysical Journal, Volume 886, Issue 2, article id. 82, 13 pp., 2019.

- V. Acciari,.....S. Gasparyan...N. Sahakyan, ... D. Zaric, "Observation of inverse Compton emission from a long γ-ray burst", Nature, Volume 575, Issue 7783, p.459-463, 2019.

- V. Acciari,.....S. Gasparyan...N. Sahakyan, ... D. Zaric, "Teraelectronvolt emission from the -ray burst GRB 190114C", Nature, Volume 575, Issue 7783, p.455-458, 2019.
- N. Sahakyan, "Origin of the multiwavelength emission of PKS 0502+049", accepted for publication in Astronomy and Astrophysics, doi.org/10.1051/0004-6361/201936715, arXiv:1911.12087, 2019.
- V. Acciari,.....S. Gasparyan...N. Sahakyan, ... D. Zaric, "New hard-TeV extreme blazars detected with the MAGIC telescopes", accepted for publication in Astrophysical Journal Supplement, arXiv:1911.06680, 2019.
- P. Giommi, C. Brandt, U. Barres de Almeida, A. Pollock, F. Arneodo, Y. Chang, O. Civitarese, M. Angelis, V. DElia, J. Del Rio Vera, S. Di Pippo, R. Middei, A. Penacchioni, M. Perri, R. Ruffini, N. Sahakyan, S. Turriziani, "Open Universe for Blazars: a new generation of astronomical products based on 14 years of Swift-XRT data", Astronomy and Astrophysics, Volume 631, id.A116, 11 pp., 2019.
- T. Glauch, P. Padovani, P. Giommi, E. Resconi, B. Arsioli, N. Sahakyan, M. Huber, "Dissecting the region around IceCube-170922A: the blazar TXS 0506+056 as the first cosmic neutrino source", EPJ Web of Conferences, Volume 207, id.02003, 2019.
- V. Acciari,.....S. Gasparyan...N. Sahakyan, ... D. Zaric, "Constraints on Gamma-Ray and Neutrino Emission from NGC 1068 with the MAGIC Telescopes", The Astrophysical Journal, Volume 883, Issue 2, article id. 135, 9 pp., 2019.
- V. Acciari,.....S. Gasparyan...N. Sahakyan, ... D. Zaric, "Measurement of the extragalactic background light using MAGIC and Fermi-LAT gamma-ray observations of blazars up to z = 1", Monthly Notices of the Royal Astronomical Society, Volume 486, Issue 3, p.4233-4251, 2019.
- V. Acciari,.....S. Gasparyan...N. Sahakyan, ... D. Zaric, "Deep observations of the globular cluster M15 with the MAGIC telescopes", Monthly Notices of the Royal Astronomical Society, Volume 484, Issue 2, p.2876-2885, 2019.
- J. Rueda, R. Ruffini, Y. Wang, C. Bianco, J. Blanco-Iglesias, M. Karlica, P. Loren-Aguilar, R. Moradi, N. Sahakyan, "Electromagnetic emission of

white dwarf binary mergers", Journal of Cosmology and Astroparticle Physics, Issue 03, article id. 044, 2019.

- N. Sahakyan, "Origin of the multiwavelength emission of PKS 0502+049", Astronomy and Astrophysics, Volume 622, id.A144, 10 pp. 2019.

- R. Ruffini, M. Karlica, N. Sahakyan, J. Rueda, Y. Wang, G. Mathews, C. Bianco, M. Muccino, "A GRB Afterglow Model Consistent with Hypernova Observations", The Astrophysical Journal, Volume 869, Issue 2, article id. 101, 9 pp. 2018.

- A. Abeysekara, ... N. Sahakyan, ... D. Zaric, "Periastron Observations of TeV Gamma-Ray Emission from a Binary System with a 50-year Period", The Astrophysical Journal Letters, Volume 867, Issue 1, article id. L19, 8 pp., 2018.

- P. Padovani, P. Giommi, E. Resconi, T. Glauch, B. Arsioli, N. Sahakyan, M. Huber, "Dissecting the region around IceCube-170922A: the blazar TXS 0506+056 as the first cosmic neutrino source", Monthly Notices of the Royal Astronomical Society, Volume 480, Issue 1, p.192-203, 2018.

- N. Sahakyan, "Lepto-hadronic γ-Ray and Neutrino Emission from the Jet of TXS 0506+056", The Astrophysical Journal, Volume 866, Issue 2, article id. 109, 6 pp. 2018.

- S. Gasparyan, N. Sahakyan, V. Baghmanyan, D. Zargaryan, "On the Multiwavelength Emission from CTA 102", The Astrophysical Journal, Volume 863, Issue 2, article id. 114, 11 pp., 2018.

- M. Aartsen, ... N. Sahakyan, ... T. Yuan, "Neutrino emission from the direction of the blazar TXS 0506+056 prior to the IceCube-170922A alert", Science, Volume 361, Issue 6398, pp. 147-151, 2018.

- V. Baghmanyan, M. Tumanyan, N. Sahakyan, Y. Vardanyan, "High-Energy γ -Ray Emission from PKS 0625-35", Astrophysics, Volume 61, Issue 2, pp.160-170, 2018.

- N. Sahakyan, V. Baghmanyan, D. Zargaryan, "Fermi-LAT observation of nonblazar AGNs", Astronomy & Astrophysics, Volume 614, id.A6, 11 pp., 2018.

- B. Fraga, U. Barres de Almeida, S. Gasparyan, P. Giommi, N. Sahakyan, "Time-Evolving SED of MKN421: a multi-band view and polarimetric signatures", Frontiers in Astronomy and Space Sciences, Volume 5, id.1, 2018.
- S. Gasparyan, N. Sahakyan, P. Chardonnet, "The origin of HE and VHE gamma-ray flares from FSRQs", International Journal of Modern Physics D, Volume 27, Issue 10, id. 1844007, 2018.
- D. Zargaryan, N. Sahakyan, H. Harutyunian, "Chandra observations of gamma-ray emitting radio galaxies", International Journal of Modern Physics D, Volume 27, Issue 10, id. 1844022, 2018.
- V. Baghmanyan, N. Sahakyan, "X-ray and γ-ray emissions from NLSy1 galaxies", International Journal of Modern Physics D, Volume 27, Issue 10, id. 1844001, 2018.
- D. Zargaryan, S. Gasparyan, V. Baghmanyan and N. Sahakyan, "Comparing 3C 120 jet emission at small and large scales", Astronomy & Astrophysics, Volume 608, id. A37, 10, 2017.
- U. Barres de Almeida, F. Bernardo, P. Giommi, N. Sahakyan, S. Gasparyann and C. Brandt, "Long-Term Multi-Band and Polarimetric View of Mkn 421: Motivations for an Integrated Open-Data Platform for Blazar Optical Polarimetry", Galaxies, vol. 5, issue 4, p. 90, 2017.
- V. Baghmanyan, S. Gasparyan and N. Sahakyan, "Rapid Gamma-Ray Variability of NGC 1275", The Astrophysical Journal, Volume 848, Issue 2, article id. 111, 8, 2017.
- N. Sahakyan and S. Gasparyan "High energy gamma-ray emission from PKS 1441+25", Monthly Notices of the Royal Astronomical Society, 470, 3, p.2861-2869, 2017.
- N. Sahakyan, V. Baghmanyan, and D. Zargaryan, "Gamma-ray Emission from Non-Blazar AGNs", AIP Conference Proceedings, Volume 1792, Issue 1, id.050002, 2017.
- N. Sahakyan and S. Gasparyan, "High Energy Gamma-Rays From PKS 1441+25", AIP Conference Proceedings, Volume 1792, Issue 1, id.050005, 2017.

- V. Baghmanyan, "Gamma-Ray Variability of NGC 1275", AIP Conference Proceedings, Volume 1792, Issue 1, id.050007, 2017.

- D. Zargaryan, "The Gamma-Ray Emission from Broad-Line Radio Galaxy 3C 120",AIP Conference Proceedings, Volume 1792, Issue 1, id.050008, 2017.

- N. Sahakyan, "Galactic sources of high energy neutrinos: Expectation from gamma-ray data", EPJ Web of Conferences, Volume 121, id.05005, 2016.

- Sahakyan, N., Zargaryan, D. and Baghmanyan, V. "On the gamma-ray emission from 3C 120", Astronomy & Astrophysics, Volume 574, id.A88, 5 pp., 2015.

- Sahakyan, N., Yang, R., Rieger, F., Aharonian, F. and de Ona-Wilhelmi, E. "High Energy Gamma Rays from Centaurus a" Proceedings of the MG13 Meeting on General Relativity ISBN 9789814623995, pp. 1028-1030, 2015.

- Sahakyan, N., Piano, G. and Tavani, M. "Hadronic Gamma-Ray and Neutrino Emission from Cygnus X-3", The Astrophysical Journal, Volume 780, Issue 1, article id. 29, 2014.

- Sahakyan, N., Rieger, F., Aharonian, F., Yang, R., and de Ona-Wilhelmi, E. "On the gamma-ray emission from the core and radio lobes of the radio galaxy Centaurus A", International Journal of Modern Physics: Conference Series, Volume 28, id. 1460182, 2014.

- Sahakyan, N., Yang, R. Aharonian, F. and Rieger, F., " Evidence for a Second Component in the High-energy Core Emission from Centaurus A?", The Astrophysical Journal Letters, Volume 770, Issue 1, L6, 2013.

- Yang, R.-Z., Sahakyan, N., de Ona Wilhelmi, E., Aharonian, F. and Rieger, F., "Deep observation of the giant radio lobes of Centaurus A with the Fermi Large Area Telescope", Astronomy & Astrophysics, 542, A19, 2012.

- Sahakyan, N., "High energy gamma-radiation from the core of radio galaxy Centaurus A", Astrophysics, 55, 14, 2012.

- Sahakyan, N., "On the Origin of High Energy Gamma-Rays from Giant Radio Lobes Centarus A", International Journal of Modern Physics Conference Series, 12, 224, 2012.

4 Modeling the Broadband Emission of 3C 454.3

4.1 Introduction

Blazars are a subclass of active galactic nuclei with a jet pointing or making a small angle with respect to the observer [144]. These jets are strong sources of electromagnetic radiation ranging from radio to high energy (HE; $>$ 100 MeV) and very high energy γ-ray bands (see **(author?)** 104 for a recent review). This emission is characterized by rapid and high-amplitude variability in almost all wavelengths, the most extreme being at γ-ray band [e.g., order of minutes, 9, 53, 52, 100, 31, 116, 130, 74, 135]. Blazars are dominant sources in the extragalactic γ-ray sky and have been observed even at very high redshifts [e.g., 7, 129]. The recent studies of 4FGL J1544.3-0649 reveal the possible existence of transient blazars; being undecteable in the X-ray and γ-ray bands, 4FGL J1544.3-0649 for a few months rose to be one of the brightest known X-ray blazars [128]. If 4FGL J1544.3-0649 does not indeed represent an isolated case but rather a common phenomenon, this would have a non-negligible role in the multimessenger astrophysics.

The broadband spectral energy distribution (SED) of blazars is characterized by two broad humps, one at optical/UV/X-ray bands and the other in the HE γ-ray band (see **(author?)** 104 for a recent review). It is believed that the first peak (low energy component) is mostly due to synchrotron emission from relativistic electrons, whereas the origin of the second component is highly debatable. Within conventional leptonic scenarios, this component is produced when the synchrotron emitting electrons inverse Compton up scatter the photons of internal [synchrotron self Compton (SSC) 58, 25, 90] or external [external inverse Compton (EIC) 24, 59, 136] origin. The nature of the external photon fields depends on the distance of the emitting region from the central black hole [137] and can be dominated either by the photons directly emitted from the accretion disk [47, 46] or disk photons reflected from

the broad-line region [BLR; 136] or IR photons emitted from the dusty torus [24]. Recently, after associating TXS 0506+056 with the IceCube-170922A neutrino event [76, 75, 105], it is more evident that the HE component could be initiated by the interaction of energetic protons when they are effectively accelerated in the blazar jets. The HE component can be either from proton synchrotron emission [97] or from secondary particles from pion decay [87, 88, 97, 98, 29]. In the latter case, blazars are also sources of very high energy neutrinos [16, 81, 99, 105, 122, 120, 37, 123, 54].

Based on the properties observed in the optical band, blazars are classified as Flat Spectrum Radio Quasars (FSRQs) when the emission lines are stronger and quasar-like or BL Lacs when these lines are weak or absent [144]. Alternatively, blazars are FSRQs when the luminosity of the broad emission lines (or accretion disk) measured in Eddington units is $L_{BLR}/L_{Edd} \geq 5 \times 10^{-4}$, otherwise they are BL Lacs [61, 132]. Depending on the position of the synchrotron component peak (ν_s), the blazars are further classified as low synchrotron peaked (LSP) sources, when $\nu_s < 10^{14}$ Hz, intermediate synchrotron peaked (ISP) and high synchrotron peaked (HSP) sources when $10^{14} < \nu_s < 10^{15}$ Hz and $\nu_s > 10^{15}$ Hz, respectively [107, 2]. However, sometimes the synchrotron peak of HSPs can reach $\sim$1 keV, ($\sim 2 \times 10^{17}$ Hz) or beyond, showing an extreme behaviour [e.g. 68, 43, 22]. Such behaviour was first observed during the flare of Mkn 501 when the synchrotron peak reached $\sim$ 100 keV [110], and then many such objects were identified in the X-ray observations. For example, during the flares of 1ES 1218+304 the X-ray spectral index hardened to $\Gamma \leq 1.80$, shifting the peak towards higher energies [124]. In this classification, FSRQs usually have a synchrotron peak at $\nu_s < 10^{14}$ Hz, so they are LSPs.

The BL Lac and FSRQ SEDs demonstrate different properties. In FSRQs, the strong external photon fields which are weak or absent in the case of BL Lacs, modify the HE component: these external photons are seen relativistically boosted in the comoving frame of the jet and can dominate over the internal synchrotron photon fields, giving rise to the EIC component [e.g., 55, 127]. Therefore, in FSRQs the luminosity of the second component is usually larger, i.e. shows a larger Compton dominance [136] due to the presence of external seed photons. The shape of this component depends on the distribution of up-scattering photons which in its turn is defined by the distance of the emitting region from the central black hole. So, the modeling of the SED or features in the γ-ray spectrum (e.g., break or cut-off) can help to localize the emission region [e.g., 112, 13, 125].

3C 454.3 is a typical FSRQ at $z = 0.859$ harboring a black hole with a mass estimated to be $1.5 \times 10^9\ M_\odot$ [152, 84]. This source was extensively studied in the multiwavelength band over the last two decades [e.g., 66]. However, after the prominent optical outburst in 2005 with a peak optical brightness of $R = 12$ mag, the source remained active showing several bright flares, it has become a target of multiwavelength studies [115, 114, 102, 3, 4, 8, 78, 14]. This multiwavelength campaigns provided unprecedented information on this source. For example, **(author?)** [26] studying the multiwavelength data observed during the high flux state in July 2008, showed that the emissions in IR, optical, UV, and γ-ray bands are well correlated while the X-ray flux is correlated with none of these fluxes. These features in the multiwavelength variability can be naturally explained within the EIC scenario. However, **(author?)** [27] found that the optical, X-ray and γ-ray fluxes correlate during the extreme brightening of 3C 454.3 in the first week of December 2009. In the γ-ray band the source was first detected by EGRET on the Compton Gamma-Ray Observatory [73] and then extensively monitored by AGILE and Fermi large area telescope (Fermi-LAT) since 2007. The AGILE observations have shown that the 3C 454.3 was in active γ-ray state in several occasions [50, 102, 148]. In 2010 during the exceptional bright γ-ray flare Fermi-LAT detected a flux above $\sim 10^{-5}\ photon\ cm^{-2}\ s^{-1}$ from 3C 454.3 which corresponds to $\sim 10^{50}\ erg\ s^{-1}$ isotropic luminosity, making 3C 454.3 one of the brightest γ-ray sources in the sky [3]. During the flaring of 3C 454.3, different extraordinary changes in terms of spectral and temporal properties were reported in the multiwavelength context and especially in the γ-ray band. For example, **(author?)** [4] found that the γ-ray spectrum of 3C 454.3 steepens above ~ 2 GeV and it is better explained by a broken power-law with photon indices of ~ 2.3 and ~ 3.5 below and above the break, respectively. This turnover in the spectrum was interpreted by the spectral break in the electron distribution; however, **(author?)** [51] interpreted the break to be due to the inverse Compton scattering of accretion disk and BLR photons.

In this paper, the evolution of the multiwavelength SED of 3C 454.3 during 2008-2018 as well as the spectral changes in different bands are investigated. These changes in the SED are expected to arise from the variation of the parameters of the emitting electrons or the physical parameters of the emission region [108], so, they directly define the physical processes taking place in the jet as well as the state of the plasma in it. For this reason, in the period from 2008 to 2018, as many SEDs of 3C 454.3 as possible that can be constructed with contemporaneous data from the radio to HE bands have been modeled

within a leptonic scenario. More explicitly, these SEDs are modeled assuming the low energy component is due to synchrotron emission whereas the second component is due to SSC and/or EIC by the same electrons. Through such modeling the jet parameters are estimated for different periods allowing to investigate their variation which could help to investigate the changes in the jet of 3C 454.3 as well as to understand the origin of the flares. 3C 454.3 was selected because of *i)* the availability of rich multiwavelength data (e.g., more than 465 observations with Neil Gehrels Swift Observatory (hereafter Swift) and continuous monitoring by Fermi-LAT) and *ii)* its large amplitude variability in almost all wavelengths.

In the current paper the origin of the multiwavelength emission from 3C 454.3 is investigated using the multiwavelength data accumulated during 2008-2018. The paper is structured as follows. Section 4.2 presents the multiwavelength data analyzed in the current study. The evolution of SED in time is presented in Section 4.3. The modeling of SEDs is presented in Section 4.4 and the discussions in Section 4.5. The conclusion is given in Section 4.6.

4.2 Multiwavelenth Observations

3C 454.3, being among the brightest γ-ray blazars, was frequently monitored in different energy bands. Here, the emission of 3C 454.3 in the optical/UV, X-ray and γ-ray bands is investigated using the data from Fermi-LAT, Swift UVOT and XRT telescopes.

4.2.1 Fermi-LAT data

Fermi-LAT on board the Fermi Gamma-ray Space Telescope is a pair-conversion telescope sensitive to γ-rays in the energy band from 20 MeV to 500 GeV. Scanning the entire sky every $\sim$ 3 hours, it provides the deepest view of the γ-ray sky [17].

In the current study, the publicly available Fermi-LAT data accumulated between August 4, 2008 and August 4, 2018 are used. The Pass 8 (P8R3) Fermi-LAT events in the energy range from 100 MeV to 500 GeV extracted from a 12° region of interest (ROI) around the γ-ray position of 3C 454.3 (RA = 343.497 and Dec = 16.149) have been analyzed using Fermi ScienceTools (1.2.1) and the P8R3_ SOURCE_ V2 instrument response functions (IRFs). With the help of gtselect tool the front and back events of type 3 and event

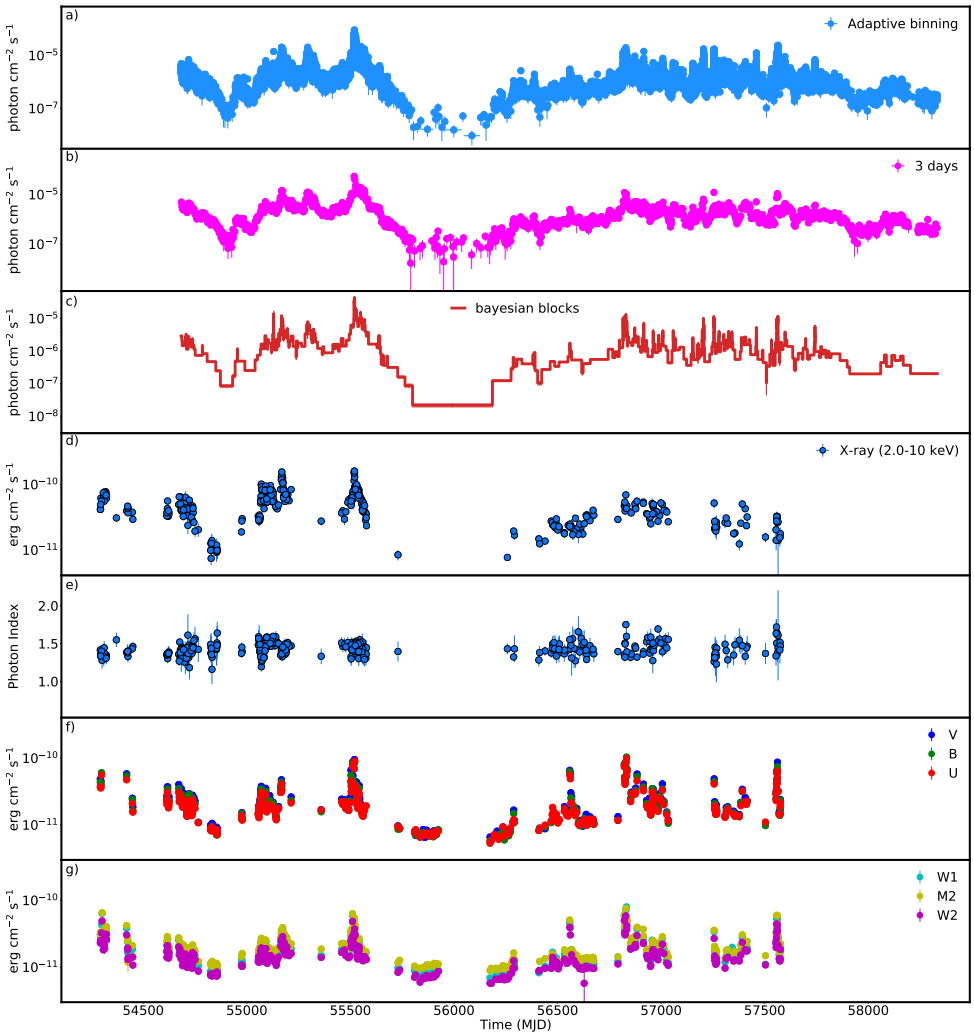

Figure 4.1 The multiwavelength light curve of 3C 454.3 between May 01, 2007 and August 04, 2018. From top to bottom: adaptively binned γ-ray light curve ($>$ 141.6 MeV), 3-day binned γ-ray light curve ($>$ 100 MeV), Bayesian block representation of the γ-ray light curve, 2.0-10 keV X-ray flux, 0.3-10.0 keV X-ray photon index, flux in V, B, and U filters and flux in W1, M2 and W2 filters.

class 128 coming from zenith angles smaller than 90°, to reduce contamination by photons from Earth's atmosphere, were selected. Instead, the good time intervals are selected with gtmktime tool using the filter expression (DATAQUAL >0) and (LAT CONFIG==1). The events are binned within a 16.9° × 16.9° square region with a stereographic projection into 0.1° × 0.1° pixels and into 37 equal logarithmically spaced energy bins with the help of gtbin tool. Then, an exposure map in the ROI with 22° radius was computed using tasks gtltcube and gtexpmap. The background point sources from the Fermi-LAT fourth source catalog [4FGL; 11] within ROI+5 from the position of 3C 454.3 were all included in the model file with the same spectral models as in the catalog. The normalization and spectral parameters of the sources within the ROI were set as free parameters, while that of the sources outside ROI were fixed to the catalog values. The model file contains the standard templates describing the diffuse emission from the Galaxy (gll_iem_v07) and the isotropic γ-ray background (iso_P8R3_SOURCE_V2_v1). The normalization of both components is considered as a free parameter in the analysis. Initially, the binned likelihood analysis is applied to the full time data set using the gtlike tool.

In the light curve calculations (shorter periods), the flux and photon index are estimated applying unbinned likelihood analysis. The photon indexes of all sources except 3C 454.3 are fixed, only keeping free the normalization of the sources within the ROI. As no variability is expected from background models, their normalization was fixed. Since the likelihood fitting is performed for short periods, the spectrum of 3C 454.3 was modeled as a power-law (PL) with the normalization and photon index as free parameters. The significance of the source emission in each interval is evaluated using test statistics defined as $TS = 2log(L_1/L_0)$, where L_0 and L_1 are the likelihoods of the model without source (null hypothesis) and the alternative likelihood (with source), respectively.

3C 454.3 is a well known strongly variable γ-ray blazar, so the light curve is computed in two different ways. Initially, the light-curve with 3-day binning was calculated (Fig. 4.1 panel b), but at this fixed time binning the fast variation of the flux will be smoothed out and the true increase or the variation of the flux cannot be investigated. In the case of short time intervals, the flux can be estimated only in the active state when the source is bright. Thus, in order to have a deeper and detailed view of the γ-ray flux variation, the light curve was generated with the help of the adaptive binning method [85]. In this case, the bin width is defined by requiring a constant relative flux

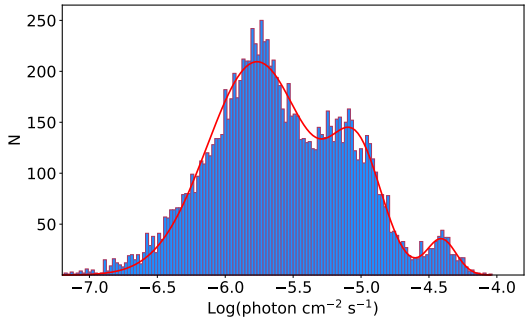

Figure 4.2 The distribution of the γ-ray flux estimated in adaptively binned intervals. The red line shows the fit with three Gaussian functions.

uncertainty, so the time bins are longer during low flux levels and narrower when the source is in flaring state. The light curve generated by this method is a powerful tool for investigation of the flux variations in short time scales and identification of flaring periods as well as it contains maximum possible information on the flux variation [e.g., see 55, 126, 153, 18, 30, 117].

The adaptively binned light curve with 20% uncertainty and above $E_0 = 141.6$ MeV [for E_0 see 85] is in Fig. 4.1 panel *a)* showing the complex behavior of 3C 454.3 in 2008-2018. The source is so bright that the flux and photon index were estimated in 11698 time intervals providing a possibility to investigate the γ-ray flux changes also in hour scales. The source exhibited several substantial γ-ray flaring events during the considered period. In the low state (e.g., MJD 55800-56140) the γ-ray flux is of the order of $\simeq 5 \times 10^{-8}$ $photon\ cm^{-2}\ s^{-1}$, however, during the flares the flux was above 10^{-5} $photon\ cm^{-2}\ s^{-1}$. The major γ-ray flaring activity was observed during MJD 55517-55522 when the highest γ-ray flux of $(9.22 \pm 1.96) \times 10^{-5}$ $photon\ cm^{-2}\ s^{-1}$ above 141.6 MeV was observed on MJD 55519.3 with 15.6σ significance which is 1844 times higher than the lowest γ-ray flux. Interestingly, there are in total 1657 time intervals when the source flux was above 10^{-5} $photon\ cm^{-2}\ s^{-1}$ which were observed in different periods, showing that from time to time the source was in a powerful γ-ray emitting state. Fig. 4.2 shows the distribution of the γ-ray flux of 3C 454.3 estimated in 11698 intervals. The distribution shows three peaks which characterize different states of the source. The fit of these peaks with three Gaussian functions is shown with red line in Fig. 4.2. The first peak is at 1.71×10^{-6} $photon\ cm^{-2}\ s^{-1}$ which is the average γ-ray flux of the source. The other two peaks are at 9.32×10^{-6} $photon\ cm^{-2}\ s^{-1}$ and

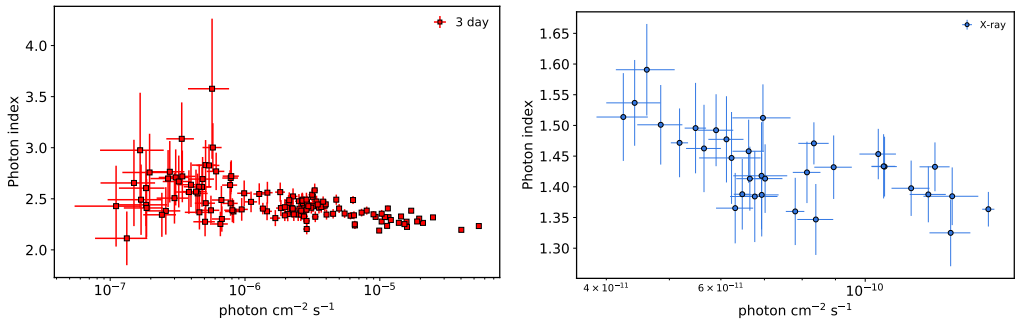

Figure 4.3 Photon index versus flux. Left panel: The γ-ray photon index vs. the flux during the major γ-ray flare (MJD 55400-55800) estimated in 3-day bins. Right panel: The X-ray photon index vs. the flux during MJD 55400-55600.

3.9×10^{-5} *photon* cm^{-2} s^{-1}, respectively, when the source was in an active γ-ray emitting state. Especially interesting are the periods when the flux exceeded the third peak; for example, in 72 intervals the source was in a hyperactive state when the γ-ray flux varied within $(5.01 - 9.22) \times 10^{-5}$ *photon* cm^{-2} s^{-1}, corresponding to an apparent isotropic γ-ray luminosity of $(0.88 - 5.69) \times 10^{50}$ *erg* s^{-1}, which is the range of the highest γ-ray luminosity observed from blazars so far. It is interesting to note that the 3C 454.3 flux was $> 10^{-5}$ *photon* cm^{-2} s^{-1} for 30.8 days in total ($\sim$ 0.84 % of the considered ten years). This once more confirms that 3C 454.3 is extremely variable in the γ-ray band.

The evolution of the γ-ray photon index in the considered ten years was also investigated. Unlike the fast γ-ray flux variation, the photon index does not vary significantly. It is hard to investigate the photon index variation when adaptive bins are considered, as the time intervals are short and the photon index is estimated with large uncertainty; the simple χ^2 test results in $\chi^2/dof \simeq 1.01$ with a probability of $P(\chi^2) = 0.12$, implying a relatively constant photon index. Instead, in the light curve with 3-day bins, the accumulation time is enough for precise estimation of the photon index showing that it varies as well. Considering only the intervals when TS > 16, the hardest photon index of 1.87 ± 0.04 was observed on MJD 56559.16 ± 1.5 with 47.5σ. The source flux was $(2.54 \pm 0.15) \times 10^{-6}$ *photon* cm^{-2} s^{-1}, implying the source was in an average γ-ray emitting state. Furthermore, the γ-ray photon index correlation was investigated. The correlation of the photon in-

dex and the flux is expected when the accelerated electrons are cooled down; the photon index is controlled by acceleration or cooling times, and depending on which of them is dominating, the photon index at the peak flux either softens or hardens [82]. Photon index hardening is observed for some blazars and radio galaxies when they get brighter [e.g., see 5, 1, 8, 18]. In the long time scale, any trend will be smoothed out because of the mix of different flux levels, so the spectral variability and flux correlation was investigated using the data around the major γ-ray flare (MJD 55400-55800). The γ-ray photon index versus flux estimated in 3-day bins is presented in Fig. 4.3 (left panel) and the possible correlation is investigated using the linear-Pearson correlation test. The test yielded $r_p = -0.41$, implying a negative correlation between the flux and photon index, i.e., the flux increases with decreasing (hardening) photon index. It should be noted that a very moderate harder when brighter trend was measured using daily bins for the period covering the outbursts in 2009 December and 2010 April [8].

4.2.2 Swift XRT

The Swift satellite with three instruments on board, the UV and Optical Telescope [UVOT, 121], the X-Ray Telescope [XRT, 34] sensitive to the 0.3-10.0 keV band, and the Burst Alert Telescope [BAT, 20] sensitive to the 15-150 keV band is an ideal instrument for simultaneous observation of blazars in the X-ray, Optical, and UV bands. 3C 454.3 was monitored by Swift 465 times during 2005 - 2016. In the current study the data collected by XRT and UVOT instruments has been analyzed.

The XRT data were taken both in photon counting mode (PC) or windowed timing mode (WT) with the single exposure ranging from 0.22 to 14.35 ks for a total exposure of $\sim$ 0.76 Ms. All the XRT data were processed using Swift_xrtproc which is an automatic tool for XRT data analysis developed within the Open Universe initiative [1] (**(author?)** [64], Giommi et al. 2021, submitted). The raw event files (Level1) were reduced, calibrated and cleaned via the XRTPIPELINE script by applying the standard filtering criteria and the latest calibration files of CALDB. The source counts were extracted from a circular region of a radius of $\sim$ 20 pixels ($47''$) centered on the position of 3C 454.3, while the background counts are taken from an annular ring centered at the source, with inner and outer radii of $\sim$ 51 pixels ($120''$) and $\sim$ 85 pixels

[1] https://openuniverse.asi.it

($200''$), respectively. For some observations, the source count rate was above $0.5\,counts\,s^{-1}$ and the data were significantly affected by the pile-up in the inner part of the point-spread function. These pile-up effects were removed by excluding events within the circle the radius of which is defined by the count rate and varying within 3-6-pixels. The ungrouped data were loaded in XSPEC (vesiopn 12.11) for spectral fitting using Cash statistics [35]. The individual spectra were fitted adopting absorbed PL and log-parabola models with the galactic absorption column density of $6.78 \times 10^{20}\,cm^{-2}$ [2].

Fig. 4.1 d) shows the 2.0-10.0 keV X-ray flux variation during 2007-2016. The X-ray variation over different observations is evident, the lowest flux being $(7.47 \pm 0.59) \times 10^{-12} erg\,cm^{-2}\,s^{-1}$ and the highest $(1.80 \pm 0.18) \times 10^{-10} erg\,cm^{-2}\,s^{-1}$. The source was observed many times around the major γ-ray brightening, showing the X-ray flux increased between MJD 55517-55520 when in seven observations the flux was above $\sim 10^{-10} erg\,cm^{-2}\,s^{-1}$. Another period of bright X-ray emission was observed in MJD 55166-55174 when again the X-ray flux was $> 10^{-10} erg\,cm^{-2}\,s^{-1}$. The X-ray flux varies albeit with lower amplitude also during the γ-ray flaring period in MJD 56800-57800.

Fig. 4.1 e) shows the variation of X-ray photon index measured in the $0.3 - 10$ keV band. The X-ray photon index is around ~ 1.5 and does not show substantial variation over different observations. However, occasionally harder or softer indexes are observed; the softest index of 1.75 ± 0.04 was observed on MJD 56829.60 while the hardest, 1.16 ± 0.20, on MJD 54831.70. The photon index variation versus the flux is investigated using the data around the flares at MJD 55130-55250 and MJD 55400-55600. In the latter case, the linear-Pearson correlation test shows no correlation, while a negative correlation ($r_p = -0.60$) is found during the first flare (Fig. 4.3 right panel). Along with the increase of the flux, the photon index hardens to ~ 1.35.

4.2.3 Swift UVOT

Simultaneously with XRT, 3C 454.3 was observed with the UVOT instrument in six filters, V (500-600 nm), B (380-500 nm), U (300-400 nm), W1 (220-400 nm), M2 (200-280 nm) and W2 (180–260 nm). All the single observations were processed. The source counts were extracted from a circular region of $5''$ around the source, while the background - from a $20''$ region away from the source not containing any significant pixel. The source magnitudes and

[2] https://heasarc.gsfc.nasa.gov/cgi-bin/Tools/w3nh/w3nh.pl

Table 4.1 Results of the γ-ray spectrum fitting with different models (PLEC and LP).

Period	Flux[1]	Γ / α	E_{cut}^2	β
54719.82 - 54730.50	3.94 ± 0.44	2.15 ± 0.05	4.03 ± 1.00	- -
54808.37 - 54850.18	0.82 ± 0.05	2.21 ± 0.06	3.61 ± 0.96	- -
54955.18 - 54990.41	0.85 ± 0.12	2.13 ± 0.06	3.20 ± 0.81	- -
55051.41-55065.48*	1.27 ± 0.05	2.14 ± 0.07	- -	$0.18 \pm$
55104.72 - 55118.41	3.10 ± 0.09	2.25 ± 0.06	3.13 ± 0.79	- -
55160.50 - 55166.10	7.84 ± 0.20	2.13 ± 0.04	5.05 ± 1.18	- -
55177.89-55182.82*	6.94 ± 0.22	2.08 ± 0.04	- -	$0.11 \pm$
55213.93 - 55223.36	5.06 ± 0.13	2.22 ± 0.05	3.34 ± 0.76	- -
55246.42 - 55264.45	3.06 ± 0.07	2.25 ± 0.05	3.83 ± 0.94	- -
55280.79 -55288.24*	5.79 ± 0.19	2.19 ± 0.04	- -	$0.11 \pm$
55303.44 - 55308.62	7.48 ± 0.19	2.17 ± 0.05	4.11 ± 1.08	- -
55371.82 - 55414.87	1.53 ± 0.04	2.20 ± 0.05	2.75 ± 0.52	- -
55414.87 - 55422.58	2.71 ± 0.30	2.07 ± 0.09	1.67 ± 0.43	- -
55464.76 - 55480.30	2.29 ± 0.38	2.03 ± 0.08	1.70 ± 0.35	- -
55480.30 - 55494.20	3.71 ± 0.41	2.27 ± 0.05	4.06 ± 1.03	- -
55494.20 -55500.87*	5.80 ± 0.18	2.23 ± 0.05	- -	$0.12 \pm$
55502.06 - 55510.51	10.54 ± 0.17	2.13 ± 0.02	10.55 ± 2.13	- -
55517.05 - 55518.06	48.96 ± 1.03	2.01 ± 0.03	8.81 ± 1.97	- -
55518.06 - 55518.68	62.37 ± 1.27	2.11 ± 0.03	6.28 ± 1.42	- -
55519.59 - 55520.19	73.59 ± 1.79	2.09 ± 0.04	6.40 ± 1.68	- -
55520.19 - 55520.80	52.29 ± 1.34	1.98 ± 0.04	6.91 ± 1.57	- -
55521.30 -55523.00*	24.94 ± 0.72	2.10 ± 0.04	- -	$0.09 \pm$
55523.00 - 55525.35	21.23 ± 0.45	2.14 ± 0.04	6.76 ± 1.65	- -
55529.04 - 55530.56	20.31 ± 0.57	2.13 ± 0.04	5.82 ± 1.61	- -
55541.35 - 55542.68	14.88 ± 0.48	2.09 ± 0.06	3.75 ± 1.03	- -
55543.94 - 55545.30	17.02 ± 0.49	2.08 ± 0.05	4.23 ± 1.10	- -
55549.00 - 55553.46	18.28 ± 0.30	2.15 ± 0.02	9.17 ± 1.83	- -
55587.20 - 55628.06	2.93 ± 0.07	2.30 ± 0.03	5.76 ± 1.15	- -
56657.96 - 56744.44	0.95 ± 0.03	2.24 ± 0.08	4.69 ± 2.05	- -
56829.85 - 56832.09	11.95 ± 0.31	1.84 ± 0.03	14.94 ± 3.54	- -
56857.26 -56863.64*	2.12 ± 0.15	1.89 ± 0.08	- -	$0.22 \pm$
57267.66 - 57278.13	2.84 ± 0.16	2.12 ± 0.06	3.06 ± 0.80	- -
57287.48 -57301.85*	2.98 ± 0.10	2.23 ± 0.05	–	$0.12 \pm$
57326.85 -57333.30*	3.25 ± 0.16	2.06 ± 0.07	- -	$0.19 \pm$
57400.81 - 57409.39	4.33 ± 0.12	1.99 ± 0.05	2.90 ± 0.54	- -
57431.33 -57456.50*	1.26 ± 0.21	2.78 ± 0.10	- -	$0.16 \pm$
57558.20 - 57562.21	7.40 ± 0.38	1.83 ± 0.07	4.67 ± 1.34	- -
57562.21 - 57562.71	16.42 ± 0.76	1.77 ± 0.08	3.86 ± 1.11	- -
57563.01 - 57564.33	17.18 ± 0.50	1.87 ± 0.04	5.52 ± 1.17	- -
57607.08 - 57635.05	2.37 ± 0.21	2.20 ± 0.04	5.41 ± 1.24	- -
57743.77 - 57763.90	1.64 ± 0.05	2.13 ± 0.05	3.66 ± 0.88	- -

[1] The flux in units of 10^{-6} $photon\ cm^{-2}\ s^{-1}$.

[1] The cut-off energy in GeV.

fluxes were extracted using uvotsource. Magnitudes are corrected for the galactic extinction [134] which were then converted to fluxes using the central wavelength values for each filter from **(author?)** [111].

Fig. 4.1 panels f) and g) show the light curves in optical and UV bands (separating V, B, U and W1, M2 and W2 filters for clarity). On the low state the optical/UV flux of the source is at the level of $(7-8)\times10^{-12}\,erg\,cm^{-2}\,s^{-1}$ which increases above $\sim 3\times10^{-11}\,erg\,cm^{-2}\,s^{-1}$ during the flares. The flux increased in all six filters with different amplitudes: the highest flux of $(1.16\pm0.03)\times10^{-10}\,erg\,cm^{-2}\,s^{-1}$ was observed on MJD 53507.85 before the Fermi-LAT operation (not shown in Fig. 4.1). This coincides with the exceptional optical outburst observed in spring 2005 [149]. The flux increased almost to the same level, $(1.03\pm0.03)\times10^{-10}\,erg\,cm^{-2}\,s^{-1}$, also in B band on MJD 56832.89. During the γ-ray major brightening around MJD 55500 and the flare in MJD 56800-57800, the UV flux in all bands substantially increased, being above $\sim 5\times10^{-11}\,erg\,cm^{-2}\,s^{-1}$.

The visual inspection of the light curves shown in Fig. 4.1 suggests that the flares in different bands are nearly correlated or appear with small legs. A cross correlation analysis of the 3C 454.3 emission in different bands has been performed in **(author?)** [14] where a detailed comparison of the emission in various bands is provided [see Table 2 and 3 in 14].

4.3 Evolution of Spectral Energy Distribution

The data presented in the previous section provide a detailed view of the long-term emission of 3C 454.3. The temporal evolution of the SEDs is investigated by generating SEDs with simultaneous or quasi simultaneous data. The SEDs are constructed in the following manner: for each interval the γ-ray data are plotted together with the Swift UVOT, XRT or, if available, archival data extracted from the ASI Space Science Data Centre (ASI/SSDC) [3]. The archival data observed both at low and high frequencies are included, allowing to constrain the SEDs from 10^6 Hz to 10^{26} Hz. The intervals are selected based on the γ-ray data as the source is being continuously monitored since 2008. Yet, in the ideal case, the γ-ray spectral points should be generated for all adaptively binned intervals and compared with the Swift observations. However, for short intervals, in the γ-ray band the spectrum will extend only

[3] https://tools.ssdc.asi.it/SED/

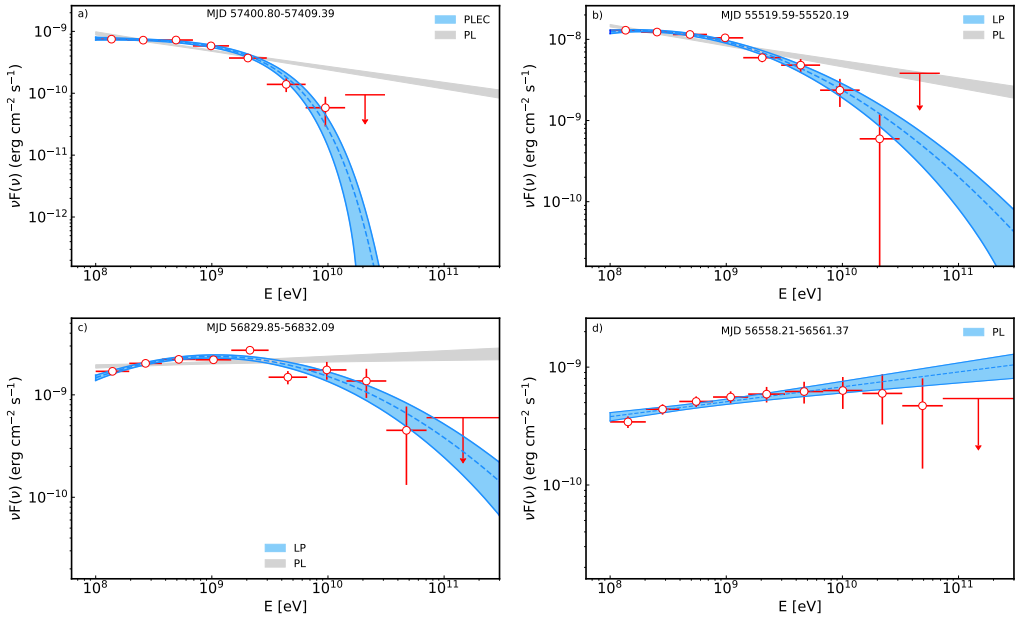

Figure 4.4 The γ-ray SEDs of 3C 454.3 in different periods. Panels a) and b) PLEC and LP spectral modeling (blue shaded area) versus PL model (gray shaded area), respectively. Panels c) and d) the periods with hard γ-ray spectra. The spectral points have been obtained by running gtlike tool for smaller energy intervals.

up to moderate energies of $\sim$ 1 GeV not enough for theoretical modeling. So, in order to overcome the problem of low statistics, the adaptively binned light curve is divided into piecewise constant blocks (Bayesian blocks) by optimizing a fitness function [133]. This gives the optimal segmentation of the data into time intervals during which the data are statistically consistent with a constant flux. These blocks provide an objective way to detect significant local variations in the light curve. In this way, the γ-ray emitting intervals with the same flux level (weather flaring or constant) will be selected and separated. These intervals are shown in Fig. 4.1 c panel. By this statistical method, the selected intervals will be longer, allowing to calculate the γ-ray spectra up to reasonable energies necessary for theoretical modeling.

The Bayesian block algorithm applied to the adaptively binned light curve produces 388 intervals each with a constant flux level. Similarly, Bayesian blocks are computed also for the 3-day binned light curve, which in general produces similar results although with less intervals. In order to have a more detailed view of the SEDs evolution, the blocks from adaptively binned light curve are considered. The spectrum in each Bayesian block is computed by applying unbinned likelihood analysis assuming the spectrum of 3C 454.3 is a PL with the normalization and index as free parameters. Then, the SEDs are calculated by fixing the source PL index and running gtlike separately for 4 to 7 energy bins (depending on the source significance) of equal width in log scale.

The resultant SED evolution in time (SED/ligh curve animation) can be found in `youtube.com/wNLVj3W6ZFg` showing dramatic changes in the broadband spectrum of 3C 454.3 during 2008-2018. The flux amplification is nearly of two orders of magnitude in the optical/UV bands while in the X-ray band it is of two-three orders of magnitude. The major changes are observed in the γ-ray band when the flux changes by four orders of magnitude. Similar changes of the flux in the optical/UV and X-ray bands show that, perhaps, in these bands the same component is contributing, whereas in the γ-ray band another component is dominating. This fits well in the synchrotron and SSC/EIC scenario for the broadband emission from 3C 454.3.

4.3.1 Gamma-ray spectrum evolution in time

The periods when the γ-ray spectrum deviates from the simple PL model (red bowtie) can be identified in the time evolution of the multiwavelength

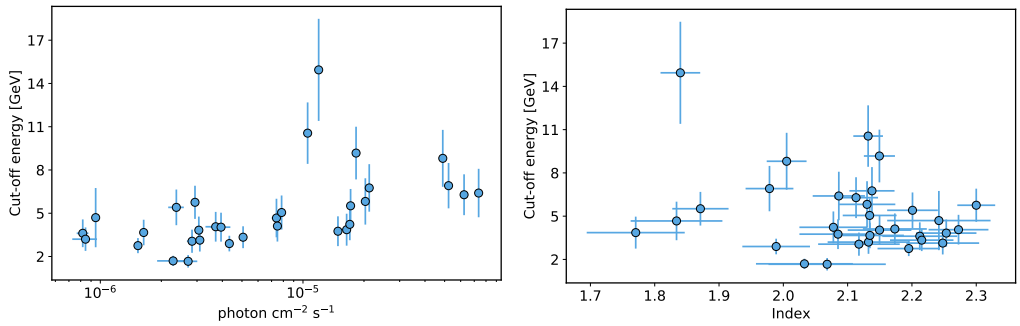

Figure 4.5 The cut-off energy versus the γ-ray flux (left panel) and photon index (right panel).

SEDs. In order to identify whether the curvature is statistically significant, alternative fits with functions in the form of $dN/dE \sim E_{\gamma}^{-\alpha} \times Exp(-E_{\gamma}/E_{cut})$ (power-law with exponential cut-off [PLEC]) and $dN/dE \sim (E_{\gamma}/E_{br})^{-(\alpha+\beta log(E_{\gamma}/E_{br}))}$ (log-parabola [LP]) were applied. These models are compared with PL modeling by applying a log likelihood ratio test where the significance is $2(\mathcal{L}_{\mathcal{PLEC}/\mathcal{LP}} - \mathcal{L}_{\mathcal{PL}})$. In the 388 Bayesian blocks, there are 41 intervals when the significance of the curvature was $> 5\sigma$. These periods are given in Table 4.1 for each interval, providing the γ-ray flux, photon index, cut-off energy or β if the model is LP, detection significance and curvature significance.

In all the periods, both PLEC and LP provide a statistically better representation of the data and only in nine periods (marked with $*$) only LP modeling was preferred over the simple PL model. In all the periods, the detection significance of the source was $> 40\,\sigma$, convincingly high to test the curvature. In these periods the γ-ray spectrum is soft with a photon index of $1.98 - 2.30$, except for five intervals when it was < 1.90. Fig. 4.4 a) and b) panels show the 3C 454.3 spectra during two periods (with a high significance of the curvature) where the PLEC and LP are compared with PL model. Interestingly, curved spectra were observed also when the source was in active and hyperactive states (MJD 55502-55554 in Table 4.1). The spectrum in the hyperactive state with a flux of $(7.36 \pm 0.18) \times 10^{-5}\ photon\ cm^{-2}\ s^{-1}$ is shown in Fig. 4.4 b).

The cut-off energy variation versus the γ-ray flux and photon index is shown in Fig. 4.5. No strong cut-off energy variation is found as compared to the flux, i.e., the flux varies by a factor of ~ 90, whereas the cut-off energy

only by $\sim$ 5. Similarly, as the photon index occasionally can be as hard as $\simeq$ 1.77, the break energy remains relatively constant. This is in agreement with the previous studies of 3C 454.3 [e.g., 3, 8]. The highest cut-off energy of $E_{cut} = 14.95 \pm 3.54$ GeV has been observed on MJD 56829.85-56832.09 when the source was in a bright γ-ray emission state with a flux of $(1.19 \pm 0.03) \times 10^{-5}$ *photon* $cm^{-2}\, s^{-1}$ and the γ-ray photon index was 1.84 ± 0.03.

Interestingly, there are periods when the γ-ray spectrum substantially hardened shifting the peak of the second emission component towards higher energies. The spectrum of 3C 454.3 in such two periods in shown in Fig. 4.4 panels c) and d). In the first period (panel c), even if the γ-ray spectrum is initially hard, it starts to curve above a few GeV, and the LP model better explains the data. On the other hand, the γ-ray spectrum measured during MJD 56558.21-56561.37 is with a photon index of 1.84 ± 0.04 and extends above $\sim$ 10 GeV with 51.50σ. Additional periods with harder γ-ray photon index of 1.88 ± 0.06, 1.89 ± 0.07 and 1.89 ± 0.06 were observed during MJD 56834.20-56834.91, 56916.17-56916.64 and 56827.09-56827.52, respectively. Although, these are short intervals as compared with the period in Fig. 4.4 d) and the spectra were measured up to $\sim$ 10 GeV, the hardening of the spectrum is evident.

4.4 Origin of multiwavelength emission

The multiwalength data obtained in Section 4.2 provide unprecedented detailed information on the emission spectrum of 3C 454.3 over different years. Yet, the large amount of the available data allows to investigate not only the emission in different states but also, through theoretical modeling, the evolution of different components of the SEDs. By modeling single snapshot SEDs constrained by (quasi) contemporaneous data, the main parameters describing the jet can be estimated, whereas modeling of the SEDs of the same source observed in different periods can provide a clue on the changes in the jet over different periods. Such an interpretation of the data is the backbone of any model aiming to self-consistently explain blazar emission. Thus, in all the periods shown in the SED/light curve animation when the data in the optical/UV, X-ray and γ-ray bands are available (362 periods) have been modeled and the corresponding parameters estimated.

The double-peaked SED of 3C 454.3 is modeled within a homogeneous one-zone leptonic scenario where the low energy component is interpreted

as synchrotron emission of relativistic electrons, while the second component is due to inverse Compton up-scattering of various photon fields. The seed photons come from the jet itself [SSC model e.g., 90, 25] and those from the accretion disk [external Compton scattering of direct disk radiation, EC disk; 46] or those reflected from the BLR clouds [EC BLR; 136] or those of the dusty torus [24], depending on the location of the emission region along the jet. However, the observed high energetics of 3C 454.3 as well as the short time variability in the γ-ray band suggest that the emission region is located close to the blazar central black hole where the dominant photon fields are those from the accretion disk and BLR. Similar assumption was made in **(author?)** [147], and **(author?)** [51] demonstrated that the combination of those two photon fields can explain the sharp break in the SED of 3C 454.3 and it gives a better fit to the quasi-simultaneous radio, optical/UV, X-ray and γ-ray data.

In this scenario, the emission is produced in a spherical blob of the jet with a size of R filled with uniform magnetic field B that moves with a Lorentz factor of Γ at a small angle to the observer. The emission from the blob is enhanced by $\delta \simeq \Gamma$ for small angles. The emission region is filled with a population of non-thermal electrons which have a broken power-law distribution in the form of

$$N(\gamma') = \begin{cases} N'_e \gamma'^{-p_1} & \gamma'_{min} \leq \gamma' \leq \gamma'_{br} \\ N'_e \gamma'^{\,p_2-p_1}_{br} \gamma'^{-p_2} & \gamma' > \gamma'_{br} \end{cases} , \tag{4.4.1}$$

where p_1 and p_2 are the low and high indexes of electrons correspondingly below and above the break energy γ'_{br}, γ'_{min} is the minimum electron energy in the jet frame. N'_e is connected with the total energy of electrons $U_e = m_e\, c^2 \int_{\gamma'_{min}}^{\gamma'_{max}} \gamma'\, N(\gamma')\, \mathrm{d}\gamma'$ which scales with the magnetic field energy density $B^2/8\pi$.

It is assumed that the emission region is within the BLR, at a distance of 10^{17} cm. **(author?)** [27] derived that for 3C 454.3 the BLR is located at a distance of $\sim 6 \times 10^{17}$ cm. Therefore, the BLR is modeled as a spherical shell with a lower boundary of $R_{in} \simeq 4.9 \times 10^{17}$ cm and an outer boundary of $R_{out} = 1.2 \times R_{in} \simeq 5.9 \times 10^{17}$ [49] and which reflects 10% of the disk luminosity L_{disk}. The disk emission is approximated as a mono-temperature black body.

In order to reduce the number of free parameters, it is assumed that the

emission region size is $R = 5 \times 10^{15}$ cm which corresponds to hour scale variability as observed in the γ-ray band. Next, in order to constrain the source parameters (e.g., the disk luminosity), the SED observed in MJD 54808.37-54750.83, where the disk contribution in the optical/UV band (blue bump) can be seen, is modeled. The fitting is performed with the open source package JetSet [91, 143, 142].

The SED well reproduced by the applied model is shown in Fig. 4.6 (upper panel). The sum of all components is shown in blue, while the disk component is in magenta peaking at 3.02×10^4 K (6.3×10^{14} Hz) with the luminosity of $L_{disk} = 4.57 \times 10^{46}\, erg\, s^{-1}$ similar to the values usually estimated for 3C 454.3. The X-ray emission is dominated by the contribution from SSC (green) while the EC of disk and BLR components (light blue and red, respectively) dominate at higher energies. The fitting resulted in $\delta \simeq 16.9$ which is typical for the bright blazars and $\gamma'_{min} = 5.88$ implying that all electrons are cooling in the emitting region. The PL indexes of electrons change from 1.34 to 3.51 at the break energy of 240.7.

When modeling the SEDs in other periods, the disk luminosity and temperature are fixed to the values obtained from the fitting of the SED in MJD 54808.37-54750.83. The other model parameters (N'_e, p_1, p_2, γ'_{min}, γ'_{br}, δ and B) have been then estimated by fitting the SEDs. The SEDs modeling animation is available here `youtube.com/dAqVjpO5Nb4`. The synchrotron/SSC components account for the data up to the X-ray band and, in principle, SSC could extend to HEs. However, as demonstrated in **(author?)** [51], the SSC component cannot explain the sharp break observed in the γ-ray band and in such case the strong contribution from BLR photons should be neglected. Considering inverse Compton scattering of only BLR photons, which have a narrower distribution than the SSC component starts to decrease and cannot explain the Fermi-LAT data. Instead, the HE spectrum can be well reproduced when considering the joint contribution from EC of disk and BLR photons. The EC disk component dominates in the sub-GeV band, while the contribution of EC BLR is significant at HEs. However, the γ-ray data can be explained also when considering the joint inverse Compton scattering of BLR and torus photons [e.g., see 79].

The modeling of the SED during the bright period in MJD 55519.59-55520.19 is shown in Fig. 4.6 (middle panel). In this active emission state, the source flux from radio to X-ray bands increased nearly by an order of magnitude while in the γ-ray band by nearly two orders of magnitude. As compared with the results of the modeling of the SED in MJD 54808.37-54750.83, the pa-

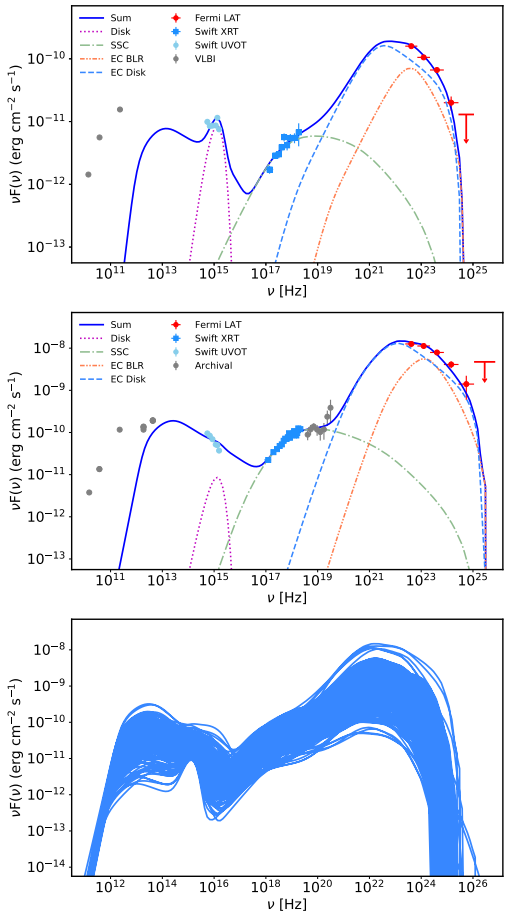

Figure 4.6 Upper panel: The multiwavelength SED during MJD 54808.37-54750.83. Fermi-LAT, Swift XRT and UVOT data are in red, blue and light blue, respectively. The VLBI radio data are from **(author?)** [147]. Middle panel: The multiwavelength SED during the bright period in MJD 55519.59-55520.19. Lower panel: The summary of all components from the modeling of all SEDs with contemporaneous data collected during 2008-2018.

rameters describing the emitting electrons did not vary substantially (e.g., $p_1 = 1.19$, $p_2 = 3.77$ and $\gamma'_{br} = 271.7$ were estimated in MJD 55519.59-55520.19), but a higher $\delta \simeq 50.8$ was estimated. This implies that the flaring activity was caused by the changes in the bulk Lorentz factor of the emitting region.

The evolution of model parameters is shown in Fig. 4.7. The photon indexes (panel a and b) are defined by different data sets and vary in the range of $p_1 = 0.77 - 1.97$ and $p_2 = 2.71 - 5.98$. The emission in the X-ray band is due to inverse Compton up-scattering of synchrotron photons in the Thomoson regime and the PL index of the emitting electrons is defined by the X-ray data. Similarly, the γ-ray data which are due to inverse Compton scattering of disk and BLR photons are defining p_2. The modeling shows that the p_1-$p_2 > 1.4$, so the index change is significantly larger than that expected from the standard cooling break. The break energy (panel d in Fig. 4.7) is in the range of $107.07 - 1220.58$ defining the low and high energy peaks to be at $\sim 3 \times 10^{12}$ Hz and 10^{22} Hz, respectively, which is characteristic for FSRQs. The minimum electron energy varies in the range of 2.03-48.88 which is shown in panel e) of Fig. 4.7. Along with p_1 this minimal energy is defined by the SSC modeling of the X-ray data.The magnetic field in the jet is in the range from 1.43 to 9.19 G (lower panel of Fig. 4.7) and the amplitude of its variation is lower than that of the parameters describing the emitting electrons. This implies that the observed flares are likely due to the changes in the emitting electrons rather than in the emitting region plasma.

4.5 Discussion

The broadband monitoring of 3C 454.3 in 2008-2018 reveals an interesting and complicated behaviour in all the considered bands. The highest amplitude flares are observed in the γ-ray band when the flux in several occasions was above 10^{-5} $photon\,cm^{-2}\,s^{-1}$ which corresponds to an apparent isotropic γ-ray luminosity exceeding $10^{50}\,erg\,s^{-1}$ (for the 5.49 Gpc distance to 3C 454.3). In these active states, in the proper frame of the jet, the total power emitted in the γ-ray band would be $L_{em,\gamma} = L_\gamma/2\,\delta^2 \simeq 10^{47}\,(\delta/20)^{-2}\,erg\,s^{-1}$ which by nearly an order of magnitude exceeds the disk luminosity L_d in agreement with the results of **(author?)** [62].

The γ-ray photon index of 3C 454.3 varies as well; occasionally the photon index can be as hard as 1.87 ± 0.04 measured during a 3-day period. During

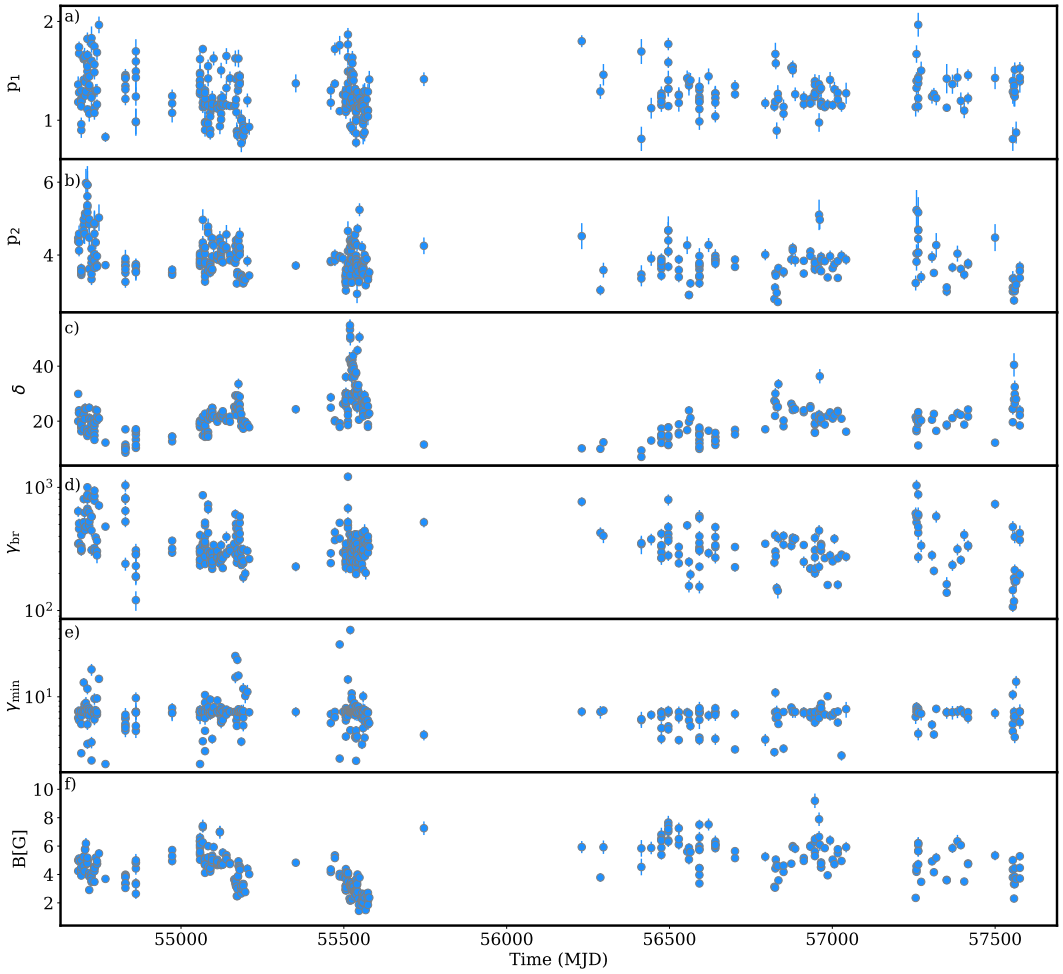

Figure 4.7 The evolution of model free parameters estimated by modeling the SEDs. a) and b) the PL indexes of electrons before and after the break, respectively. c) the Doppler boosting factor changes in 2008-2018. d) and e) the break and minimum energy of emitting electrons in different periods. f) the change of magnetic field in the emitting region.

this period, the highest energy event with $E_\gamma = 14.92$ GeV has been observed in MJD 56559.89 within a circle of 0.006° around 3C 454.3, with the probability of 0.99987 being associated with it (computed with gtsrcprob tool). Such hardening of the γ-ray spectrum is unusual for FSRQs which are characterized by a soft γ-ray photon index (e.g., the mean of FSRQ photon index distribution is 2.2 in 4FGL). However, during the γ-ray flares, occasional hardening of the the γ-ray photon index of FSRQs have been already observed [e.g., see 101, 55, 125, 109, 15]. In some periods the γ-ray spectrum of 3C 454.3 deviates from the simple PL model and PLEC and LP models give a better explanation to the overall spectrum. Such modification of the spectrum was observed when the γ-ray emission of the source was in an average or active emitting state, but unlike the strong changes in the flux ($\sim$ 90 times), the cut-off energy is within $2 - 10$ GeV.

In the X-ray band 3C 454.3 behaves like a classical FSRQ with a hard X-ray photon index of $\sim$ 1.5. Unlike the changes in the X-ray flux, which can increase up to $10^{-10} erg\, cm^{-2}\, s^{-1}$, the photon index is relatively constant. The linear-Pearson correlation test reveals a negative correlation ($r_p = -0.60$) between the flux and photon index during the flare at MJD 55130-55250. In the optical/UV band 3C 454.3 is in an active state after the large outburst in 2005: in several occasions the flux was as high as $10^{-10}\, erg\, cm^{-2}\, s^{-1}$. The available optical/UV data allows to shape the peak of the low energy component to be around $10^{13}\, Hz$ and unlike the increase of the flux it remains relatively constant. In the past, short transition of the low energy component to higher frequencies during the flares was observed in several FSRQs [e.g., see 36, 45, 131, 69, 44]. For 3C 454.3, in this band either the contribution of the disk is observed or, when the synchrotron jet emission dominates during the flares, it corresponds to the falling part of the low energy component which consequently defines the HE tail of the electron distribution. This implies that even during the flares, the processes limiting the maximum energy of the accelerated electrons (e.g., cooling or a limit from the accelerator size) do not change and produce the same effect on the electron acceleration.

The multiwavelength SEDs observed in various periods during the considered ten years are well modeled within one-zone leptonic model taking into account the inverse Compton scattering of synchrotron, disk and BLR photons. The adopted model with physically realistic parameters can satisfactorily reproduce the observed SEDs; the models obtained in 362 periods are in Fig. 4.6 (lower panel) which shows the multiwavelength behaviour of 3C 454.3 in 2008-2018. It is evident that the broadband emission varies

significantly, except for the radio band which is most likely produced from electrons in more extended regions. This is more evident when comparing the SEDs in the upper and middle panels of Fig. 4.6 where two different emission states of the source are shown. Unlike the changes in the flux, the peak of both components remains relatively stable. Within the adopted scenario, this could be interpreted by strong cooling of the electrons, i.e., due to the existence of dense photon fields (internal and external), the injected particles cool down, limiting their maximum energy, thus affecting the emission of photons. The different rising and decaying spectra of both components are most likely related with the initial injection (cooling) of electrons.

The modeling reveals that the emitting electrons initially are distributed with a hard PL index with a mean of $p_{1,mean} = 1.27$ which substantially hardens to $p_{2,mean} = 3.87$. The break energy varies in the range of $107.08 - 1220.58$ and is defined by the interplay between the particle acceleration and cooling times. The electron cooling time is defined as

$$t_{cool} = \frac{3\, m_e c\, (1+z)}{4\sigma_T\, u'_{tot}\, \gamma'_e} \tag{4.5.1}$$

where $u'_{tot} = u_B + u_{SSC} + u_{disc} + u_{BLR}$. The densities of disk and BLR photons are constant whereas u_B and u_{SSC}, which depend on the synchrotron and SSC components, vary in different periods (Fig. 4.6 lower panel). Thus, the small variation of the break energy (see Fig. 4.7) is defined by the changes in u_B and u_{SSC}. Yet, in the vast majority of cases the ratio of u_{SSC}/u_B is ≥ 1 implying that the SSC cooling cannot be neglected, so the nonlinear effects are important for the formation of particle distribution, i.e., γ_{br} and p_2. Because of these nonlinear effects the difference between p_1 and p_2 is larger than that expected from traditional cooling break ($\Delta p = 1$). Alternatively, large Δp could be due to the nature of the injection process or due to the inhomogeneities in the source [119].

In the modeling, some SEDs can be modeled only when considering very hard electron spectra; p_1 is $0.77 - 1.97$. This index depends on the combination of the data in the X-ray and γ-ray bands and sometimes because of their hard photon indexes, $p_1 < 1$ is required. In the fast electron cooling regime, a much softer γ^{-2} spectrum will be formed below γ_{min}, whereas in the slow cooling regime the hard spectrum of electrons may be due to their initial injection. However, the PL index of ≤ 1.0 is challenging for many particle acceleration scenarios. The diffuse shock acceleration of particles can

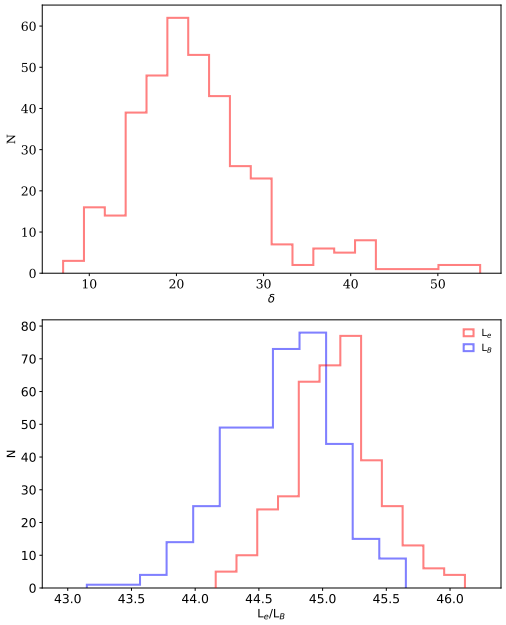

Figure 4.8 Upper panel: The distribution of Doppler boosting factor. Lower panel: The distribution of the jet luminosity in the form of electrons (red) and magnetic field (blue).

form a spectrum as hard as -1 depending on the parameters of the shocks [e.g., 140]. Similarly, a very hard electron spectrum will be formed in the relativistic magnetic reconnection [154, 72, 138, 151] only under extremely high magnetization conditions ($\geq$ 100).

The distribution of Doppler boosting factor is presented in the upper panel of Fig. 4.8 which has a peak at $\delta \simeq 20$ which is characteristic for bright FSRQs [60]. However, in some periods substantially higher values for δ are estimated: there are 26 periods when $\delta > 35$. As can be seen from Fig. 4.7 (panel c), high δ were estimated around MJD 55500 when the source was in a bright γ-ray emission state. For example, the highest $\delta = 54.8$ was estimated in MJD 55518.68-55519.10 when the γ-ray flux was as high as $(5.97 \pm 0.14) \times 10^{-5}\ photon\ cm^{-2}\ s^{-1}$ and that in the X-ray band-$(1.59 \pm 0.07) \times 10^{-10}\ erg\ cm^{-2}\ s^{-1}$. So, in this period the emission region has a larger Doppler boosting factor which results in a strong increase in the Compton dominance (hence an increase of the HE component) as the external pho-

ton density in the comoving frame of the jet depends on the Doppler boosting factor. This faster moving emitting region could be either re-accelerated during the propagation or could be newly injected and emits close to the central source. Another possibility for the Doppler boosting factor increase can be due to geometrical effects, i.e, when the jet regions may have different orientations; e.g., jets in a jet [63] or twisted inhomogeneous jet model [113]. So, during the flares the photons may be produced in a region viewed at smaller angles as compared to the entire jet, which increases the Doppler boosting factor.

The modeling provides also information on the power of the jet. The distribution of the jet luminosities in the form of magnetic field and electron kinetic energy computed as $L_B = \pi c R_b^2 \Gamma^2 U_B$ and $L_e = \pi c R_b^2 \Gamma^2 U_e$ is given in Fig. 4.8 (lower panel). L_e is in the range of $(0.79 - 9.35) \times 10^{44}\, erg\, s^{-1}$ while L_B in $(0.12 - 5.07) \times 10^{44}\, erg\, s^{-1}$, implying the system is not far from the equipartition condition. The peak of L_e is around $3 \times 10^{44}\, erg\, s^{-1}$ and L_B is at $1.2 \times 10^{44}\, erg\, s^{-1}$. For the majority of SEDs, the jet is slightly particle-dominated with $L_e/L_B \geq 1$ and only in a few periods when the low energy components exceed the X-ray flux $L_e/L_B < 1$. The total jet luminosity defined as $L_{tot} = L_e + L_B + L_p + L_{rad}$ [57], where L_p and L_{rad} are the power carried by the cold protons and the produced radiation, respectively, is $\leq 2.08 \times 10^{46}\, erg\, s^{-1}$, being smaller than the total Eddington luminosity of $1.9 \times 10^{47}\, erg\, s^{-1}$ for the black hole mass of $1.5 \times 10^9\, M_\odot$ in 3C 454.3.

4.6 Conclusions

In this paper the broadband emission from 3C 454.3 during 2008-2018 is investigated. In this period the source was in active emission state displaying extraordinary flares in the γ-ray band. In several occasions the γ-ray flux exceeded $5 \times 10^{-5}\, photon\, cm^{-2}\, s^{-1}$ corresponding to an apparent isotropic γ-ray luminosity of $> 10^{50}\, erg\, s^{-1}$. Similarly, the source was active (although with lower amplitude) also in the X-ray and optical/UV bands.

The multiwavelength SEDs of 3C 454.3 (in 362 periods) constrained with contemporaneous data collected during 2008-2018 have been modeled within a one-zone leptonic scenario taking into account the inverse Compton scattering of synchrotron, disk and BLR reflected photons. Through the modeling, the main parameters describing the jet in different periods have been estimated providing an insight into the jet evolution in 2008-2018. It is shown

that during the large γ-ray flares the Doppler boosting factor substantially increased which points that the emission during the flares comes most likely from a region which either moves faster or has a different geometrical orientation.

5 The strange case of the transient HBL blazar 4FGL J1544.3-0649

5.1 Introduction

Blazars are a special type of active galactic nuclei (AGN) hosting a relativistic jet that happens to be pointing very close to the observer's line of sight [e.g. 23, 103]. The emission in these sources is dominated by non-thermal radiation across the electromagnetic spectrum, often exhibiting large variations on timescales ranging from years to a few hundred seconds. Blazars are usually grouped into BL Lacertae (BL Lac) objects and Flat Spectrum Radio Quasars (FSRQs), based on their properties in the optical band: the optical spectrum of FSRQs shows broad emission lines while that of BL Lacs is featureless, shows narrow lines or features of the host galaxy [145].
Blazars are the most luminous and energetic persistent emitters in the known Universe, dominating in the extragalactic γ-ray sky. Among the total $\sim 5,800$ sources in the Fermi Large Area Telescope (Fermi-LAT) fourth source catalog of γ-ray sources [4FGL-DR2 ; 6, 12, 19, 86] $\sim 3,100$ are blazars, 47 are radio galaxies, and 19 are other types of AGNs. Interestingly, γ-ray emission has been detected also from blazars at very high redshifts [e.g., 7, 129] which enables the study of the evolution of the most luminous relativistic jets over cosmic time.
The broadband spectral energy distribution (SED) of blazars has a characteristic double hump shape. The low energy peak (radio to UV/X-ray) is usually explained by synchrotron emission of relativistic electrons propagating along the jet, although recent models developed to explain the emission of high-energy neutrinos in blazars assume that this component may be due to proton synchrotron radiation, at least during flares [94]. The second SED component extends to High Energies (HEs; > 100 MeV), its origin being debatable. In the leptonic scenarios, this component is interpreted as inverse Compton upscattering of synchrotron photons (Synchrotron self Compton

[SSC] **(author?)** [89, 25, 58]) or of external photons (external inverse Compton) [136, 48]. On the other hand, in hadronic models the HE component is mainly due to proton synchrotron emission [10, 97] or pion decay [87, 88, 97, 98, 29]. In the latter case, blazars are also sources of Very High Energy (VHE; $>$ 100 GeV) neutrinos [76, 75, 16, 81, 99, 105, 122, 120, 37, 54].
Depending on the peak of the low energy component (ν_{peak-s}) blazars can be further grouped into three subcategories, namely low-energy peaked blazars (LBLs; $\nu_{peak-s} < 10^{14}$ Hz), intermediate peaked blazars (IBLs; $10^{14}\ Hz < \nu_{peak-s} < 10^{15}$ Hz) and high-energy peaked blazars (HBLs; $\nu_{peak-s} > 10^{15}$ Hz) [107, 2]. Observations in the X-ray band reveal that sometimes the synchrotron peak of HBLs can reach energies of $\sim$1 keV, ($\sim 2 \times 10^{17}$ Hz) or even larger, showing an extreme behaviour [extreme HBLs, e.g. 68, 43, 22]. For example, during the flares of Mkn 501 the synchrotron peak reached $\sim$ 100 keV [110] or during the flares of 1ES 1218+304 the X-ray spectral index hardened to $\Gamma \leq 1.80$ shifting the peak towards higher energies [124]. The third catalog of high energy peaked blazars [3HSP, 38] includes several objects in this category. Recent observations in the HE and VHE γ-ray bands have revealed an additional class of BL Lac objects VHE γ-ray spectrum of which is characterized by a hard intrinsic photon index of up to 1 TeV after correction for the extragalactic background light (EBL) absorption effects (BL Lacs extreme in γ-rays; **(author?)** [28, 141]).
The BL Lacs having featureless optical spectra have been traditionally discovered in radio or X-ray surveys [e.g., 70]. Currently, the γ-ray data from Fermi-LAT observations combined with the data at the lower energy bands [e.g., infrared, IR, 92] are a powerful additional method; nearly 38% of detected blazars are BL Lacs in the fourth catalog of AGNs detected by Fermi-LAT [38, 11]. Nearly all these γ-ray emitting BL Lacs have detected radio counterparts, which makes radio observations crucial also for the understanding of their physics. In this regard of a particular interest is the identification of radio-weak BL Lac objects, i.e., BL Lacs from which radio emission is detected in follow-up observations but which do not have counterparts in the major radio surveys. A handful observations of radio-weak BL Lac objects will have an impact on our understanding of AGN unification as well as on BL Lac associations based on the radio surveys [93, 38].
In May 2017 Fermi-LAT detected a new γ-ray source (4FGL J1544.3-0649) not associated with any previously known γ-ray object; it was bright in the γ-ray band in two consecutive weeks after the discovery [41]. The X-ray follow-up

observations by Neil Gehrels Swift Observatory [56], (hereafter Swift) found a new bright X-ray source at a position corresponding to the optical transient ASASSN-17gs detected at $V = 17.3$ mag on May 25 [41]. The MAXI team [80] also reported a detection of this source on May 12-13 at a flux level similar to that observed by Swift, with a flux increase of a factor $\sim$2 in the period May 21 to May 25. The spectroscopic redshift of the host galaxy, 2MASX J15441967-0649156, was estimated to be $z = 0.171$ using the MDM 2.4m Hiltner telescope [40]. The source has a counterpart in the radio band with flux densities of 46.6 mJy at 1.4 GHz [NRAO VLA Sky Survey; 42], 35.8 mJy at 3 GHz [Very Large Array Sky Survey, epoch 1; 71] and 67 mJy at 150 MHz [TIFR GMRT Sky Survey; 77]. In addition, **(author?)** [32] monitored 4FGL J1544.3-0649 with the Effelsberg-100 m single dish radio telescope for a four-month follow-up after the brightening in the γ-ray band. These data imply a flat radio spectrum very similar to that of most blazars, and a radio luminosity of $\sim 5 \times 10^{40}$ erg s^{-1}, at 1.4 GHz, more than a factor 10 larger than that of Mrk 501 and Mrk 421. Considering the post-burst data at 5 GHz, the radio to X-ray flux ratio is log ($F_{1.4\,GHz}/F_{1\,kev}$) = -4.3 typical of HBL Blazars. Follow up XMM-Newtown (XMM) observations showed that the source exhibits strong variability both in the X-ray flux and spectral shape on timescales of $\sim$ 10 ks and the X-ray spectrum is described by a broken power-law [146].
The transient nature of 4FGL J1544.3-0649 makes it a unique object and an interesting target for broadband studies. Understanding of the changes in the jet of 4FGL J1544.3-0649 which led to its brightening in the X-ray and γ-ray bands can shed light on the physics at work in the BL Lac jets. In this regard, the many monitoring observations of 4FGL J1544.3-0649 with Swift provide unprecedented data both in the optical/UV and X-ray bands while that of Fermi-LAT in the 100 MeV-500 GeV band allowing to shape the low and high energy components in the SED of 4FGL J1544.3-0649 and investigate its evolution in time. Also, this broadband data can be used for theoretical modeling allowing to derive the main parameters characterizing the jet of 4FGL J1544.3-0649.
The purpose of this paper is to investigate the origin of the broadband emission from 4FGL J1544.3-0649 and the astrophysical multi-messenger implications of the dual behaviour of this source. The paper is organized as follows. The Fermi-LAT and Swift data extraction and analyses are described in Section 5.2. In Section 5.3 the origin of the multiwavelength emission is investigated, and the discussion and conclusion are given in Section 5.4.

5.2 Data analyses

5.2.1 Fermi-LAT observations of 4FGL J1544.3-0649

The γ-ray data used in this work was collected by Fermi-LAT from August 2008 to July 2020 (from MJD 54683 to MJD 59058). The Pass 8 SOURCE data in the energy range from 100 MeV to 600 GeV have been downloaded and analyzed using the standard reduction methodology suggested by the LAT collaboration. The events classified as evclass=128 and evtype=3 within a circular region of 12° centered on the γ-ray position of 4FGL J1544.3-0649 (R.A., decl.=236.078, -6.825) are analyzed using Fermi ScienceTools (1.2.1) with P8R3_ SOURCE_ V2 instrument response functions. The good time intervals were selected with the filter "DATA_ QUAL¿0" and "LAT_ CONFIG==1" in the gtmktime tool whereas the Earth limb photons were removed by applying a maximum zenith angle cut of 90°. The data are divided into 38 logarithmically equal energy bins and binned into the $16.9° \times 16.9°$ square region of interest. Then, binned likelihood analysis implemented in gtlike tool was used to estimate the γ-ray flux and photon index of the sources. The model file is generated from the Fermi-LAT fourth source catalog of γ-ray sources (4FGL) using the 4FGL-DR2 version of the 4FGL which is based on 10 years of survey; it includes all point-like sources within a region with a radius of 17° around 4FGL J1544.3-0649 to account for the sources outside the region which may contribute photons to the data. The latest background models, gll_iem_v07 and iso_P8R3_SOURCE_V2_v1, were also included in the model file. The spectral shapes of all sources are adopted from the 4FGL catalog and all spectral parameters of the sources falling between 12° and $12° + 5°$ are kept fixed. The γ-ray spectrum of 4FGL J1544.3-0649 is modeled with a power-law function. The significance of the γ-ray signal is evaluated by the test statistic (TS) [96] defined as $TS = 2 \times (logL_1 - logL_0)$ where L_1 and L_0 are the likelihood of the data with and without a point source at the position of the source under investigation.
The γ-ray light curves were calculated by performing an unbinned maximum likelihood analysis with the appropriate quality cuts as described above. Initially the light curve was computed by dividing the entire observation time into 21-day intervals and selecting events in the energy range from 500 MeV to 300 GeV. The lower limit was selected 500 MeV, since due to the hard γ-ray photon index of 4FGL J1544.3-0649 the source is undetected below $\sim$ 500 MeV. Also, the normalization of both diffuse components was fixed to the

values obtained for the whole time period, as no variability is expected from the background. Next, the γ-ray variability of the 4FGL J1544.3-0649 was investigated by generating the light curves with the help of an adaptive binning method [85]. This produces light curves with flexible time bins, requiring a fixed uncertainty for the flux estimation in each time interval. The fluxes are computed above the optimal energy, which is $E_p = 801.6$ MeV in this case. This allows a detailed investigation of the γ-ray flux variation and is a powerful method for identifying flaring periods (if any).

The analysis of entire $\sim$ 11.9 years data yielded the source detection with $TS = 778.7$ ($27.9\,\sigma$) and with a hard γ-ray spectrum ($\sim E^{-1.87\pm0.04}$) consistent with the value given in 4FGL. The integral flux estimated above 100 MeV is $(8.0 \pm 0.9) \times 10^{-9}$ $photon\,cm^{-2}\,s^{-1}$. Panels a) and b) of Fig. 5.1 show the γ-ray flux and photon index (Γ_γ) evolution in time calculated for 21-day (red) bins where only the intervals when $TS > 12$ are presented. The source was in the bright γ-ray flaring state around MJD 58000 with the highest γ-ray flux of $(2.59 \pm 0.43) \times 10^{-8}$ $photon\,cm^{-2}\,s^{-1}$ observed on MJD 57997.5 ± 10.5 with a detection significance of $15.0\,\sigma$. Yet, the adaptively binned light curve illustrates the changes in the γ-ray flux better; the source being mostly undetected in the γ-ray band shows significant ($> 5\sigma$) γ-ray emission with a flux of $(7.75 \pm 2.96) \times 10^{-10}$ $photon\,cm^{-2}\,s^{-1}$ above $E_p = 801.6$ MeV starting from MJD 57484.7. However, the γ-ray flux of the source substantially increased during MJD 57869.3-58052.0; the highest γ-ray flux of $(2.35 \pm 0.55) \times 10^{-8}$ $photon\,cm^{-2}\,s^{-1}$ above $E_p = 801.6$ MeV was observed on MJD 57998.9 ± 4.60. The flux was above 10^{-8} $photon\,cm^{-2}\,s^{-1}$ in other eight periods (see Fig. 5.1). Despite the increase in the γ-ray flux, the photon index does not vary significantly (panel b in Fig. 5.1); even though there are periods when the spectrum hardens, no definite conclusion can be drawn because of large uncertainties. For example, in the adaptively binned intervals the hardest indexes of 1.43 ± 0.19 and 1.44 ± 0.18 were observed on MJD 57955.64 ± 4.49 and MJD 58241.06 ± 8.70 which within the uncertainty agree with the averaged photon index estimated during $\sim$ 11.9 years. Interestingly, in the 21-day binned light curve, when the highest γ-ray flux was observed on MJD 57997.5 ± 10.5, the γ-ray spectrum is hard with a photon index of 1.57 ± 0.11. The distribution of HE photons arrival time (computed using the gtsrcprob tool) is shown in panel f) of Fig. 5.1. The highest energy event with $E_\gamma = 174.20$ GeV has been observed on MJD 57951.92 within a circle of 0.054° around 4FGL J1544.3-0649, with the probability of 0.99428 being associated

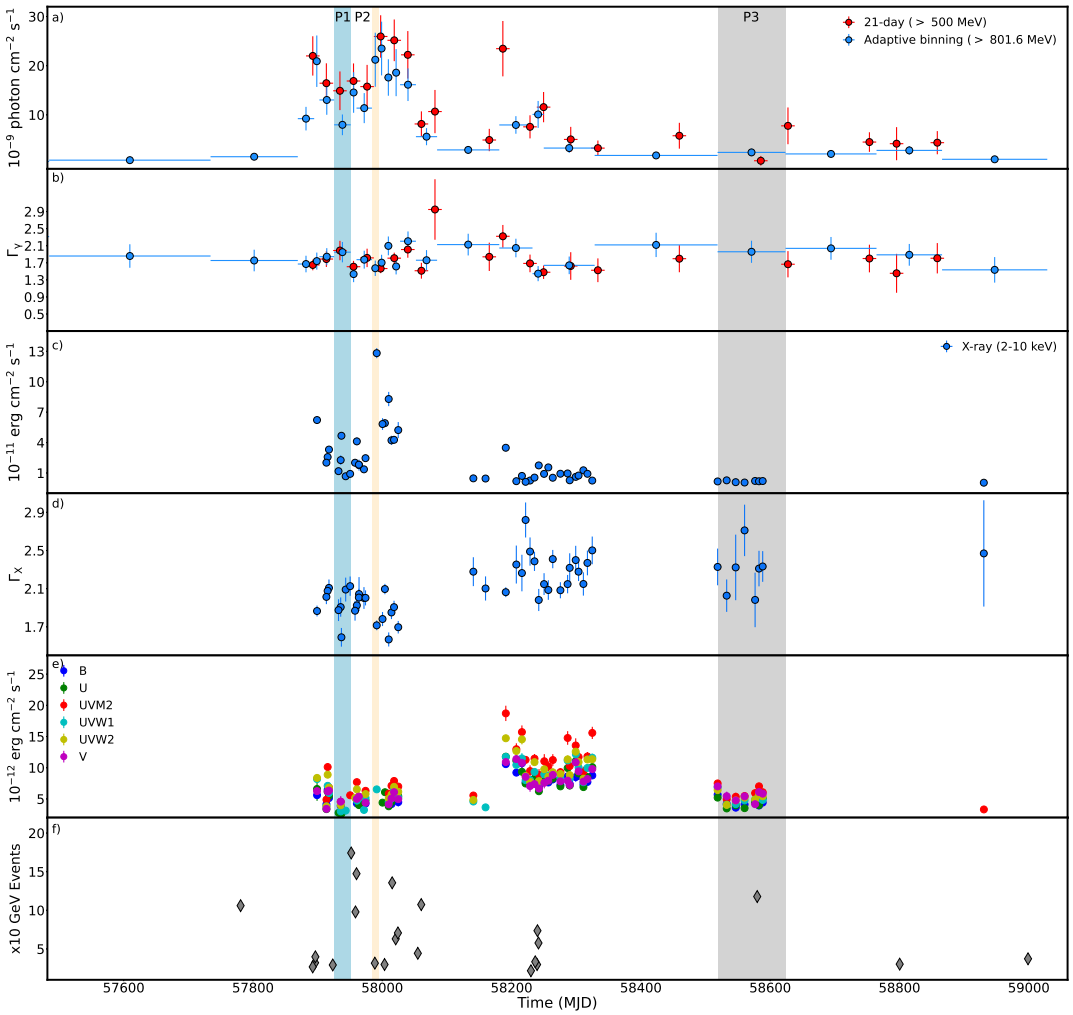

Figure 5.1 Multiwavelength light curves for 4FGL J1544.3-0649. a) and b) the γ-ray flux and photon index computed for 21-day (red; $>$ 500 MeV) and adaptive bins (blue; $>$ 801.6 MeV); c) and d) Swift XRT flux and photon index; e) UV/optical fluxes in V, B, U, W1, M2, and W2 bands; f) the arrival time of HE photons from the direction of 4FGL J1544.3-0649. Shadowed areas indicate the periods P1, P2 and P3 defined in Sect. 5.3.

with it. There are four additional events from the innermost region around 4FGL J1544.3-0649 with an energy exceeding 100 GeV; the 107.4, 106.0, 147.4 and 117.8 GeV events were observed on MJD 58060.2, 57780.9, 57960.1 and 58579.9, respectively.

5.2.2 Swift XRT observations

4FGL J1544.3-0649 was pointed by Swift 51 times, starting shortly after the discovery of the γ-ray and optical transient in May 2017 to mid 2020. All the XRT data were processed using Swift_xrtproc, a data reduction, spectral and imaging analysis tool, that was developed within the Open Universe initiative [1] [64], in collaboration with the ASI Space Science Data Center (SSDC) [2]. It allows to analyse all the XRT observations of a large sample of blazars and the data of all the Gamma Ray Bursts (GRBs) observed by Swift-XRT. Details of the Swift_xrtproc data processing pipeline are given in Giommi et al. (2020, submitted). Here we briefly list the features of the tool that are most relevant to this paper, which include a) the automatic download of raw data and calibration files from one of the official Swift archives; b) the reduction, calibration of XRT data taken in PC or WT readout modes [see 33] using the official XRTDAS software, following a standard procedure; c) spectra and X-ray image generation; d) spectral fitting to a power law and a log-parabola model using XSPEC-V12.11 and Cash statistics, followed by conversion to $\nu f(\nu)$ fluxes and data rebinning to produce 30 SED bins. d) photometric flux estimation in standard energy bands with the XIMAGE-V4.5.1.

The 2-10 keV X-ray flux and best-fit photon index of 4FGL J1544.3-0649 are shown in panels c) and d) of Fig. 5.1, respectively. The source was in a high X-ray state contemporaneously with the γ-ray flare around MJD 58000 with the highest X-ray flux of $(1.28 \pm 0.05) \times 10^{-10}\, erg\, cm^{-2}\, s^{-1}$ observed on MJD 57991.40. Then, the source is in a quiescent state with the flux of the order of $(1.0 - 5.0) \times 10^{-12}\, erg\, cm^{-2}\, s^{-1}$. The X-ray photon index (Γ_X) shows an interesting evolution in time; the X-ray spectrum is hard (< 2.0) during the bright X-ray state around MJD 58000 which then softens during the moderately bright or quiescent states. The hardest X-ray photon index of 1.57 ± 0.07 was observed on MJD 58009.92; there are additional 12 periods with an X-ray photon index of ≤ 1.9. This hardening clearly shifts the peak of synchrotron

[1] https://openuniverse.asi.it
[2] https://www.ssdc.asi.it

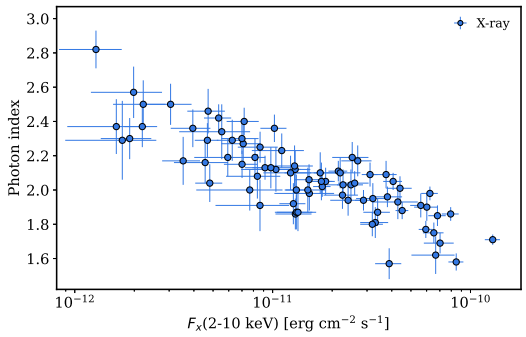

Figure 5.2 The X-ray flux versus photon index.

component to higher energies. The relation between the X-ray flux and the photon index was further investigated by considering XRT observations in each orbit. The X-ray flux (2-10 keV) versus the photon index is shown in Fig. 5.2. The spectrum clearly tends to harden as the source gets brighter. The linear-Pearson correlation test yields $r_d = -0.71$ which suggests a negative correlation between the flux and photon index, i.e., when the photon index decreases (hardens) the flux increases.

5.2.3 Swift UVOT

Along with the XRT observations, the source was also targeted with Swift UVOT in the ultraviolet UVW1, UVM2, and UVW2 and optical V, B and U bands. For each observation, the aperture photometry analysis was performed using the standard UVOT software distributed within the HEASoft package (v6.26.1) and the calibration included in the latest release of CALDB. Source counts were extracted from a circular region with 5″ radius, and the background ones from a source-free region with 20″ radius. Each individual observation was checked to validate that in any filter the background was not contaminated by the nearby objects. The counts were extracted and converted to fluxes using UVOTSOURCE tool and the conversion factors from **(author?)** [111]. The flux values were then de-reddened using the value of E (B - V) = 0.138 [134].
The optical/UV light curve is shown in Fig. 5.1 e). The source appears to be in a quiescent state in the optical/UV bands when it was bright in the

X-ray and γ-ray bands (MJD 58000). However, the optical/UV flux substantially increased around MJD $\sim$ 58250. The highest flux of $(1.87 \pm 0.12) \times 10^{-11}$ *erg* cm^{-2} s^{-1} was observed on MJD 58191.08 in UVM2 filter. In this period the flux increased in other UVOT filters as well, being at the level of $(1.06 - 1.47) \times 10^{-11}$ *erg* cm^{-2} s^{-1}.

5.3 The origin of multiwavelength emission

Multiwavelength observations of 4FGL J1544.3-0649 allow us to build the SEDs with simultaneous and archival data as well as to investigate the time evolution of SEDs. The γ-ray data for each adaptively binned interval has been combined with the Swift optical/UV and X-ray data, with the Effelsberg-100 m observations of 4FGL J1544.3-0649 [in the frequencies from 5 to 15 GHz 32] and with archival data from the VOU-Blazar [39] and the SSDC[3] SED tools, to form the SED/light curve animation that is available here `youtu.be/9feaNWi1RDs`. Moving over each γ-ray light curve interval, the spectrum observed in different bands evolves showing the time evolution of the SED. The months before the large γ-ray flare on MJD 58000 (May 2017) the source is barely detected in the γ-ray band, i.e., the SED on MJD 57274.73 contain upper limits and large uncertainties in the flux estimation. Then the γ-ray emission substantially increases which is sometimes accompanied by increases in the other bands. The γ-ray emission from the source is still detectable with a high significance until MJD 58865.87, but in the last interval (MJD 58947.23 $\pm$ 81.36) the detection significance drops to $TS = 17$. To investigate the nature of the multiwavelength emission from 4FGL J1544.3-0649, data from the following periods are considered:

Period 1 (P1): averaged γ-ray emission state on MJD 57938.35 $\pm$ 12.80 with contemporaneous Swift UVOT/XRT (Obsid: 10145008) and radio data.

Period 2 (P2): from MJD 57984.00 to MJD 57994.33 corresponding to the period when the highest X-ray flux was observed (Obsid: 10145018).

Period 3 (P3): 105.06-days interval centered on MJD 58571.12 when the source was in a low state in the γ-ray, X-ray and optical/UV bands (Obsid: 10145057).

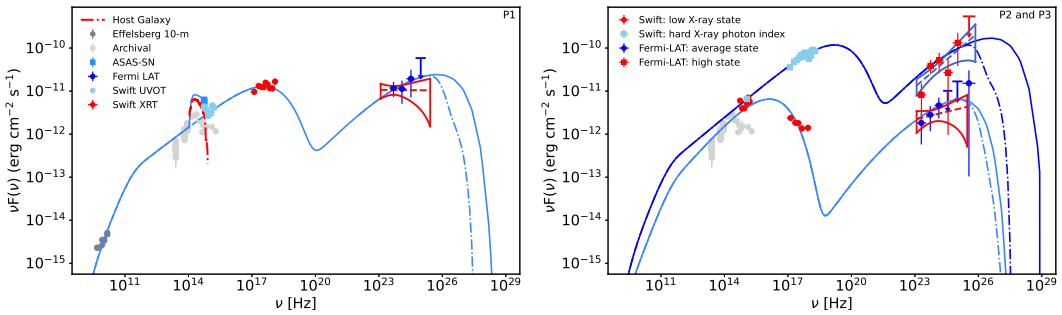

Figure 5.3 Modeling of multiwavelength SEDs of 4FGL J1544.3-0649 during the MJD 57938.35 ± 12.80 (left panel) and MJD 57989.16 ± 5.16 and MJD 58571.12 ± 52.53 (right panel; squares and circles, respectively). The model is presented in the text and the parameters are given in Table 5.1.

Table 5.1 Parameters of modeling of the broadband SED of 4FGL J1544.3-0649 within a simple one zone synchrotron/SSC scenario.

Parameter	P1	P2	P3
δ	25.6	25.6	25.6
α	2.25	2.19	1.90
γ'_{min}	481.1	481.1	481.1
$\gamma'_{cut} \times 10^6$	1.16	6.82	0.11
B [G] 10^{-3}	7.82	8.54	13.71
L_e [$\times 10^{44}$ erg cm^{-3}]	1.60	2.47	0.50
L_B [$\times 10^{40}$ erg cm^{-3}]	5.73	6.83	17.61

The broadband SED of 4FGL J1544.3-0649 shows the usual double humped shape that can be interpreted within a common one-zone synchrotron/SSC model (Fig. 5.3). It is assumed that the broadband emission is produced by relativistic electrons in a spherical blob of radius R with a uniform magnetic field B. The emitting region is seen in the direction close to the line of sight which moves with the bulk Lorentz factor of $\Gamma \approx \delta$. It is assumed that the emitting electrons have commonly used powerlaw with an exponential cut-off energy distribution in the form of $N'_e(\gamma'_e) = N'_0\,\gamma'^{-\alpha}_e\,Exp[-\gamma'_e/\gamma'_{cut}]$ for $\gamma'_e \geq \gamma'_{min}$ where $\gamma'_{min} = E'_e/m_e\,c^2$ is the minimum electron energy. These electrons interacting with the magnetic field radiate via the synchrotron mechanism which explains the low energy component in the SED while the HE hump is described by up-scattering of the synchrotron photons by the same electrons.
The model includes seven free parameters to describe the emitting electrons (α, N'_0, γ'_{min} and γ'_{cut}) and specify the emitting region (δ, B and R). In order to reduce the number of free parameters, we assume the emission is produced in a compact region with $R = 5 \times 10^{16}\,cm$ which corresponds to flux changes on days time scales, as it has been found in the γ-ray band (adaptive bins in Fig. 5.1). In order to constrain δ and γ'_{min} initially the SED on MJD 57938.35 ± 12.8 (P1) with (quasi) simultaneous data ranging from radio to HE γ-ray bands is modeled, resulting in $\delta = 25.6$ and $\gamma'_{min} = 481.1$ which are typical values usually obtained for BL Lacs. These were fixed parameters when modeling the SEDs observed on MJD 57989.16 (P2) and MJD 58571.12 (P3) for which the low energy data are lacking. In order to account for the contribution of the host galaxy (see the excess in the IR/optical part of the SED on MJD 57938.35 ± 12.8), in addition to synchrotron/SSC component also we adopted a template of giant elliptical galaxy. The fitting is performed with the open source package JetSet [91, 143, 142].
The SED modeling results are shown in Fig. 5.3 and the corresponding parameters presented in Table 5.1. In the left panel of Fig. 5.3, the Swift UVOT and ASAS-SN data [downloaded from the ASAS-SN Sky Patrol web site 83][4] allow to estimate or at least constrain the contribution of the host galaxy; the peak of the host galaxy component is at $6.13 \times 10^{-12}\,erg\,cm^{-2}\,s^{-1}$. The dip in the UV data points corresponding to period P1, which appears to be evident also because of the lack of UVM2 data (red points in Fig. 5.1 panel e),

[3] https://tools.ssdc.asi.it/SED
[4] https://asas-sn.osu.edu/

is likely real non-thermal flux decrease, as the possible contribution from the disk/blue bump, as constrained from archival data shown in Fig. 5.3, is significantly lower. When the SED in the quiescent state is considered (P3), the data can be reproduced when $\alpha = 1.96$ and $\gamma'_{cut} = 1.13 \times 10^5$ and the magnetic field is $B = 1.37 \times 10^{-2}\ G$. In this case low energy component peak is at $\sim 2.42 \times 10^{16}\ Hz$ which, however, shifts to higher frequencies when the active states of the source are considered; i.e., during MJD 57938.35 ± 12.8 the X-ray data defines the peak to be at $\sim 10^{17}\ Hz$ whereas during the hardest X-ray state the peak is shifted well beyond $\sim 10^{18}\ Hz$. This shift changes also the maximum energy up to which the particles are effectively accelerated; γ'_{cut} increases to 1.16×10^6 and 6.82×10^6 when the SEDs on P1 and P2 are considered, respectively. The modeling resulted in a similar power-law index and magnetic field for these active X-ray periods, namely $\alpha = 2.25$ and $7.82 \times 10^{-3}\ G$ for P1 and $\alpha = 2.19$ and $8.54 \times 10^{-3}\ G$ for P2. In all the considered periods the jet is particle dominated with $U_e/U_B > 3000$ for P1 and P2 and $U_e/U_B \simeq 350$ for P3. However, U_e strongly depends on γ'_{min} which is not well constrained, and when allowing γ'_{min} to vary U_e/U_B ratio can change. The jet power in the form of magnetic field and electron kinetic energy are calculated by $L_B = \pi c R^2 \Gamma^2 U_B$ and $L_e = \pi c R^2 \Gamma^2 U_e$, respectively, and are given in Table 5.1.

5.4 Discussion and Conclusion

We have presented the results of the analysis of optical/UV, X-ray and γ-ray observations of 4FGL J1544.3-0649, a remarkable blazar showing transient-like high-energy multiwavelength emission. This object, in fact, remained below the sensitivity limits of all the high-energy surveys until May 2017, when it suddenly rose above the background to become one of the brightest HBL blazars in the sky, a source so intense to be detectable in short exposures by Fermi-LAT and by the MAXI X-ray sky monitor [95]. The transient behaviour of this so far unique object has never been observed before in AGNs. If this dual behaviour is common to other so far undiscovered objects it might have important implications in blazar research, especially in high-energy and multi-messenger astrophysics, depending on how numerous transient blazars are and how frequently they enter a bright phase.

During the brightening, the 2-10 keV X-ray flux strongly varies increasing

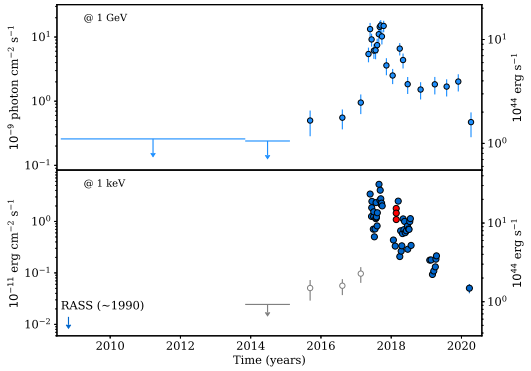

Figure 5.4 The γ-ray (@ 1 GeV) and the reconstructed X-ray (@ 1 keV) light curve of 4FGL J1544.3-0649 (see text for details).

from $(1.0 - 5.0) \times 10^{-12}\, erg\, cm^{-2}\, s^{-1}$ to $(1.28 \pm 0.05) \times 10^{-10}\, erg\, cm^{-2}\, s^{-1}$. This variability, which is even larger when the flux is estimated in each Swift orbit, is clearly associated to a harder-when-brighter behavior, as also noted by [146] based on XMM observations. Such flux and photon index correlation is well known in HBL blazars [e.g. 65], and is usually interpreted by the relation between the acceleration and cooling processes. As shown in **(author?)** [82], when the injection decreases and particles are loosing energy by synchrotron cooling or any other cooling process that is faster at higher energies, the spectrum becomes steeper.
During the γ-ray brightening of the source, the X-ray spectrum modifies as well. The available optical/UV and X-ray data defines the peak of the low energy component to be within $\nu_{peak-s} = 10^{15} - 10^{17}$ Hz, implying 4FGL J1544.3-0649 is a classical HBL. However, occasionally (e.g., on MJD 57898.70, 57989.16, 57998.92, 58009.40 and 58021.40, see the SED/Light curve animation) the source shows a synchrotron component peak above 10^{18} Hz which is more typical for extreme synchrotron BL Lacs. Yet, in all these periods the γ-ray photon index hardens as well, e.g., 1.74 ± 0.20 on MJD 57898.70, 1.57 ± 0.18 on MJD 57989.16 or 1.61 ± 0.19 on MJD 58021.40, shifting the HE peak to VHEs. The peaks in the SED are determined by $\gamma'_{cut} \simeq \sqrt{\frac{\nu_{c,\,peak}}{\nu_{s,\,peak}}}$ implying in P1 and P2 when $\nu_{peak} \geq 10^{18}$ Hz the second peak is around $2 \times 10^{26} - 2 \times 10^{27}$ Hz $(1 - 10$ TeV) (solid line in Fig. 5.3). However, this peak and the flux is suppressed by Klein Nishina effects and EBL absorption, which for the distance of 4FGL J1544.3-0649 starts at $\sim 5 \times 10^{25}$ Hz

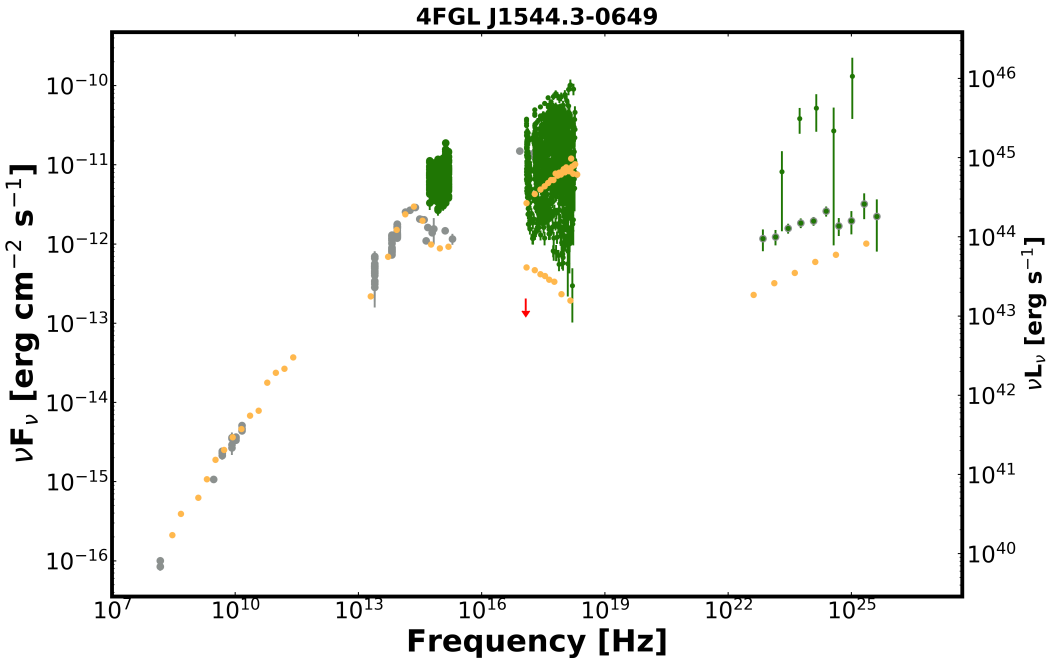

Figure 5.5 The SED of 4FGL J1544.3-0649. Green points are from Swift UVOT, Swift XRT and Fermi-LAT; grey points are archival multi-frequency data retrieved with VOU-Blazars. For comparison the average SED of Mrk 501, scaled to flux level of 4FGL J1544.3-0649, in the radio/infrared bands, is plotted as orange points. In the X-ray band instead of the average spectrum we plot the the spectra observed in Mrk 501 when it was at maximum and minimum intensity. The red arrow is an upper limit resulting from the non-detection of 4FGL J1544.3-0649 during the RASS survey in 1990.

($\sim$ 200 GeV; dot dashed line in Fig. 5.3). Despite this reduction, during the bright γ-ray and X-ray states the source flux at 1 TeV is expected to be $\simeq 10^{-11}\, erg\, cm^{-2}\, s^{-1}$, well above the sensitivity of the current ground-based Cherenkov telescopes. In addition, the hard γ-ray photon index observed in the MeV/GeV band and the applied SSC model predict also a very hard photon index in TeV band after EBL correction. So, 4FGL J1544.3-0649 mimics properties similar to those of extreme BL Lacs in γ-rays [28, 141], which are an interesting sub-class not only because of their possible association with VHE neutrinos and cosmic rays [106, 118] but also because they pose major difficulties for the understanding of particle acceleration and emission processes in blazar jets.

The multiwavelength light curve of Fig. 5.1, shows that the optical/UV flux increase is delayed compared to that in the X-ray and γ-ray bands. In general, lags in different energy bands are expected either from changes in the global parameters (magnetic field, Lorentz factor, etc.) or from the temporal evolution of emitting particles. For example, **(author?)** [21] proposed that if the low energy component is produced when the blob is closer to the base of the jet and the HE photons are emitted at larger distances from the jet base, at which the blob has accelerated to a higher Lorentz factor, this could result in delays between the low energy and HE flares. Or, in complex jet geometry if the flare is caused by the collision between a relativistic shock wave and a stationary feature in the jet, it results in a complex variation of fluxes in different bands [139]. However, a simple consideration of particle acceleration and cooling can naturally explain the observed delay in the multiwavelength light curve of 4FGL J1544.3-0649. The SED in different epochs is well reproduced by a one-zone synchrotron/SSC model with physically reasonable parameters. Within this model, the flare and modification of the spectra can be interpreted by an increase in the luminosity of electrons and γ'_{cut}; during the bright X-ray period the luminosity increased $\sim$ 4.9 times whereas $\gamma'_{cut} \sim$ 62 times. This implies that the X-ray and γ-ray flare was most likely caused by injection of new freshly accelerated electrons. The cooling time of these electrons is

$$t_{cooling} = \frac{3}{4}\,\frac{m_e\, c}{\sigma_T (u_B + u_{syn})\,\gamma} = \frac{6\,\pi\, m_e\, c}{\sigma_T\,\gamma\, B^2\,(1 + u_{syn}/u_B)}. \tag{5.4.1}$$

where u_{syn} is the synchrotron photon energy density in the jet frame. Considering the peak frequency of synchrotron emission is $\nu = 1.2 \times 10^6\, B\, \delta\, \gamma^2$, the cooling time of the electron emitting photons with frequency $\nu_{15} = \nu/10^{15}\, Hz$

is $t_{cooling} = 2.7 \times 10^4 \, (\delta/1+z)^{0.5} \, B^{-1.5} \, \nu_{15}^{-0.5}$ s. Considering the parameters obtained for the P1, the delay between X-ray emission (10^{18} Hz) and optical/UV (5×10^{14} Hz) is of the order of $\sim$ 114 days which is very similar to that observed. However, in order to investigate in details the time lags and thus to infer the underlying physics, much denser monitoring of 4FGL J1544.3-0649 in optical/UV band is needed.
Figure 5.4 plots the high-energy light-curves of 4FGL J1544.3-0649 spanning the entire operational period of the Fermi mission. The upper panel, reporting the γ-ray data, illustrate the transient nature of this source, which was not detected by the LAT instrument until late 2015, peaked in 2017-2018 and then faded. The lower panel reconstructs the long-term light-curve of 4FGL J1544.3-0649 in the X-ray band, combining the Swift-XRT measurements (blue points), with the XMM data from [146] (red points) and the expected X-ray flux level estimated from the flux in the γ-ray band, based on the average x-ray/γ-ray flux ratio (open grey circles). An upper limit derived from the non-detection of the source in the RASS X-ray sky survey, which was carried out in 1990-1991 [150], is also shown in the leftmost part of the plot. The reconstructed X-ray light-curve implies a rise time of approximately two years, and a decay of approximately three years.

The SED of 4FGL J1544.3-0649 (Fig. 5.5) assembled with Swift-XRT, Swift-UVOT, Fermi-LAT (green points) and archival data (grey points), shows a highly variable X-ray spectrum, changing its intensity by large factors and often peaking in the X-ray band. For comparison the average SED of the well known HBL blazar Mrk501, rescaled to match the radio emission of 4FGL J1544.3-0649, together with its X-ray spectra observed during its minimum and maximum intensity state, is plotted as light orange points in the same figure. The nearly identical shape of the radio to optical SEDs and the range of observed X-ray fluxes, confirms that 4FGL J1544.3-0649 during the active phase is a typical HBL blazar, with X-ray and γ-ray emission that are even stronger than that of Mrk 501. The upper limit from the RASS all sky survey (red arrow) sets the magnitude of the intensity variations in the soft X-ray band, which ranged from below $\approx 10^{-13} \, erg \, cm^{-2} \, s^{-1}$ in 1990 to such a high value to place 4FGL J1544.3-0649 amongst the 20 brightest X-ray blazars.

The existence of transient (HBL) blazars was never considered in the literature before the discovery of 4FGL J1544.3-0649 and, consequently, never taken into account in population studies. We don't know if 4FGL J1544.3-0649 represents the tip of the iceberg, or it is simply an isolated event. Most

likely the discovery of 4FGL J1544.3-0649 is a rare favorable selection effect, as similar transient events would probably remain unnoticed in sources where the γ-ray flux during flares is only a factor of a few lower than that of 4FGL J1544.3-0649, or their γ-ray spectrum is softer, or even in cases where the γ-ray intensity remains low during strong X-ray flares associated to neutrino emission as in scenarios similar to that presented by [94]. It is therefore probable that similar events in other blazars are present in the existing data or will emerge from future more sensitive observations. The identification of similar objects would add crucial information to our knowledge of the population of extragalactic sources, especially in the high-energy domain. Areas of research that might be affected would be e.g. the determination of the LogN-LogS, luminosity function and cosmological evolution of HBL blazars, the identification of still unassociated γ-ray and VHE sources, and the contribution of discrete sources to the γ-ray and possibly high-energy neutrino cosmic backgrounds. A transient nature of some electromagnetic counterparts of astrophysical neutrinos would on one side increase the level of difficulty in the process of the association, but on the other it would strengthen the association in case X-ray or γ-ray flares are detected in association with the neutrino arrival. A recent study [67] reported a 3.23 σ post trial excess of HBL Blazars in the error regions of a sample of 70 Ice Cube astrophysical neutrinos with good positional accuracy. If HBL blazars are indeed counterparts of high-energy neutrinos, some of them could be transient sources somewhat fainter than 4FGL J1544.3-0649 that would difficult to locate since they are not listed in catalogues and no full coverage of the still large Ice Cube neutrino positional uncertainty can be achieved with current X-ray imaging instruments. A full census of these so far elusive objects would be possible only when sensitive all-sky X-ray (or γ-ray) monitor detectors become available. Meanwhile a careful search for weak transients in the Fermi-LAT data on the positions of flat-spectrum radio sources with radio to infrared flux ratio similar to that of HBL objects could lead to the discovery of additional transient blazars and set limits to their duty cycle and space density.

Bibliography

[1] A. A. Abdo, M. Ackermann, I. Agudo, M. Ajello, A. Allafort, H. D. Aller, M. F. Aller, E. Antolini, A. A. Arkharov, M. Axelsson, U. Bach, L. Baldini, J. Ballet, G. Barbiellini, D. Bastieri, K. Bechtol, R. Bellazzini, A. Berdyugin, B. Berenji, R. D. Blandford, D. A. Blinov, E. D. Bloom, M. Boettcher, E. Bonamente, A. W. Borgland, A. Bouvier, J. Bregeon, A. Brez, M. Brigida, P. Bruel, R. Buehler, C. S. Buemi, T. H. Burnett, S. Buson, G. A. Caliandro, R. A. Cameron, P. A. Caraveo, D. Carosati, S. Carrigan, J. M. Casandjian, E. Cavazzuti, C. Cecchi, Ö. Çelik, A. Chekhtman, W. P. Chen, C. C. Cheung, J. Chiang, S. Ciprini, R. Claus, J. Cohen-Tanugi, J. Conrad, S. Corbel, L. Costamante, C. D. Dermer, A. de Angelis, F. de Palma, D. Donato, E. do Couto e. Silva, P. S. Drell, R. Dubois, D. Dumora, C. Farnier, C. Favuzzi, S. J. Fegan, E. C. Ferrara, W. B. Focke, E. Forné, P. Fortin, Y. Fukazawa, S. Funk, P. Fusco, F. Gargano, D. Gasparrini, N. Gehrels, S. Germani, B. Giebels, N. Giglietto, F. Giordano, M. Giroletti, T. Glanzman, G. Godfrey, I. A. Grenier, J. E. Grove, S. Guiriec, M. A. Gurwell, C. Gusbar, J. L. Gómez, D. Hadasch, V. A. Hagen-Thorn, M. Hayashida, E. Hays, D. Horan, R. E. Hughes, G. Jóhannesson, A. S. Johnson, W. N. Johnson, T. Kamae, H. Katagiri, J. Kataoka, N. Kawai, G. Kimeridze, J. Knödlseder, T. S. Konstantinova, E. N. Kopatskaya, E. Koptelova, Y. Y. Kovalev, O. M. Kurtanidze, M. Kuss, A. Lahteenmaki, J. Lande, V. M. Larionov, E. G. Larionova, L. V. Larionova, S. Larsson, L. Latronico, S. H. Lee, P. Leto, M. L. Lister, F. Longo, F. Loparco, B. Lott, M. N. Lovellette, P. Lubrano, G. M. Madejski, A. Makeev, E. Massaro, M. N. Mazziotta, W. McConville, J. E. McEnery, I. M. McHardy, P. F. Michelson, W. Mitthumsiri, T. Mizuno, A. A. Moiseev, C. Monte, M. E. Monzani, D. A. Morozova, A. Morselli, I. V. Moskalenko, S. Murgia, M. Naumann-Godo, M. G. Nikolashvili, P. L. Nolan, J. P. Norris, E. Nuss, M. Ohno, T. Ohsugi, A. Okumura, N. Omodei, E. Orlando, J. F. Ormes, M. Ozaki, D. Paneque, J. H. Panetta, D. Par-

ent, M. Pasanen, V. Pelassa, M. Pepe, M. Pesce-Rollins, F. Piron, T. A. Porter, A. B. Pushkarev, S. Rainò, C. M. Raiteri, R. Rando, M. Razzano, A. Reimer, O. Reimer, R. Reinthal, J. Ripken, S. Ritz, M. Roca-Sogorb, A. Y. Rodriguez, M. Roth, P. Roustazadeh, F. Ryde, H. F. W. Sadrozinski, A. Sander, J. D. Scargle, C. Sgrò, L. A. Sigua, P. D. Smith, K. Sokolovsky, G. Spandre, P. Spinelli, J. L. Starck, M. S. Strickman, D. J. Suson, H. Takahashi, T. Takahashi, L. O. Takalo, T. Tanaka, B. Taylor, J. B. Thayer, J. G. Thayer, D. J. Thompson, L. Tibaldo, M. Tornikoski, D. F. Torres, G. Tosti, A. Tramacere, C. Trigilio, I. S. Troitsky, G. Umana, T. L. Usher, J. Vandenbroucke, V. Vasileiou, N. Vilchez, M. Villata, V. Vitale, A. P. Waite, P. Wang, B. L. Winer, K. S. Wood, Z. Yang, T. Ylinen, and M. Ziegler.

Fermi Large Area Telescope and Multi-wavelength Observations of the Flaring Activity of PKS 1510-089 between 2008 September and 2009 June.

ApJ, 721(2):1425–1447, October 2010.

[2] A. A. Abdo, M. Ackermann, I. Agudo, M. Ajello, H. D. Aller, M. F. Aller, E. Angelakis, A. A. Arkharov, M. Axelsson, U. Bach, L. Baldini, J. Ballet, G. Barbiellini, D. Bastieri, B. M. Baughman, K. Bechtol, R. Bellazzini, E. Benitez, A. Berdyugin, B. Berenji, R. D. Bland ford, E. D. Bloom, M. Boettcher, E. Bonamente, A. W. Borgland, J. Bregeon, A. Brez, M. Brigida, P. Bruel, T. H. Burnett, D. Burrows, S. Buson, G. A. Caliandro, L. Calzoletti, R. A. Cameron, M. Capalbi, P. A. Caraveo, D. Carosati, J. M. Casand jian, E. Cavazzuti, C. Cecchi, Ö. Çelik, E. Charles, S. Chaty, A. Chekhtman, W. P. Chen, J. Chiang, G. Chincarini, S. Ciprini, R. Claus, J. Cohen-Tanugi, S. Colafrancesco, L. R. Cominsky, J. Conrad, L. Costamante, S. Cutini, F. D'ammando, R. Deitrick, V. D'Elia, C. D. Dermer, A. de Angelis, F. de Palma, S. W. Digel, I. Donnarumma, E. do Couto e. Silva, P. S. Drell, R. Dubois, D. Dultzin, D. Dumora, A. Falcone, C. Farnier, C. Favuzzi, S. J. Fegan, W. B. Focke, E. Forné, P. Fortin, M. Frailis, L. Fuhrmann, Y. Fukazawa, S. Funk, P. Fusco, J. L. Gómez, F. Gargano, D. Gasparrini, N. Gehrels, S. Germani, B. Giebels, N. Giglietto, P. Giommi, F. Giordano, A. Giuliani, T. Glanzman, G. Godfrey, I. A. Grenier, C. Gronwall, J. E. Grove, L. Guillemot, S. Guiriec, M. A. Gurwell, D. Hadasch, Y. Hanabata, A. K. Harding, M. Hayashida, E. Hays, S. E. Healey, J. Heidt,

D. Hiriart, D. Horan, E. A. Hoversten, R. E. Hughes, R. Itoh, M. S. Jackson, G. Jóhannesson, A. S. Johnson, W. N. Johnson, S. G. Jorstad, M. Kadler, T. Kamae, H. Katagiri, J. Kataoka, N. Kawai, J. Kennea, M. Kerr, G. Kimeridze, J. Knödlseder, M. L. Kocian, E. N. Kopatskaya, E. Koptelova, T. S. Konstantinova, Y. Y. Kovalev, Yu. A. Kovalev, O. M. Kurtanidze, M. Kuss, J. Lande, V. M. Larionov, L. Latronico, P. Leto, E. Lindfors, F. Longo, F. Loparco, B. Lott, M. N. Lovellette, P. Lubrano, G. M. Madejski, A. Makeev, P. Marchegiani, A. P. Marscher, F. Marshall, W. Max-Moerbeck, M. N. Mazziotta, W. McConville, J. E. McEnery, C. Meurer, P. F. Michelson, W. Mitthumsiri, T. Mizuno, A. A. Moiseev, C. Monte, M. E. Monzani, A. Morselli, I. V. Moskalenko, S. Murgia, I. Nestoras, K. Nilsson, N. A. Nizhelsky, P. L. Nolan, J. P. Norris, E. Nuss, T. Ohsugi, R. Ojha, N. Omodei, E. Orlando, J. F. Ormes, J. Osborne, M. Ozaki, L. Pacciani, P. Padovani, C. Pagani, K. Page, D. Paneque, J. H. Panetta, D. Parent, M. Pasanen, V. Pavlidou, V. Pelassa, M. Pepe, M. Perri, M. Pesce-Rollins, S. Piranomonte, F. Piron, C. Pittori, T. A. Porter, S. Puccetti, F. Rahoui, S. Rainò, C. Raiteri, R. Rando, M. Razzano, A. Reimer, O. Reimer, T. Reposeur, J. L. Richards, S. Ritz, L. S. Rochester, A. Y. Rodriguez, R. W. Romani, J. A. Ros, M. Roth, P. Roustazadeh, F. Ryde, H. F. W. Sadrozinski, A. Sadun, D. Sanchez, A. Sander, P. M. Saz Parkinson, J. D. Scargle, A. Sellerholm, C. Sgrò, M. S. Shaw, L. A. Sigua, E. J. Siskind, D. A. Smith, P. D. Smith, G. Spandre, P. Spinelli, J. L. Starck, M. Stevenson, G. Stratta, M. S. Strickman, D. J. Suson, H. Tajima, H. Takahashi, T. Takahashi, L. O. Takalo, T. Tanaka, J. B. Thayer, J. G. Thayer, D. J. Thompson, L. Tibaldo, D. F. Torres, G. Tosti, A. Tramacere, Y. Uchiyama, T. L. Usher, V. Vasileiou, F. Verrecchia, N. Vilchez, M. Villata, V. Vitale, A. P. Waite, P. Wang, B. L. Winer, K. S. Wood, T. Ylinen, J. A. Zensus, G. V. Zhekanis, and M. Ziegler.
The Spectral Energy Distribution of Fermi Bright Blazars.
ApJ, 716(1):30–70, June 2010.

[3] A. A. Abdo, M. Ackermann, M. Ajello, A. Allafort, L. Baldini, J. Ballet, G. Barbiellini, D. Bastieri, R. Bellazzini, B. Berenji, R. D. Bland ford, E. D. Bloom, E. Bonamente, A. W. Borgland , A. Bouvier, J. Bregeon, M. Brigida, P. Bruel, R. Buehler, S. Buson, G. A. Caliandro, R. A. Cameron, P. A. Caraveo, J. M. Casandjian, E. Cavaz-

zuti, C. Cecchi, E. Charles, A. Chekhtman, C. C. Cheung, J. Chiang, S. Ciprini, R. Claus, J. Conrad, S. Cutini, F. D'Ammando, A. de Angelis, F. de Palma, C. D. Dermer, S. W. Digel, E. do Couto e. Silva, P. S. Drell, R. Dubois, D. Dumora, L. Escande, C. Favuzzi, S. J. Fegan, E. C. Ferrara, P. Fortin, Y. Fukazawa, P. Fusco, F. Gargano, D. Gasparrini, N. Gehrels, S. Germani, N. Giglietto, P. Giommi, F. Giordano, M. Giroletti, T. Glanzman, G. Godfrey, I. A. Grenier, J. E. Grove, S. Guiriec, D. Hadasch, M. Hayashida, E. Hays, D. Horan, R. Itoh, G. Jóhannesson, A. S. Johnson, T. Kamae, H. Katagiri, J. Kataoka, J. Knödlseder, M. Kuss, J. Lande, S. Larsson, L. Latronico, S. H. Lee, F. Longo, F. Loparco, B. Lott, M. N. Lovellette, P. Lubrano, G. M. Madejski, A. Makeev, M. N. Mazziotta, W. McConville, J. E. McEnery, P. F. Michelson, W. Mitthumsiri, T. Mizuno, A. A. Moiseev, C. Monte, M. E. Monzani, A. Morselli, I. V. Moskalenko, S. Murgia, M. Naumann-Godo, S. Nishino, P. L. Nolan, J. P. Norris, E. Nuss, T. Ohsugi, A. Okumura, E. Orlando, J. F. Ormes, D. Paneque, V. Pelassa, M. Pesce-Rollins, M. Pierbattista, F. Piron, T. A. Porter, S. Rainò, R. Rando, S. Razzaque, A. Reimer, O. Reimer, S. Ritz, M. Roth, H. F. W. Sadrozinski, D. Sanchez, J. D. Scargle, T. L. Schalk, C. Sgrò, E. J. Siskind, P. D. Smith, G. Spandre, P. Spinelli, M. S. Strickman, H. Takahashi, T. Takahashi, T. Tanaka, Y. Tanaka, J. G. Thayer, J. B. Thayer, D. J. Thompson, L. Tibaldo, D. F. Torres, G. Tosti, A. Tramacere, E. Troja, J. Vand enbroucke, V. Vasileiou, G. Vianello, N. Vilchez, V. Vitale, A. P. Waite, P. Wang, B. L. Winer, K. S. Wood, Z. Yang, and M. Ziegler.

Fermi Gamma-ray Space Telescope Observations of the Gamma-ray Outburst from 3C454.3 in November 2010.

ApJL, 733(2):L26, June 2011.

[4] A. A. Abdo, M. Ackermann, M. Ajello, W. B. Atwood, M. Axelsson, L. Baldini, J. Ballet, G. Barbiellini, D. Bastieri, M. Battelino, B. M. Baughman, K. Bechtol, R. Bellazzini, B. Berenji, R. D. Blandford, E. D. Bloom, E. Bonamente, A. W. Borgland, A. Bouvier, J. Bregeon, A. Brez, M. Brigida, P. Bruel, T. H. Burnett, G. A. Caliandro, R. A. Cameron, P. A. Caraveo, J. M. Casandjian, E. Cavazzuti, C. Cecchi, E. Charles, S. Chaty, A. Chekhtman, C. C. Cheung, J. Chiang, S. Ciprini, R. Claus, J. Cohen-Tanugi, L. R. Cominsky, J. Conrad, L. Costamante, S. Cutini, C. D. Dermer, A. de Angelis, F. de Palma,

S. W. Digel, E. do Couto e. Silva, D. Donato, P. S. Drell, R. Dubois, D. Dumora, C. Farnier, C. Favuzzi, W. B. Focke, L. Foschini, M. Frailis, L. Fuhrmann, Y. Fukazawa, S. Funk, P. Fusco, F. Gargano, D. Gasparrini, N. Gehrels, S. Germani, B. Giebels, N. Giglietto, P. Giommi, F. Giordano, T. Glanzman, G. Godfrey, I. A. Grenier, M. H. Grondin, J. E. Grove, L. Guillemot, S. Guiriec, Y. Hanabata, A. K. Harding, R. C. Hartman, M. Hayashida, E. Hays, R. E. Hughes, G. Jóhannesson, A. S. Johnson, R. P. Johnson, W. N. Johnson, T. Kamae, H. Katagiri, J. Kataoka, N. Kawai, M. Kerr, J. Knödlseder, M. L. Kocian, F. Kuehn, M. Kuss, L. Latronico, S. H. Lee, M. Lemoine-Goumard, F. Longo, F. Loparco, B. Lott, M. N. Lovellette, P. Lubrano, G. M. Madejski, A. Makeev, E. Massaro, M. N. Mazziotta, J. E. McEnery, S. McGlynn, C. Meurer, P. F. Michelson, W. Mitthumsiri, T. Mizuno, A. A. Moiseev, C. Monte, M. E. Monzani, A. Morselli, I. V. Moskalenko, S. Murgia, P. L. Nolan, J. P. Norris, E. Nuss, T. Ohsugi, N. Omodei, E. Orlando, J. F. Ormes, D. Paneque, J. H. Panetta, D. Parent, V. Pelassa, M. Pepe, M. Pesce-Rollins, F. Piron, T. A. Porter, S. Rainò, R. Rando, M. Razzano, A. Reimer, O. Reimer, T. Reposeur, L. C. Reyes, S. Ritz, L. S. Rochester, A. Y. Rodriguez, F. Rahoui, F. Ryde, H. F. W. Sadrozinski, R. Sambruna, D. Sanchez, A. Sander, P. M. Saz Parkinson, C. Sgrò, M. S. Shaw, D. A. Smith, P. D. Smith, G. Spandre, P. Spinelli, J. L. Starck, M. S. Strickman, D. J. Suson, H. Tajima, H. Takahashi, T. Takahashi, T. Tanaka, J. B. Thayer, J. G. Thayer, D. J. Thompson, L. Tibaldo, D. F. Torres, G. Tosti, A. Tramacere, Y. Uchiyama, T. L. Usher, N. Vilchez, M. Villata, V. Vitale, A. P. Waite, B. L. Winer, K. S. Wood, T. Ylinen, J. A. Zensus, and M. Ziegler.

Early Fermi Gamma-ray Space Telescope Observations of the Quasar 3C 454.3.

ApJ, 699(1):817–823, July 2009.

[5] A. A. Abdo, M. Ackermann, M. Ajello, W. B. Atwood, M. Axelsson, L. Baldini, J. Ballet, G. Barbiellini, D. Bastieri, B. M. Baughman, K. Bechtol, R. Bellazzini, B. Berenji, E. D. Bloom, G. Bogaert, E. Bonamente, A. W. Borgland, J. Bregeon, A. Brez, M. Brigida, P. Bruel, T. H. Burnett, G. A. Caliandro, R. A. Cameron, P. A. Caraveo, J. M. Casandjian, E. Cavazzuti, C. Cecchi, Ö. Çelik, A. Chekhtman, C. C. Cheung, J. Chiang, S. Ciprini, R. Claus, J. Cohen-Tanugi, J. Conrad,

S. Cutini, C. D. Dermer, A. de Angelis, F. de Palma, S. W. Digel, E. do Couto e. Silva, P. S. Drell, R. Dubois, D. Dumora, C. Farnier, C. Favuzzi, S. J. Fegan, E. C. Ferrara, W. B. Focke, M. Frailis, L. Fuhrmann, Y. Fukazawa, S. Funk, P. Fusco, F. Gargano, D. Gasparrini, N. Gehrels, S. Germani, B. Giebels, N. Giglietto, F. Giordano, M. Giroletti, T. Glanzman, G. Godfrey, I. A. Grenier, M. H. Grondin, J. E. Grove, L. Guillemot, S. Guiriec, Y. Hanabata, A. K. Harding, M. Hayashida, E. Hays, R. E. Hughes, G. Jóhannesson, A. S. Johnson, R. P. Johnson, W. N. Johnson, M. Kadler, T. Kamae, H. Katagiri, J. Kataoka, M. Kerr, J. Knödlseder, M. L. Kocian, F. Kuehn, M. Kuss, J. Lande, L. Latronico, M. Lemoine-Goumard, F. Longo, F. Loparco, B. Lott, M. N. Lovellette, P. Lubrano, G. M. Madejski, A. Makeev, M. Marelli, E. Massaro, W. Max-Moerbeck, M. N. Mazziotta, W. McConville, J. E. McEnery, C. Meurer, P. F. Michelson, W. Mitthumsiri, T. Mizuno, A. A. Moiseev, C. Monte, M. E. Monzani, A. Morselli, I. V. Moskalenko, S. Murgia, P. L. Nolan, J. P. Norris, E. Nuss, T. Ohsugi, N. Omodei, E. Orlando, J. F. Ormes, M. Ozaki, D. Paneque, J. H. Panetta, D. Parent, V. Pavlidou, T. J. Pearson, V. Pelassa, M. Pepe, M. Pesce-Rollins, F. Piron, T. A. Porter, S. Rainò, R. Rando, M. Razzano, S. Razzaque, A. Readhead, A. Reimer, O. Reimer, T. Reposeur, J. L. Richards, S. Ritz, L. S. Rochester, A. Y. Rodriguez, R. W. Romani, M. Roth, F. Ryde, H. F. W. Sadrozinski, D. Sanchez, A. Sander, P. M. Saz Parkinson, J. D. Scargle, C. Sgrò, M. S. Shaw, E. J. Siskind, D. A. Smith, P. D. Smith, G. Spandre, P. Spinelli, M. Stevenson, M. S. Strickman, D. J. Suson, H. Tajima, H. Takahashi, T. Tanaka, J. B. Thayer, J. G. Thayer, D. J. Thompson, L. Tibaldo, O. Tibolla, D. F. Torres, G. Tosti, A. Tramacere, P. Ubertini, Y. Uchiyama, T. L. Usher, V. Vasileiou, N. Vilchez, V. Vitale, A. P. Waite, P. Wang, B. L. Winer, K. S. Wood, H. Yasuda, T. Ylinen, J. A. Zensus, M. Ziegler, Fermi LAT Collaboration, E. Angelakis, T. Hovatta, E. Hoversten, Y. Ikejiri, K. S. Kawabata, Y. Y. Kovalev, Yu. A. Kovalev, T. P. Krichbaum, M. L. Lister, A. Lähteenmäki, N. Marchili, P. Ogle, C. Pagani, A. B. Pushkarev, K. Sakimoto, M. Sasada, M. Tornikoski, M. Uemura, M. Yamanaka, T. Yamashita, Fermi LAT Collaboration, and Multifrequency Campaign Collaboration.

PKS 1502+106: A New and Distant Gamma-ray Blazar in Outburst Discovered by the Fermi Large Area Telescope.

ApJ, 710(1):810–827, February 2010.

[6] S. Abdollahi, F. Acero, M. Ackermann, M. Ajello, W. B. Atwood, M. Axelsson, L. Baldini, J. Ballet, G. Barbiellini, D. Bastieri, J. Becerra Gonzalez, R. Bellazzini, A. Berretta, E. Bissaldi, R. D. Bland ford, E. D. Bloom, R. Bonino, E. Bottacini, T. J. Brandt, J. Bregeon, P. Bruel, R. Buehler, T. H. Burnett, S. Buson, R. A. Cameron, R. Caputo, P. A. Caraveo, J. M. Casandjian, D. Castro, E. Cavazzuti, E. Charles, S. Chaty, S. Chen, C. C. Cheung, G. Chiaro, S. Ciprini, J. Cohen-Tanugi, L. R. Cominsky, J. Coronado-Blázquez, D. Costantin, A. Cuoco, S. Cutini, F. D'Ammando, M. DeKlotz, P. de la Torre Luque, F. de Palma, A. Desai, S. W. Digel, N. Di Lalla, M. Di Mauro, L. Di Venere, A. Domínguez, D. Dumora, F. Fana Dirirsa, S. J. Fegan, E. C. Ferrara, A. Franckowiak, Y. Fukazawa, S. Funk, P. Fusco, F. Gargano, D. Gasparrini, N. Giglietto, P. Giommi, F. Giordano, M. Giroletti, T. Glanzman, D. Green, I. A. Grenier, S. Griffin, M. H. Grondin, J. E. Grove, S. Guiriec, A. K. Harding, K. Hayashi, E. Hays, J. W. Hewitt, D. Horan, G. Jóhannesson, T. J. Johnson, T. Kamae, M. Kerr, D. Kocevski, M. Kovac'evic', M. Kuss, D. Landriu, S. Larsson, L. Latronico, M. Lemoine-Goumard, J. Li, I. Liodakis, F. Longo, F. Loparco, B. Lott, M. N. Lovellette, P. Lubrano, G. M. Madejski, S. Maldera, D. Malyshev, A. Manfreda, E. J. Marchesini, L. Marcotulli, G. Martí-Devesa, P. Martin, F. Massaro, M. N. Mazziotta, J. E. McEnery, I. Mereu, M. Meyer, P. F. Michelson, N. Mirabal, T. Mizuno, M. E. Monzani, A. Morselli, I. V. Moskalenko, M. Negro, E. Nuss, R. Ojha, N. Omodei, M. Orienti, E. Orlando, J. F. Ormes, M. Palatiello, V. S. Paliya, D. Paneque, Z. Pei, H. Peña-Herazo, J. S. Perkins, M. Persic, M. Pesce-Rollins, V. Petrosian, L. Petrov, F. Piron, H. Poon, T. A. Porter, G. Principe, S. Rainò, R. Rando, M. Razzano, S. Razzaque, A. Reimer, O. Reimer, Q. Remy, T. Reposeur, R. W. Romani, P. M. Saz Parkinson, F. K. Schinzel, D. Serini, C. Sgrò, E. J. Siskind, D. A. Smith, G. Spandre, P. Spinelli, A. W. Strong, D. J. Suson, H. Tajima, M. N. Takahashi, D. Tak, J. B. Thayer, D. J. Thompson, L. Tibaldo, D. F. Torres, E. Torresi, J. Valverde, B. Van Klaveren, P. van Zyl, K. Wood, M. Yassine, and G. Zaharijas.
Fermi Large Area Telescope Fourth Source Catalog.
ApJSS, 247(1):33, March 2020.

[7] M. Ackermann, M. Ajello, L. Baldini, J. Ballet, G. Barbiellini, D. Bastieri, J. Becerra Gonzalez, R. Bellazzini, E. Bissaldi, R. D. Blandford, E. D. Bloom, R. Bonino, E. Bottacini, J. Bregeon, P. Bruel, R. Buehler, S. Buson, R. A. Cameron, M. Caragiulo, P. A. Caraveo, E. Cavazzuti, C. Cecchi, C. C. Cheung, J. Chiang, G. Chiaro, S. Ciprini, J. Conrad, D. Costantin, F. Costanza, S. Cutini, F. D'Ammando, F. de Palma, R. Desiante, S. W. Digel, N. Di Lalla, M. Di Mauro, L. Di Venere, A. Domínguez, P. S. Drell, C. Favuzzi, S. J. Fegan, E. C. Ferrara, J. Finke, W. B. Focke, Y. Fukazawa, S. Funk, P. Fusco, F. Gargano, D. Gasparrini, N. Giglietto, F. Giordano, M. Giroletti, D. Green, I. A. Grenier, L. Guillemot, S. Guiriec, D. H. Hartmann, E. Hays, D. Horan, T. Jogler, G. Jóhannesson, A. S. Johnson, M. Kuss, G. La Mura, S. Larsson, L. Latronico, J. Li, F. Longo, F. Loparco, M. N. Lovellette, P. Lubrano, J. D. Magill, S. Maldera, A. Manfreda, L. Marcotulli, M. N. Mazziotta, P. F. Michelson, N. Mirabal, W. Mitthumsiri, T. Mizuno, M. E. Monzani, A. Morselli, I. V. Moskalenko, M. Negro, E. Nuss, T. Ohsugi, R. Ojha, N. Omodei, M. Orienti, E. Orlando, J. F. Ormes, V. S. Paliya, D. Paneque, J. S. Perkins, M. Persic, M. Pesce-Rollins, F. Piron, T. A. Porter, G. Principe, S. Rainò, R. Rando, B. Rani, M. Razzano, S. Razzaque, A. Reimer, O. Reimer, R. W. Romani, C. Sgrò, D. Simone, E. J. Siskind, F. Spada, G. Spandre, P. Spinelli, C. S. Stalin, L. Stawarz, D. J. Suson, M. Takahashi, K. Tanaka, J. B. Thayer, D. J. Thompson, D. F. Torres, E. Torresi, G. Tosti, E. Troja, G. Vianello, and K. S. Wood.
Gamma-Ray Blazars within the First 2 Billion Years.
ApJL, 837(1):L5, March 2017.

[8] M. Ackermann, M. Ajello, L. Baldini, J. Ballet, G. Barbiellini, D. Bastieri, K. Bechtol, R. Bellazzini, B. Berenji, R. D. Blandford, E. Bonamente, A. W. Borgland, J. Bregeon, M. Brigida, P. Bruel, R. Buehler, T. H. Burnett, S. Buson, G. A. Caliandro, R. A. Cameron, P. A. Caraveo, S. Carrigan, J. M. Casandjian, E. Cavazzuti, C. Cecchi, Ö. Çelik, A. Chekhtman, C. C. Cheung, J. Chiang, S. Ciprini, R. Claus, J. Cohen-Tanugi, S. Corbel, S. Cutini, F. D'Ammando, C. D. Dermer, A. de Angelis, F. de Palma, S. W. Digel, E. do Couto e. Silva, P. S. Drell, R. Dubois, D. Dumora, L. Escande, C. Favuzzi, S. J. Fegan, E. C. Ferrara, L. Fuhrmann, Y. Fukazawa, P. Fusco, F. Gargano, D. Gasparrini, N. Gehrels, S. Germani, B. Giebels, N. Giglietto,

P. Giommi, F. Giordano, M. Giroletti, T. Glanzman, G. Godfrey, I. A. Grenier, J. E. Grove, S. Guiriec, D. Hadasch, M. Hayashida, E. Hays, G. Jóhannesson, A. S. Johnson, W. N. Johnson, T. Kamae, H. Katagiri, J. Kataoka, J. Knödlseder, M. Kuss, J. Lande, S. Larsson, L. Latronico, S. H. Lee, M. Llena Garde, F. Longo, F. Loparco, B. Lott, P. Lubrano, G. M. Madejski, A. Makeev, N. Marchili, M. N. Mazziotta, J. E. McEnery, J. Mehault, P. F. Michelson, T. Mizuno, C. Monte, M. E. Monzani, A. Morselli, I. V. Moskalenko, S. Murgia, T. Nakamori, K. Nalewajko, M. Naumann-Godo, P. L. Nolan, J. P. Norris, E. Nuss, T. Ohsugi, A. Okumura, N. Omodei, E. Orland o, J. F. Ormes, V. Pelassa, M. Pepe, M. Pesce-Rollins, F. Piron, T. A. Porter, S. Rainò, R. Rando, M. Razzano, A. Reimer, O. Reimer, L. C. Reyes, J. Ripken, S. Ritz, M. Roth, H. F. W. Sadrozinski, D. Sanchez, A. Sand er, J. D. Scargle, C. Sgrò, M. Sikora, E. J. Siskind, G. Spandre, P. Spinelli, M. S. Strickman, D. J. Suson, H. Takahashi, T. Takahashi, T. Tanaka, Y. Tanaka, J. B. Thayer, J. G. Thayer, D. J. Thompson, L. Tibaldo, D. F. Torres, G. Tosti, A. Tramacere, T. L. Usher, J. Vandenbroucke, N. Vilchez, V. Vitale, A. P. Waite, P. Wang, A. E. Wehrle, B. L. Winer, Z. Yang, T. Ylinen, and M. Ziegler.
Fermi Gamma-ray Space Telescope Observations of Gamma-ray Outbursts from 3C 454.3 in 2009 December and 2010 April.
ApJ, 721(2):1383–1396, October 2010.

[9] M. Ackermann, R. Anantua, and et al.
Minute-timescale 100 MeV γ-Ray Variability during the Giant Outburst of Quasar 3C 279 Observed by Fermi-LAT in 2015 June.
ApJL, 824:L20, June 2016.

[10] F. A. Aharonian.
TeV gamma rays from BL Lac objects due to synchrotron radiation of extremely high energy protons.
, 5(7):377–395, November 2000.

[11] M. Ajello, R. Angioni, M. Axelsson, J. Ballet, G. Barbiellini, D. Bastieri, J. Becerra Gonzalez, R. Bellazzini, E. Bissaldi, E. D. Bloom, R. Bonino, E. Bottacini, P. Bruel, S. Buson, F. Cafardo, R. A. Cameron, E. Cavazzuti, S. Chen, C. C. Cheung, S. Ciprini, D. Costantin, S. Cutini, F. D'Ammando, P. de la Torre Luque, R. de Menezes, F. de Palma, A. Desai, N. Di Lalla, L. Di Venere, A. Domínguez,

F. Fana Dirirsa, E. C. Ferrara, J. Finke, A. Franckowiak, Y. Fukazawa, S. Funk, P. Fusco, F. Gargano, S. Garrappa, D. Gasparrini, N. Giglietto, F. Giordano, M. Giroletti, D. Green, I. A. Grenier, S. Guiriec, S. Harita, E. Hays, D. Horan, R. Itoh, G. Jóhannesson, M. Kovac'evic', F. Krauss, M. Kreter, M. Kuss, S. Larsson, C. Leto, J. Li, I. Liodakis, F. Longo, F. Loparco, B. Lott, M. N. Lovellette, P. Lubrano, G. M. Madejski, S. Maldera, A. Manfreda, G. Martí-Devesa, F. Massaro, M. N. Mazziotta, I. Mereu, M. Meyer, G. Migliori, N. Mirabal, T. Mizuno, M. E. Monzani, A. Morselli, I. V. Moskalenko, M. Negro, R. Nemmen, E. Nuss, L. S. Ojha, R. Ojha, N. Omodei, M. Orienti, E. Orlando, J. F. Ormes, V. S. Paliya, Z. Pei, H. Peña-Herazo, M. Persic, M. Pesce-Rollins, L. Petrov, F. Piron, H. Poon, G. Principe, S. Rainò, R. Rando, B. Rani, M. Razzano, S. Razzaque, A. Reimer, O. Reimer, F. K. Schinzel, D. Serini, C. Sgrò, E. J. Siskind, G. Spandre, P. Spinelli, D. J. Suson, Y. Tachibana, D. J. Thompson, D. F. Torres, E. Torresi, E. Troja, J. Valverde, P. van Zyl, and M. Yassine.

The Fourth Catalog of Active Galactic Nuclei Detected by the Fermi Large Area Telescope.

ApJ, 892(2):105, April 2020.

[12] M. Ajello, R. Angioni, M. Axelsson, J. Ballet, G. Barbiellini, D. Bastieri, J. Becerra Gonzalez, R. Bellazzini, E. Bissaldi, E. D. Bloom, R. Bonino, E. Bottacini, P. Bruel, S. Buson, F. Cafardo, R. A. Cameron, E. Cavazzuti, S. Chen, C. C. Cheung, S. Ciprini, D. Costantin, S. Cutini, F. D'Ammando, P. de la Torre Luque, R. de Menezes, F. de Palma, A. Desai, N. Di Lalla, L. Di Venere, A. Domínguez, F. Fana Dirirsa, E. C. Ferrara, J. Finke, A. Franckowiak, Y. Fukazawa, S. Funk, P. Fusco, F. Gargano, S. Garrappa, D. Gasparrini, N. Giglietto, F. Giordano, M. Giroletti, D. Green, I. A. Grenier, S. Guiriec, S. Harita, E. Hays, D. Horan, R. Itoh, G. Jóhannesson, M. Kovac'evic', F. Krauss, M. Kreter, M. Kuss, S. Larsson, C. Leto, J. Li, I. Liodakis, F. Longo, F. Loparco, B. Lott, M. N. Lovellette, P. Lubrano, G. M. Madejski, S. Maldera, A. Manfreda, G. Martí-Devesa, F. Massaro, M. N. Mazziotta, I. Mereu, M. Meyer, G. Migliori, N. Mirabal, T. Mizuno, M. E. Monzani, A. Morselli, I. V. Moskalenko, M. Negro, R. Nemmen, E. Nuss, L. S. Ojha, R. Ojha, N. Omodei, M. Orienti, E. Orlando, J. F. Ormes, V. S. Paliya, Z. Pei,

H. Peña-Herazo, M. Persic, M. Pesce-Rollins, L. Petrov, F. Piron, H. Poon, G. Principe, S. Rainò, R. Rando, B. Rani, M. Razzano, S. Razzaque, A. Reimer, O. Reimer, F. K. Schinzel, D. Serini, C. Sgrò, E. J. Siskind, G. Spandre, P. Spinelli, D. J. Suson, Y. Tachibana, D. J. Thompson, D. F. Torres, E. Torresi, E. Troja, J. Valverde, P. van Zyl, and M. Yassine.

The Fourth Catalog of Active Galactic Nuclei Detected by the Fermi Large Area Telescope.

ApJ, 892(2):105, April 2020.

[13] J. Aleksić, L. A. Antonelli, P. Antoranz, M. Backes, J. A. Barrio, D. Bastieri, J. Becerra González, W. Bednarek, A. Berdyugin, K. Berger, E. Bernardini, A. Biland, O. Blanch, R. K. Bock, A. Boller, G. Bonnoli, D. Borla Tridon, I. Braun, T. Bretz, A. Cañellas, E. Carmona, A. Carosi, P. Colin, E. Colombo, J. L. Contreras, J. Cortina, L. Cossio, S. Covino, F. Dazzi, A. De Angelis, E. De Cea del Pozo, B. De Lotto, C. Delgado Mendez, A. Diago Ortega, M. Doert, A. Domínguez, D. Dominis Prester, D. Dorner, M. Doro, D. Elsaesser, D. Ferenc, M. V. Fonseca, L. Font, C. Fruck, R. J. García López, M. Garczarczyk, D. Garrido, G. Giavitto, N. Godinović, D. Hadasch, D. Häfner, A. Herrero, D. Hildebrand, D. Höhne-Mönch, J. Hose, D. Hrupec, B. Huber, T. Jogler, S. Klepser, T. Krähenbühl, J. Krause, A. La Barbera, D. Lelas, E. Leonardo, E. Lindfors, S. Lombardi, M. López, E. Lorenz, M. Makariev, G. Maneva, N. Mankuzhiyil, K. Mannheim, L. Maraschi, M. Mariotti, M. Martínez, D. Mazin, M. Meucci, J. M. Miranda, R. Mirzoyan, H. Miyamoto, J. Moldón, A. Moralejo, D. Nieto, K. Nilsson, R. Orito, I. Oya, D. Paneque, R. Paoletti, S. Pardo, J. M. Paredes, S. Partini, M. Pasanen, F. Pauss, M. A. Perez-Torres, M. Persic, L. Peruzzo, M. Pilia, J. Pochon, F. Prada, P. G. Prada Moroni, E. Prandini, I. Puljak, I. Reichardt, R. Reinthal, W. Rhode, M. Ribó, J. Rico, S. Rügamer, A. Saggion, K. Saito, T. Y. Saito, M. Salvati, K. Satalecka, V. Scalzotto, V. Scapin, C. Schultz, T. Schweizer, M. Shayduk, S. N. Shore, A. Sillanpää, J. Sitarek, D. Sobczynska, F. Spanier, S. Spiro, A. Stamerra, B. Steinke, J. Storz, N. Strah, T. Surić, L. Takalo, F. Tavecchio, P. Temnikov, T. Terzić, D. Tescaro, M. Teshima, M. Thom, O. Tibolla, D. F. Torres, A. Treves, H. Vankov, P. Vogler, R. M. Wagner, Q. Weitzel, V. Zabalza, F. Zandanel, R. Zanin, MAGIC Collaboration, Y. T.

Tanaka, D. L. Wood, and S. Buson.
MAGIC Discovery of Very High Energy Emission from the FSRQ PKS 1222+21.
ApJL, 730(1):L8, March 2011.

[14] Raúl A. Amaya-Almazán, Vahram Chavushyan, and Victor M. Patiño-Álvarez.
Multiwavelength Analysis and the Difference in the Behavior of the Spectral Features during the 2010 and 2014 Flaring Periods of the Blazar 3C 454.3.
ApJ, 906(1):5, January 2021.

[15] R. Angioni, R. Nesci, J. D. Finke, S. Buson, and S. Ciprini.
The large gamma-ray flare of the flat-spectrum radio quasar PKS 0346-27.
A&A, 627:A140, July 2019.

[16] S. Ansoldi, L. A. Antonelli, C. Arcaro, D. Baack, A. Babić, B. Banerjee, P. Bangale, U. Barres de Almeida, J. A. Barrio, J. Becerra González, W. Bednarek, E. Bernardini, R. C. Berse, A. Berti, J. Besenrieder, W. Bhattacharyya, C. Bigongiari, A. Biland, O. Blanch, G. Bonnoli, R. Carosi, G. Ceribella, A. Chatterjee, S. M. Colak, P. Colin, E. Colombo, J. L. Contreras, J. Cortina, S. Covino, P. Cumani, V. D'Elia, P. Da Vela, F. Dazzi, A. De Angelis, B. De Lotto, M. Delfino, J. Delgado, F. Di Pierro, A. Domínguez, D. Dominis Prester, D. Dorner, M. Doro, S. Einecke, D. Elsaesser, V. Fallah Ramazani, A. Fattorini, A. Fernández-Barral, G. Ferrara, D. Fidalgo, L. Foffano, M. V. Fonseca, L. Font, C. Fruck, S. Gallozzi, R. J. García López, M. Garczarczyk, M. Gaug, P. Giammaria, N. Godinović, D. Guberman, D. Hadasch, A. Hahn, T. Hassan, M. Hayashida, J. Herrera, J. Hoang, D. Hrupec, S. Inoue, K. Ishio, Y. Iwamura, Y. Konno, H. Kubo, J. Kushida, A. Lamastra, D. Lelas, F. Leone, E. Lindfors, S. Lombardi, F. Longo, M. López, C. Maggio, P. Majumdar, M. Makariev, G. Maneva, M. Manganaro, K. Mannheim, L. Maraschi, M. Mariotti, M. Martínez, S. Masuda, D. Mazin, K. Mielke, M. Minev, J. M. Miranda, R. Mirzoyan, A. Moralejo, V. Moreno, E. Moretti, V. Neustroev, A. Niedzwiecki, M. Nievas Rosillo, C. Nigro, K. Nilsson, D. Ninci, K. Nishijima, K. Noda,

L. Nogués, S. Paiano, J. Palacio, D. Paneque, R. Paoletti, J. M. Paredes, G. Pedaletti, P. Peñil, M. Peresano, M. Persic, K. Pfrang, P. G. Prada Moroni, E. Prandini, I. Puljak, J. R. Garcia, W. Rhode, M. Ribó, J. Rico, C. Righi, A. Rugliancich, L. Saha, T. Saito, K. Satalecka, T. Schweizer, J. Sitarek, I. Šnidarić, D. Sobczynska, A. Stamerra, M. Strzys, T. Surić, F. Tavecchio, P. Temnikov, T. Terzić, M. Teshima, N. Torres-Albá, S. Tsujimoto, G. Vanzo, M. Vazquez Acosta, I. Vovk, J. E. Ward, M. Will, D. Zarić, and M. Cerruti.

The Blazar TXS 0506+056 Associated with a High-energy Neutrino: Insights into Extragalactic Jets and Cosmic-Ray Acceleration.

ApJL, 863:L10, August 2018.

[17] W. B. Atwood, A. A. Abdo, M. Ackermann, W. Althouse, B. Anderson, M. Axelsson, L. Baldini, J. Ballet, D. L. Band, G. Barbiellini, J. Bartelt, D. Bastieri, B. M. Baughman, K. Bechtol, D. Bédérède, F. Bellardi, R. Bellazzini, B. Berenji, G. F. Bignami, D. Bisello, E. Bissaldi, R. D. Blandford, E. D. Bloom, J. R. Bogart, E. Bonamente, J. Bonnell, A. W. Borgland, A. Bouvier, J. Bregeon, A. Brez, M. Brigida, P. Bruel, T. H. Burnett, G. Busetto, G. A. Caliandro, R. A. Cameron, P. A. Caraveo, S. Carius, P. Carlson, J. M. Casandjian, E. Cavazzuti, M. Ceccanti, C. Cecchi, E. Charles, A. Chekhtman, C. C. Cheung, J. Chiang, R. Chipaux, A. N. Cillis, S. Ciprini, R. Claus, J. Cohen-Tanugi, S. Condamoor, J. Conrad, R. Corbet, L. Corucci, L. Costamante, S. Cutini, D. S. Davis, D. Decotigny, M. DeKlotz, C. D. Dermer, A. de Angelis, S. W. Digel, E. do Couto e Silva, P. S. Drell, R. Dubois, D. Dumora, Y. Edmonds, D. Fabiani, C. Farnier, C. Favuzzi, D. L. Flath, P. Fleury, W. B. Focke, S. Funk, P. Fusco, F. Gargano, D. Gasparrini, N. Gehrels, F. X. Gentit, S. Germani, B. Giebels, N. Giglietto, P. Giommi, F. Giordano, T. Glanzman, G. Godfrey, I. A. Grenier, M. H. Grondin, J. E. Grove, L. Guillemot, S. Guiriec, G. Haller, A. K. Harding, P. A. Hart, E. Hays, S. E. Healey, M. Hirayama, L. Hjalmarsdotter, R. Horn, R. E. Hughes, G. Jóhannesson, G. Johansson, A. S. Johnson, R. P. Johnson, T. J. Johnson, W. N. Johnson, T. Kamae, H. Katagiri, J. Kataoka, A. Kavelaars, N. Kawai, H. Kelly, M. Kerr, W. Klamra, J. Knödlseder, M. L. Kocian, N. Komin, F. Kuehn, M. Kuss, D. Landriu, L. Latronico, B. Lee, S. H. Lee, M. Lemoine-Goumard, A. M. Lionetto, F. Longo, F. Loparco, B. Lott, M. N. Lovellette, P. Lubrano, G. M. Madejski, A. Makeev, B. Marangelli, M. M.

Massai, M. N. Mazziotta, J. E. McEnery, N. Menon, C. Meurer, P. F. Michelson, M. Minuti, N. Mirizzi, W. Mitthumsiri, T. Mizuno, A. A. Moiseev, C. Monte, M. E. Monzani, E. Moretti, A. Morselli, I. V. Moskalenko, S. Murgia, T. Nakamori, S. Nishino, P. L. Nolan, J. P. Norris, E. Nuss, M. Ohno, T. Ohsugi, N. Omodei, E. Orlando, J. F. Ormes, A. Paccagnella, D. Paneque, J. H. Panetta, D. Parent, M. Pearce, M. Pepe, A. Perazzo, M. Pesce-Rollins, P. Picozza, L. Pieri, M. Pinchera, F. Piron, T. A. Porter, L. Poupard, S. Rainò, R. Rando, E. Rapposelli, M. Razzano, A. Reimer, O. Reimer, T. Reposeur, L. C. Reyes, S. Ritz, L. S. Rochester, A. Y. Rodriguez, R. W. Romani, M. Roth, J. J. Russell, F. Ryde, S. Sabatini, H. F. W. Sadrozinski, D. Sanchez, A. Sander, L. Sapozhnikov, P. M. Saz Parkinson, J. D. Scargle, T. L. Schalk, G. Scolieri, C. Sgrò, G. H. Share, M. Shaw, T. Shimokawabe, C. Shrader, A. Sierpowska-Bartosik, E. J. Siskind, D. A. Smith, P. D. Smith, G. Spandre, P. Spinelli, J. L. Starck, T. E. Stephens, M. S. Strickman, A. W. Strong, D. J. Suson, H. Tajima, H. Takahashi, T. Takahashi, T. Tanaka, A. Tenze, S. Tether, J. B. Thayer, J. G. Thayer, D. J. Thompson, L. Tibaldo, O. Tibolla, D. F. Torres, G. Tosti, A. Tramacere, M. Turri, T. L. Usher, N. Vilchez, V. Vitale, P. Wang, K. Watters, B. L. Winer, K. S. Wood, T. Ylinen, and M. Ziegler.
The Large Area Telescope on the Fermi Gamma-Ray Space Telescope Mission.
ApJ, 697(2):1071–1102, June 2009.

[18] V. Baghmanyan, S. Gasparyan, and N. Sahakyan.
Rapid Gamma-Ray Variability of NGC 1275.
ApJ, 848(2):111, October 2017.

[19] J. Ballet, T. H. Burnett, S. W. Digel, and B. Lott.
Fermi Large Area Telescope Fourth Source Catalog Data Release 2.
arXiv e-prints, page arXiv:2005.11208, May 2020.

[20] Scott D. Barthelmy, Louis M. Barbier, Jay R. Cummings, Ed E. Fenimore, Neil Gehrels, Derek Hullinger, Hans A. Krimm, Craig B. Markwardt, David M. Palmer, Ann Parsons, Goro Sato, Masaya Suzuki, Tadayuki Takahashi, Makota Tashiro, and Jack Tueller.
The Burst Alert Telescope (BAT) on the SWIFT Midex Mission.
Space Science Reviews, 120(3-4):143–164, October 2005.

[21] W. Bednarek and R. M. Wagner.
A model for delayed emission in a very-high energy gamma-ray flare in Markarian 501.
A&A, 486(3):679–682, August 2008.

[22] J. Biteau, E. Prandini, L. Costamante, M. Lemoine, P. Padovani, E. Pueschel, E. Resconi, F. Tavecchio, A. Taylor, and A. Zech.
Progress in unveiling extreme particle acceleration in persistent astrophysical jets.
Nature Astronomy, 4:124–131, February 2020.

[23] R. Blandford and M. Rees.
Some comments on radiation mechanisms in Lacertids.
In A. M. Wolfe, editor, *Pittsburgh Conference on BL Lac Objects*, pages 341–347, Pittsburgh, 1978. University of Pittsburgh press.

[24] M. Błażejowski, M. Sikora, R. Moderski, and G. M. Madejski.
Comptonization of Infrared Radiation from Hot Dust by Relativistic Jets in Quasars.
ApJ, 545:107–116, December 2000.

[25] S. D. Bloom and A. P. Marscher.
An Analysis of the Synchrotron Self-Compton Model for the Multi–Wave Band Spectra of Blazars.
ApJ, 461:657, April 1996.

[26] E. W. Bonning, C. Bailyn, C. M. Urry, M. Buxton, G. Fossati, L. Maraschi, P. Coppi, R. Scalzo, J. Isler, and A. Kaptur.
Correlated Variability in the Blazar 3C 454.3.
ApJL, 697(2):L81–L85, June 2009.

[27] G. Bonnoli, G. Ghisellini, L. Foschini, F. Tavecchio, and G. Ghirlanda.
The γ-ray brightest days of the blazar 3C 454.3.
MNRAS, 410(1):368–380, January 2011.

[28] G. Bonnoli, F. Tavecchio, G. Ghisellini, and T. Sbarrato.
An emerging population of BL Lacs with extreme properties: towards a class of EBL and cosmic magnetic field probes?
MNRAS, 451(1):611–621, July 2015.

[29] M. Böttcher, A. Reimer, K. Sweeney, and A. Prakash.
Leptonic and Hadronic Modeling of Fermi-detected Blazars.
ApJ, 768:54, May 2013.

[30] Richard J. Britto, Eugenio Bottacini, Benoît Lott, Soebur Razzaque, and Sara Buson.
Fermi-LAT Observations of the 2014 May-July Outburst from 3C 454.3.
ApJ, 830(2):162, October 2016.

[31] A. M. Brown.
Locating the γ-ray emission region of the flat spectrum radio quasar PKS 1510-089.
MNRAS, 431:824–835, May 2013.

[32] Gabriele Bruni, Francesca Panessa, Gabriele Ghisellini, Vahram Chavushyan, Harold A. Peña-Herazo, Lorena Hernández-García, Angela Bazzano, Pietro Ubertini, and Alex Kraus.
Fermi Transient J1544-0649: A Flaring Radio-weak BL Lac.
ApJL, 854(2):L23, February 2018.

[33] D. N. Burrows, J. E. Hill, J. A. Nousek, J. A. Kennea, A. Wells, J. P. Osborne, A. F. Abbey, A. Beardmore, K. Mukerjee, A. D. T. Short, G. Chincarini, S. Campana, O. Citterio, A. Moretti, C. Pagani, G. Tagliaferri, P. Giommi, M. Capalbi, F. Tamburelli, L. Angelini, G. Cusumano, H. W. Bräuninger, W. Burkert, and G. D. Hartner.
The Swift X-Ray Telescope.
Space Science Reviews, 120:165–195, October 2005.

[34] David N. Burrows, J. E. Hill, J. A. Nousek, J. A. Kennea, A. Wells, J. P. Osborne, A. F. Abbey, A. Beardmore, K. Mukerjee, A. D. T. Short, G. Chincarini, S. Campana, O. Citterio, A. Moretti, C. Pagani, G. Tagliaferri, P. Giommi, M. Capalbi, F. Tamburelli, L. Angelini, G. Cusumano, H. W. Bräuninger, W. Burkert, and G. D. Hartner.
The Swift X-Ray Telescope.
Space Science Reviews, 120(3-4):165–195, October 2005.

[35] W. Cash.
Parameter estimation in astronomy through application of the likelihood ratio.
ApJ, 228:939–947, March 1979.

[36] A. Cavaliere and V. D'Elia.
The Blazar Main Sequence.
ApJ, 571(1):226–233, May 2002.

[37] M. Cerruti, A. Zech, C. Boisson, G. Emery, S. Inoue, and J.-P. Lenain.
Leptohadronic single-zone models for the electromagnetic and neutrino emission of TXS 0506+056.
MNRAS, 483:L12–L16, February 2019.

[38] Y. L. Chang, B. Arsioli, P. Giommi, P. Padovani, and C. H. Brandt.
The 3HSP catalogue of extreme and high-synchrotron peaked blazars.
A&A, 632:A77, December 2019.

[39] Y. L. Chang, C. H. Brandt, and P. Giommi.
The Open Universe VOU-Blazars tool.
Astronomy and Computing, 30:100350, January 2020.

[40] R. Chornock and R. Margutti.
MDM Redshift of the Host of ASASSN-17gs.
The Astronomer's Telegram, 10491:1, June 2017.

[41] S. Ciprini, C. C. Cheung, D. Kocevski, J. Chiang, Fermi Large Area Telescope Collaboration, and S. N. Shore.
Fermi LAT detection and Swift X-ray follow-up of a new gamma-ray/X-ray transient source Fermi J1544-0649 (Swift 154419.7-064915).
The Astronomer's Telegram, 10482:1, June 2017.

[42] J. J. Condon, W. D. Cotton, E. W. Greisen, Q. F. Yin, R. A. Perley, G. B. Taylor, and J. J. Broderick.
The NRAO VLA Sky Survey.
AJ, 115(5):1693–1716, May 1998.

[43] L. Costamante, G. Ghisellini, P. Giommi, G. Tagliaferri, A. Celotti, M. Chiaberge, G. Fossati, L. Maraschi, F. Tavecchio, A. Treves, and A. Wolter.
Extreme synchrotron BL Lac objects. Stretching the blazar sequence.
A&A, 371:512–526, May 2001.

[44] S. Cutini, S. Ciprini, M. Orienti, A. Tramacere, F. D'Ammando, F. Verrecchia, G. Polenta, L. Carrasco, V. D'Elia, P. Giommi, J. González-Nuevo, P. Grandi, D. Harrison, E. Hays, S. Larsson, A. Lähteenmäki, J. León-Tavares, M. López-Caniego, P. Natoli, R. Ojha, B. Partridge, A. Porras, L. Reyes, E. Recillas, and E. Torresi.
Radio-gamma-ray connection and spectral evolution in 4C +49.22 (S4 1150+49): the Fermi, Swift and Planck view.
MNRAS, 445(4):4316–4334, December 2014.

[45] F. D'Ammando, C. M. Raiteri, M. Villata, P. Romano, G. Pucella, H. A. Krimm, S. Covino, M. Orienti, G. Giovannini, S. Vercellone, E. Pian, I. Donnarumma, V. Vittorini, M. Tavani, A. Argan, G. Barbiellini, F. Boffelli, A. Bulgarelli, P. Caraveo, P. W. Cattaneo, A. W. Chen, V. Cocco, E. Costa, E. Del Monte, G. de Paris, G. Di Cocco, Y. Evangelista, M. Feroci, A. Ferrari, M. Fiorini, T. Froysland, M. Frutti, F. Fuschino, M. Galli, F. Gianotti, A. Giuliani, C. Labanti, I. Lapshov, F. Lazzarotto, P. Lipari, F. Longo, M. Marisaldi, S. Mereghetti, A. Morselli, L. Pacciani, A. Pellizzoni, F. Perotti, G. Piano, P. Picozza, M. Pilia, G. Porrovecchio, M. Prest, M. Rapisarda, A. Rappoldi, A. Rubini, S. Sabatini, P. Soffitta, E. Striani, M. Trifoglio, A. Trois, E. Vallazza, A. Zambra, D. Zanello, I. Agudo, H. D. Aller, M. F. Aller, A. A. Arkharov, U. Bach, E. Benitez, A. Berdyugin, D. A. Blinov, C. S. Buemi, W. P. Chen, A. di Paola, M. Dolci, E. Forné, L. Fuhrmann, J. L. Gómez, M. A. Gurwell, B. Jordan, S. G. Jorstad, J. Heidt, D. Hiriart, T. Hovatta, H. Y. Hsiao, G. Kimeridze, T. S. Konstantinova, E. N. Kopatskaya, E. Koptelova, O. M. Kurtanidze, S. O. Kurtanidze, V. M. Larionov, A. Lähteenmäki, P. Leto, E. Lindfors, A. P. Marscher, B. McBreen, I. M. McHardy, D. A. Morozova, K. Nilsson, M. Pasanen, M. Roca-Sogorb, A. Sillanpää, L. O. Takalo, M. Tornikoski, C. Trigilio, I. S. Troitsky, G. Umana, L. A. Antonelli, S. Colafrancesco, C. Pittori, P. Santolamazza, F. Verrecchia, P. Giommi, and L. Salotti.
AGILE detection of extreme γ-ray activity from the blazar PKS 1510-089 during March 2009. Multifrequency analysis.
A&A, 529:A145, May 2011.

[46] C. D. Dermer, R. Schlickeiser, and A. Mastichiadis.
High-energy gamma radiation from extragalactic radio sources.

A&A, 256:L27–L30, March 1992.

[47] Charles D. Dermer and Reinhard Schlickeiser.
Model for the High-Energy Emission from Blazars.
ApJ, 416:458, October 1993.

[48] Charles D. Dermer and Reinhard Schlickeiser.
On the Location of the Acceleration and Emission Sites in Gamma-Ray Blazars.
ApJSS, 90:945, February 1994.

[49] Alina-C. Donea and R. J. Protheroe.
Radiation fields of disk, BLR and torus in quasars and blazars: implications for /γ-ray absorption.
Astroparticle Physics, 18(4):377–393, January 2003.

[50] I. Donnarumma, G. Pucella, V. Vittorini, F. D'Ammando, S. Vercellone, C. M. Raiteri, M. Villata, M. Perri, W. P. Chen, R. L. Smart, J. Kataoka, N. Kawai, Y. Mori, G. Tosti, D. Impiombato, T. Takahashi, R. Sato, M. Tavani, A. Bulgarelli, A. W. Chen, A. Giuliani, F. Longo, L. Pacciani, A. Argan, G. Barbiellini, F. Boffelli, P. Caraveo, P. W. Cattaneo, V. Cocco, T. Contessi, E. Costa, E. Del Monte, G. De Paris, G. Di Cocco, Y. Evangelista, M. Feroci, A. Ferrari, M. Fiorini, T. Froysland, M. Frutti, F. Fuschino, M. Galli, F. Gianotti, C. Labanti, I. Lapshov, F. Lazzarotto, P. Lipari, M. Marisaldi, M. Mastropietro, S. Mereghetti, E. Morelli, E. Moretti, A. Morselli, A. Pellizzoni, F. Perotti, G. Piano, P. Picozza, M. Pilia, G. Porrovecchio, M. Prest, M. Rapisarda, A. Rappoldi, A. Rubini, S. Sabatini, E. Scalise, P. Soffitta, E. Striani, M. Trifoglio, A. Trois, E. Vallazza, A. Zambra, D. Zanello, C. Pittori, P. Santolamazza, F. Verrecchia, P. Giommi, L. A. Antonelli, S. Colafrancesco, and L. Salotti.
Multiwavelength Observations of 3C 454.3. II. The AGILE 2007 December Campaign.
ApJ, 707(2):1115–1123, December 2009.

[51] Justin D. Finke and Charles D. Dermer.
On the Break in the Fermi-Large Area Telescope Spectrum of 3C 454.3.
ApJL, 714(2):L303–L307, May 2010.

[52] L. Foschini, G. Bonnoli, G. Ghisellini, G. Tagliaferri, F. Tavecchio, and A. Stamerra.
Fermi/LAT detection of extraordinary variability in the gamma-ray emission of the blazar PKS 1510-089.
A&A, 555:A138, July 2013.

[53] L. Foschini, G. Ghisellini, F. Tavecchio, G. Bonnoli, and A. Stamerra.
Search for the shortest variability at gamma rays in flat-spectrum radio quasars.
A&A, 530:A77, June 2011.

[54] S. Gao, A. Fedynitch, W. Winter, and M. Pohl.
Modelling the coincident observation of a high-energy neutrino and a bright blazar flare.
Nature Astronomy, 3:88–92, January 2019.

[55] S. Gasparyan, N. Sahakyan, V. Baghmanyan, and D. Zargaryan.
On the Multiwavelength Emission from CTA 102.
ApJ, 863(2):114, August 2018.

[56] N. Gehrels, G. Chincarini, P. Giommi, K. O. Mason, J. A. Nousek, A. A. Wells, N. E. White, S. D. Barthelmy, D. N. Burrows, L. R. Cominsky, K. C. Hurley, F. E. Marshall, P. Mészáros, P. W. A. Roming, L. Angelini, L. M. Barbier, T. Belloni, S. Campana, P. A. Caraveo, M. M. Chester, O. Citterio, T. L. Cline, M. S. Cropper, J. R. Cummings, A. J. Dean, E. D. Feigelson, E. E. Fenimore, D. A. Frail, A. S. Fruchter, G. P. Garmire, K. Gendreau, G. Ghisellini, J. Greiner, J. E. Hill, S. D. Hunsberger, H. A. Krimm, S. R. Kulkarni, P. Kumar, F. Lebrun, N. M. Lloyd-Ronning, C. B. Markwardt, B. J. Mattson, R. F. Mushotzky, J. P. Norris, J. Osborne, B. Paczynski, D. M. Palmer, H. S. Park, A. M. Parsons, J. Paul, M. J. Rees, C. S. Reynolds, J. E. Rhoads, T. P. Sasseen, B. E. Schaefer, A. T. Short, A. P. Smale, I. A. Smith, L. Stella, G. Tagliaferri, T. Takahashi, M. Tashiro, L. K. Townsley, J. Tueller, M. J. L. Turner, M. Vietri, W. Voges, M. J. Ward, R. Willingale, F. M. Zerbi, and W. W. Zhang.
The Swift Gamma-Ray Burst Mission.
ApJ, 611(2):1005–1020, August 2004.

[57] G. Ghisellini and A. Celotti.

Relativistic large-scale jets and minimum power requirements.
MNRAS, 327(3):739–743, November 2001.

[58] G. Ghisellini, L. Maraschi, and A. Treves.
Inhomogeneous synchrotron-self-Compton models and the problem of relativistic beaming of BL Lac objects.
A&A, 146:204–212, May 1985.

[59] G. Ghisellini and F. Tavecchio.
Canonical high-power blazars.
MNRAS, 397:985–1002, August 2009.

[60] G. Ghisellini and F. Tavecchio.
Fermi/LAT broad emission line blazars.
MNRAS, 448(2):1060–1077, April 2015.

[61] G. Ghisellini, F. Tavecchio, L. Foschini, and G. Ghirlanda.
The transition between BL Lac objects and flat spectrum radio quasars.
MNRAS, 414:2674–2689, July 2011.

[62] G. Ghisellini, F. Tavecchio, L. Maraschi, A. Celotti, and T. Sbarrato.
The power of relativistic jets is larger than the luminosity of their accretion disks.
Nature, 515(7527):376–378, November 2014.

[63] Dimitrios Giannios, Dmitri A. Uzdensky, and Mitchell C. Begelman.
Fast TeV variability in blazars: jets in a jet.
MNRAS, 395(1):L29–L33, May 2009.

[64] P. Giommi, G. Arrigo, U. Barres De Almeida, M. De Angelis, J. Del Rio Vera, S. Di Ciaccio, S. Di Pippo, S. Iacovoni, and A. M. T. Pollock.
The Open Universe Initiative.
In Ferrretti S., editor, *Space Capacity Building in the XXI Century. Studies in Space Policy*, pages 377–386. Springer, 2020.

[65] P. Giommi, P. Barr, B. Garilli, D. Maccagni, and A. M. T. Pollock.
A Study of BL Lacertae–Type Objects with EXOSAT. I. Flux Correlations, Luminosity, Variability, and Spectral Variability.
ApJ, 356:432, June 1990.

[66] P. Giommi, A. J. Blustin, M. Capalbi, S. Colafrancesco, A. Cucchiara, L. Fuhrmann, H. A. Krimm, N. Marchili, E. Massaro, M. Perri, G. Tagliaferri, G. Tosti, A. Tramacere, D. N. Burrows, G. Chincarini, A. Falcone, N. Gehrels, J. Kennea, and R. Sambruna.
Swift and infra-red observations of the blazar 3C 454.3 during the giant X-ray flare of May 2005.
A&A, 456(3):911–916, September 2006.

[67] P. Giommi, T. Glauch, P. Padovani, E. Resconi, A. Turcati, and Y. L. Chang.
Dissecting the regions around IceCube high-energy neutrinos: growing evidence for the blazar connection.
MNRAS, 497(1):865–878, July 2020.

[68] P Giommi, M T Menna, and P Padovani.
The Sedentary Multi-Frequency Survey . I . arXiv : astro-ph / 9907014v1 1 Jul 1999.
MNRAS, 310:465–475, 1999.

[69] P. Giommi, P. Padovani, G. Polenta, S. Turriziani, V. D'Elia, and S. Piranomonte.
A simplified view of blazars: clearing the fog around long-standing selection effects.
MNRAS, 420(4):2899–2911, March 2012.

[70] P. Giommi, S. Piranomonte, M. Perri, and P. Padovani.
The sedentary survey of extreme high energy peaked BL Lacs.
A&A, 434(1):385–396, April 2005.

[71] Yjan A. Gordon, Michelle M. Boyce, Christopher P. O'Dea, Lawrence Rudnick, Heinz Andernach, Adrian N. Vantyghem, Stefi A. Baum, Jean-Paul Bui, and Mathew Dionyssiou.
A Catalog of Very Large Array Sky Survey Epoch 1 Quick Look Components, Sources, and Host Identifications.
Research Notes of the American Astronomical Society, 4(10):175, October 2020.

[72] Fan Guo, Hui Li, William Daughton, and Yi-Hsin Liu.
Formation of Hard Power Laws in the Energetic Particle Spectra Resulting from Relativistic Magnetic Reconnection.

Phys. Rev. Lett., 113(15):155005, October 2014.

[73] R. C. Hartman, D. L. Bertsch, B. L. Dingus, C. E. Fichtel, S. D. Hunter, G. Kanbach, D. A. Kniffen, Y. C. Lin, J. R. Mattox, H. A. Mayer-Hasselwander, P. F. Michelson, C. von Montigny, P. L. Nolan, B. G. Piner, E. Schneid, P. Sreekumar, and D. J. Thompson.
EGRET Detection of High-Energy Gamma Radiation from the OVV Quasar 3C 454.3.
ApJL, 407:L41, April 1993.

[74] M. Hayashida, K. Nalewajko, and et al.
Rapid Variability of Blazar 3C 279 during Flaring States in 2013-2014 with Joint Fermi-LAT, NuSTAR, Swift, and Ground-Based Multi-wavelength Observations.
ApJ, 807:79, July 2015.

[75] IceCube Collaboration, M. G. Aartsen, M. Ackermann, J. Adams, J. A. Aguilar, M. Ahlers, M. Ahrens, I. Al Samarai, D. Altmann, K. Andeen, T. Anderson, I. Ansseau, G. Anton, C. Argüelles, J. Auffenberg, S. Axani, H. Bagherpour, X. Bai, J. P. Barron, S. W. Barwick, V. Baum, R. Bay, J. J. Beatty, J. Becker Tjus, K. H. Becker, S. Ben-Zvi, D. Berley, E. Bernardini, D. Z. Besson, G. Binder, D. Bindig, E. Blaufuss, S. Blot, C. Bohm, M. Börner, F. Bos, S. Böser, O. Botner, E. Bourbeau, J. Bourbeau, F. Bradascio, J. Braun, M. Brenzke, H. P. Bretz, S. Bron, J. Brostean-Kaiser, A. Burgman, R. S. Busse, T. Carver, E. Cheung, D. Chirkin, A. Christov, K. Clark, L. Classen, S. Coenders, G. H. Collin, J. M. Conrad, P. Coppin, P. Correa, D. F. Cowen, R. Cross, P. Dave, M. Day, J. P. A. M. de André, C. De Clercq, J. J. DeLaunay, H. Dembinski, S. De Ridder, P. Desiati, K. D. de Vries, G. de Wasseige, M. de With, T. DeYoung, J. C. Díaz-Vélez, V. di Lorenzo, H. Dujmovic, J. P. Dumm, M. Dunkman, E. Dvorak, B. Eberhardt, T. Ehrhardt, B. Eichmann, P. Eller, P. A. Evenson, S. Fahey, A. R. Fazely, J. Felde, K. Filimonov, C. Finley, S. Flis, A. Franckowiak, E. Friedman, A. Fritz, T. K. Gaisser, J. Gallagher, L. Gerhardt, K. Ghorbani, T. Glauch, T. Glüsenkamp, A. Goldschmidt, J. G. Gonzalez, D. Grant, Z. Griffith, C. Haack, A. Hallgren, F. Halzen, K. Hanson, D. Hebecker, D. Heereman, K. Helbing, R. Hellauer, S. Hickford, J. Hignight, G. C. Hill, K. D. Hoffman, R. Hoffmann, T. Hoinka, B. Hokanson-Fasig, K. Hoshina, F. Huang,

M. Huber, K. Hultqvist, M. Hünnefeld, R. Hussain, S. In, N. Iovine, A. Ishihara, E. Jacobi, G. S. Japaridze, M. Jeong, K. Jero, B. J. P. Jones, P. Kalaczynski, W. Kang, A. Kappes, D. Kappesser, T. Karg, A. Karle, U. Katz, M. Kauer, A. Keivani, J. L. Kelley, A. Kheirandish, J. Kim, M. Kim, T. Kintscher, J. Kiryluk, T. Kittler, S. R. Klein, R. Koirala, H. Kolanoski, L. Köpke, C. Kopper, S. Kopper, J. P. Koschinsky, D. J. Koskinen, M. Kowalski, K. Krings, M. Kroll, G. Krückl, S. Kunwar, N. Kurahashi, T. Kuwabara, A. Kyriacou, M. Labare, J. L. Lanfranchi, M. J. Larson, F. Lauber, K. Leonard, M. Lesiak-Bzdak, M. Leuermann, Q. R. Liu, C. J. Lozano Mariscal, L. Lu, J. Lünemann, W. Luszczak, J. Madsen, G. Maggi, K. B. M. Mahn, S. Mancina, R. Maruyama, K. Mase, R. Maunu, K. Meagher, M. Medici, M. Meier, T. Menne, G. Merino, T. Meures, S. Miarecki, J. Micallef, G. Momenté, T. Montaruli, R. W. Moore, S, R. Morse, M. Moulai, R. Nahnhauer, P. Nakarmi, U. Naumann, G. Neer, H. Niederhausen, S. C. Nowicki, D. R. Nygren, A. Obertacke Pollmann, A. Olivas, A. O'Murchadha, E. O'Sullivan, T. Palczewski, H. Pandya, D. V. Pankova, P. Peiffer, J. A. Pepper, C. Pérez de los Heros, D. Pieloth, E. Pinat, M. Plum, P. B. Price, G. T. Przybylski, C. Raab, L. Rädel, M. Rameez, L. Rauch, K. Rawlins, I. C. Rea, R. Reimann, B. Relethford, M. Relich, E. Resconi, W. Rhode, M. Richman, S. Robertson, M. Rongen, C. Rott, T. Ruhe, D. Ryckbosch, D. Rysewyk, I. Safa, T. Sälzer, S. E. Sanchez Herrera, A. Sandrock, J. Sandroos, M. Santander, S. Sarkar, S. Sarkar, K. Satalecka, P. Schlunder, T. Schmidt, A. Schneider, S. Schoenen, S. Schöneberg, L. Schumacher, S. Sclafani, D. Seckel, S. Seunarine, J. Soedingrekso, D. Soldin, M. Song, G. M. Spiczak, C. Spiering, J. Stachurska, M. Stamatikos, T. Stanev, A. Stasik, R. Stein, J. Stettner, A. Steuer, T. Stezelberger, R. G. Stokstad, A. Stößl, N. L. Strotjohann, T. Stuttard, G. W. Sullivan, M. Sutherland, I. Taboada, J. Tatar, F. Tenholt, S. Ter-Antonyan, A. Terliuk, S. Tilav, P. A. Toale, M. N. Tobin, C. Toennis, S. Toscano, D. Tosi, M. Tselengidou, C. F. Tung, A. Turcati, C. F. Turley, B. Ty, E. Unger, M. Usner, J. Vandenbroucke, W. Van Driessche, D. van Eijk, N. van Eijndhoven, S. Vanheule, J. van Santen, E. Vogel, M. Vraeghe, C. Walck, A. Wallace, M. Wallraff, F. D. Wandler, N. Wandkowsky, A. Waza, C. Weaver, M. J. Weiss, C. Wendt, J. Werthebach, S. Westerhoff, B. J. Whelan, N. Whitehorn, K. Wiebe, C. H. Wiebusch, L. Wille, D. R. Williams, L. Wills, M. Wolf, J. Wood,

T. R. Wood, K. Woschnagg, D. L. Xu, X. W. Xu, Y. Xu, J. P. Yanez, G. Yodh, S. Yoshida, T. Yuan, Fermi-LAT Collaboration, S. Abdollahi, M. Ajello, R. Angioni, L. Baldini, J. Ballet, G. Barbiellini, D. Bastieri, K. Bechtol, R. Bellazzini, B. Berenji, E. Bissaldi, R. D. Blandford, R. Bonino, E. Bottacini, J. Bregeon, P. Bruel, R. Buehler, T. H. Burnett, E. Burns, S. Buson, R. A. Cameron, R. Caputo, P. A. Caraveo, E. Cavazzuti, E. Charles, S. Chen, C. C. Cheung, J. Chiang, G. Chiaro, S. Ciprini, J. Cohen-Tanugi, J. Conrad, D. Costantin, S. Cutini, F. D'Ammando, F. de Palma, S. W. Digel, N. Di Lalla, M. Di Mauro, L. Di Venere, A. Domínguez, C. Favuzzi, A. Franckowiak, Y. Fukazawa, S. Funk, P. Fusco, F. Gargano, D. Gasparrini, N. Giglietto, M. Giomi, P. Giommi, F. Giordano, M. Giroletti, T. Glanzman, D. Green, I. A. Grenier, M. H. Grondin, S. Guiriec, A. K. Harding, M. Hayashida, E. Hays, J. W. Hewitt, D. Horan, G. Jóhannesson, M. Kadler, S. Kensei, D. Kocevski, F. Krauss, M. Kreter, M. Kuss, G. La Mura, S. Larsson, L. Latronico, M. Lemoine-Goumard, J. Li, F. Longo, F. Loparco, M. N. Lovellette, P. Lubrano, J. D. Magill, S. Maldera, D. Malyshev, A. Manfreda, M. N. Mazziotta, J. E. McEnery, M. Meyer, P. F. Michelson, T. Mizuno, M. E. Monzani, A. Morselli, I. V. Moskalenko, M. Negro, E. Nuss, R. Ojha, N. Omodei, M. Orienti, E. Orlando, M. Palatiello, V. S. Paliya, J. S. Perkins, M. Persic, M. Pesce-Rollins, F. Piron, T. A. Porter, G. Principe, S. Rainò, R. Rando, B. Rani, M. Razzano, S. Razzaque, A. Reimer, O. Reimer, N. Renault-Tinacci, S. Ritz, L. S. Rochester, P. M. Saz Parkinson, C. Sgrò, E. J. Siskind, G. Spandre, P. Spinelli, D. J. Suson, H. Tajima, M. Takahashi, Y. Tanaka, J. B. Thayer, D. J. Thompson, L. Tibaldo, D. F. Torres, E. Torresi, G. Tosti, E. Troja, J. Valverde, G. Vianello, M. Vogel, K. Wood, M. Wood, G. Zaharijas, MAGIC Collaboration, M. L. Ahnen, S. Ansoldi, L. A. Antonelli, C. Arcaro, D. Baack, A. Babić, B. Banerjee, P. Bangale, U. Barres de Almeida, J. A. Barrio, J. Becerra González, W. Bednarek, E. Bernardini, A. Berti, W. Bhattacharyya, A. Biland, O. Blanch, G. Bonnoli, A. Carosi, R. Carosi, G. Ceribella, A. Chatterjee, S. M. Colak, P. Colin, E. Colombo, J. L. Contreras, J. Cortina, S. Covino, P. Cumani, P. Da Vela, F. Dazzi, A. De Angelis, B. De Lotto, M. Delfino, J. Delgado, F. Di Pierro, A. Domínguez, D. Dominis Prester, D. Dorner, M. Doro, S. Einecke, D. Elsaesser, V. Fallah Ramazani, A. Fernández-Barral, D. Fidalgo, L. Foffano, K. Pfrang,

M. V. Fonseca, L. Font, A. Franceschini, C. Fruck, D. Galindo, S. Gallozzi, R. J. García López, M. Garczarczyk, M. Gaug, P. Giammaria, N. Godinović, D. Gora, D. Guberman, D. Hadasch, A. Hahn, T. Hassan, M. Hayashida, J. Herrera, J. Hose, D. Hrupec, S. Inoue, K. Ishio, Y. Konno, H. Kubo, J. Kushida, D. Lelas, E. Lindfors, S. Lombardi, F. Longo, M. López, C. Maggio, P. Majumdar, M. Makariev, G. Maneva, M. Manganaro, K. Mannheim, L. Maraschi, M. Mariotti, M. Martínez, S. Masuda, D. Mazin, M. Minev, J. M. M, R. Mirzoyan, A. Moralejo, V. Moreno, E. Moretti, T. Nagayoshi, V. Neustroev, A. Niedzwiecki, M. Nievas Rosillo, C. Nigro, K. Nilsson, D. Ninci, K. Nishijima, K. Noda, L. Nogués, S. Paiano, J. Palacio, D. Paneque, R. Paoletti, J. M. Paredes, G. Pedaletti, M. Peresano, M. Persic, P. G. Prada Moroni, E. Prandini, I. Puljak, J. Rodriguez Garcia, I. Reichardt, W. Rhode, M. Ribó, J. Rico, C. Righi, A. Rugliancich, T. Saito, K. Satalecka, T. Schweizer, J. Sitarek, I. Šnidaric , D. Sobczynska, A. Stamerra, M. Strzys, T. Surić, M. Takahashi, F. Tavecchio, P. Temnikov, T. Terzić, M. Teshima, N. Torres-Albà, A. Treves, S. Tsujimoto, G. Vanzo, M. Vazquez Acosta, I. Vovk, J. E. Ward, M. Will, S, D. Zaric , AGILE Team, F. Lucarelli, M. Tavani, G. Piano, I. Donnarumma, C. Pittori, F. Verrecchia, G. Barbiellini, A. Bulgarelli, P. Caraveo, P. W. Cattaneo, S. Colafrancesco, E. Costa, G. Di Cocco, A. Ferrari, F. Gianotti, A. Giuliani, P. Lipari, S. Mereghetti, A. Morselli, L. Pacciani, F. Paoletti, N. Parmiggiani, A. Pellizzoni, P. Picozza, M. Pilia, A. Rappoldi, A. Trois, S. Vercellone, V. Vittorini, ASAS-SN Team, A. Franckowiak K. Z. Stanek, C. S. Kochanek, J. F. Beacom, T. A. Thompson, T. W. S. Holoien, S. Dong, J. L. Prieto, B. J. Shappee, S. Holmbo, HAWC Collaboration, A. U. Abeysekara, A. Albert, R. Alfaro, C. Alvarez, R. Arceo, J. C. Arteaga-Velázquez, D. Avila Rojas, H. A. Ayala Solares, A. Becerril, E. Belmont-Moreno, A. Bernal, K. S. Caballero-Mora, T. Capistrán, A. Carramiñana, S. Casanova, M. Castillo, U. Cotti, J. Cotzomi, S. Coutiño de León, C. De León, E. De la Fuente, R. Diaz Hernandez, S. Dichiara, B. L. Dingus, M. A. DuVernois, J. C. Díaz-Vélez, R. W. Ellsworth, K. Engel, D. W. Fiorino, H. Fleischhack, N. Fraija, J. A. García-González, F. Garfias, A. González Muñoz, M. M. González, J. A. Goodman, Z. Hampel-Arias, J. P. Harding, S. Hernand ez, B. Hona, F. Hueyotl-Zahuantitla, C. M. Hui, P. Hüntemeyer, A. Iriarte, A. Jardin-Blicq, V. Joshi, S. Kaufmann, G. J. Kunde, A. Lara,

R. J. Lauer, W. H. Lee, D. Lennarz, H. León Vargas, J. T. Linnemann, A. L. Longinotti, G. Luis-Raya, R. Luna-García, K. Malone, S. S. Marinelli, O. Martinez, I. Martinez-Castellanos, J. Martínez-Castro, H. Martínez-Huerta, J. A. Matthews, P. Miranda-Romagnoli, E. Moreno, M. Mostafá, A. Nayerhoda, L. Nellen, M. Newbold, M. U. Nisa, R. Noriega-Papaqui, R. Pelayo, J. Pretz, E. G. Pérez-Pérez, Z. Ren, C. D. Rho, C. Rivière, D. Rosa-González, M. Rosenberg, E. Ruiz-Velasco, E. Ruiz-Velasco, F. Salesa Greus, A. Sandoval, M. Schneider, H. Schoorlemmer, G. Sinnis, A. J. Smith, R. W. Springer, P. Surajbali, O. Tibolla, K. Tollefson, I. Torres, L. Villaseñor, T. Weisgarber, F. Werner, T. Yapici, Y. Gaurang, A. Zepeda, H. Zhou, J. D. Álvarez, H. E. S. S. Collaboration, H. Abdalla, E. O. Angüner, C. Armand, M. Backes, Y. Becherini, D. Berge, M. Böttcher, C. Boisson, J. Bolmont, S. Bonnefoy, P. Bordas, F. Brun, M. Büchele, T. Bulik, S. Caroff, A. Carosi, S. Casanova, M. Cerruti, N. Chakraborty, S. Chandra, A. Chen, S. Colafrancesco, I. D. Davids, C. Deil, J. Devin, A. Djannati-Ataï, K. Egberts, G. Emery, S. Eschbach, A. Fiasson, G. Fontaine, S. Funk, M. Füßling, Y. A. Gallant, F. Gaté, G. Giavitto, D. Glawion, J. F. Glicenstein, D. Gottschall, M. H. Grondin, M. Haupt, G. Henri, J. A. Hinton, C. Hoischen, T. L. Holch, D. Huber, M. Jamrozy, D. Jankowsky, F. Jankowsky, L. Jouvin, I. Jung-Richardt, D. Kerszberg, B. Khélifi, J. King, S. Klepser, W. Kluz niak, Nu. Komin, M. Kraus, J. Lefaucheur, A. Lemière, M. Lemoine-Goumard, J. P. Lenain, E. Leser, T. Lohse, R. López-Coto, M. Lorentz, I. Lypova, V. Marandon, G. Guillem Martí-Devesa, G. Maurin, A. M. W. Mitchell, R. Moderski, M. Mohamed, L. Mohrmann, E. Moulin, T. Murach, M. de Naurois, F. Niederwanger, J. Niemiec, L. Oakes, P. O'Brien, S. Ohm, M. Ostrowski, I. Oya, M. Panter, R. D. Parsons, C. Perennes, Q. Piel, S. Pita, V. Poireau, A. Priyana Noel, H. Prokoph, G. Pühlhofer, A. Quirrenbach, S. Raab, R. Rauth, M. Renaud, F. Rieger, L. Rinchiuso, C. Romoli, G. Rowell, B. Rudak, D. A. Sasaki, M. Sanchez, R. Schlickeiser, F. Schüssler, A. Schulz, U. Schwanke, M. Seglar-Arroyo, N. Shafi, R. Simoni, H. Sol, C. Stegmann, C. Steppa, T. Tavernier, A. M. Taylor, D. Tiziani, C. Trichard, M. Tsirou, C. van Eldik, C. van Rensburg, B. van Soelen, J. Veh, P. Vincent, F. Voisin, S. J. Wagner, R. M. Wagner, A. Wierzcholska, R. Zanin, A. A. Zdziarski, A. Zech, A. Ziegler, J. Zorn, N. Żywucka, INTEGRAL Team, V. Savchenko, C. Ferrigno,

A. Bazzano, R. Diehl, E. Kuulkers, P. Laurent, S. Mereghetti, L. Natalucci, F. Panessa, J. Rodi, P. Ubertini, Kiso Kanata, Subaru Observing Teams, T. Morokuma, K. Ohta, Y. T. Tanaka, H. Mori, M. Yamanaka, K. S. Kawabata, Y. Utsumi, T. Nakaoka, M. Kawabata, H. Nagashima, M. Yoshida, Y. Matsuoka, R. Itoh, Kapteyn Team, W. Keel, Liverpool Telescope Team, C. Copperwheat, I. Steele, Swift/NuSTAR Team, S. B. Cenko, D. F. Cowen, J. J. DeLaunay, P. A. Evans, D. B. Fox, A. Keivani, J. A. Kennea, F. E. Marshall, J. P. Osborne, M. Santander, A. Tohuvavohu, C. F. Turley, VERITAS Collaboration, A. U. Abeysekara, A. Archer, W. Benbow, R. Bird, A. Brill, R. Brose, M. Buchovecky, J. H. Buckley, V. Bugaev, J. L. Christiansen, M. P. Connolly, W. Cui, M. K. Daniel, M. Errando, A. Falcone, Q. Feng, J. P. Finley, L. Fortson, A. Furniss, O. Gueta, M. Hütten, O. Hervet, G. Hughes, T. B. Humensky, C. A. Johnson, P. Kaaret, P. Kar, N. Kelley-Hoskins, M. Kertzman, D. Kieda, M. Krause, F. Krennrich, S. Kumar, M. J. Lang, T. T. Y. Lin, G. Maier, S. McArthur, P. Moriarty, R. Mukherjee, D. Nieto, S. O'Brien, R. A. Ong, A. N. Otte, N. Park, A. Petrashyk, M. Pohl, A. Popkow, S. E. Pueschel, J. Quinn, K. Ragan, P. T. Reynolds, G. T. Richards, E. Roache, C. Rulten, I. Sadeh, M. Santander, S. S. Scott, G. H. Sembroski, K. Shahinyan, I. Sushch, S. Trépanier, J. Tyler, V. V. Vassiliev, S. P. Wakely, A. Weinstein, R. M. Wells, P. Wilcox, A. Wilhelm, D. A. Williams, B. Zitzer, VLA/B Team, A. J. Tetarenko, A. E. Kimball, J. C. A. Miller-Jones, and G. R. Sivakoff.

Multimessenger observations of a flaring blazar coincident with high-energy neutrino IceCube-170922A.

Science, 361(6398):eaat1378, July 2018.

[76] IceCube Collaboration, M. G. Aartsen, M. Ackermann, J. Adams, J. A. Aguilar, M. Ahlers, M. Ahrens, I. Al Samarai, D. Altmann, K. Andeen, T. Anderson, I. Ansseau, G. Anton, C. Argüelles, B. Arsioli, J. Auffenberg, S. Axani, H. Bagherpour, X. Bai, J. P. Barron, S. W. Barwick, V. Baum, R. Bay, J. J. Beatty, J. Becker Tjus, K. H. Becker, S. BenZvi, D. Berley, E. Bernardini, D. Z. Besson, G. Binder, D. Bindig, E. Blaufuss, S. Blot, C. Bohm, M. Börner, F. Bos, S. Böser, O. Botner, E. Bourbeau, J. Bourbeau, F. Bradascio, J. Braun, M. Brenzke, H. P. Bretz, S. Bron, J. Brostean-Kaiser, A. Burgman, R. S. Busse, T. Carver, E. Cheung, D. Chirkin, A. Christov, K. Clark, L. Classen,

S. Coenders, G. H. Collin, J. M. Conrad, P. Coppin, P. Correa, D. F. Cowen, R. Cross, P. Dave, M. Day, J. P. A. M. de André, C. De Clercq, J. J. DeLaunay, H. Dembinski, S. DeRidder, P. Desiati, K. D. de Vries, G. de Wasseige, M. de With, T. DeYoung, J. C. Díaz-Vélez, V. di Lorenzo, H. Dujmovic, J. P. Dumm, M. Dunkman, E. Dvorak, B. Eberhardt, T. Ehrhardt, B. Eichmann, P. Eller, P. A. Evenson, S. Fahey, A. R. Fazely, J. Felde, K. Filimonov, C. Finley, S. Flis, A. Franckowiak, E. Friedman, A. Fritz, T. K. Gaisser, J. Gallagher, L. Gerhardt, K. Ghorbani, P. Giommi, T. Glauch, T. Glüsenkamp, A. Goldschmidt, J. G. Gonzalez, D. Grant, Z. Griffith, C. Haack, A. Hallgren, F. Halzen, K. Hanson, D. Hebecker, D. Heereman, K. Helbing, R. Hellauer, S. Hickford, J. Hignight, G. C. Hill, K. D. Hoffman, R. Hoffmann, T. Hoinka, B. Hokanson-Fasig, K. Hoshina, F. Huang, M. Huber, K. Hultqvist, M. Hünnefeld, R. Hussain, S. In, N. Iovine, A. Ishihara, E. Jacobi, G. S. Japaridze, M. Jeong, K. Jero, B. J. P. Jones, P. Kalaczynski, W. Kang, A. Kappes, D. Kappesser, T. Karg, A. Karle, U. Katz, M. Kauer, A. Keivani, J. L. Kelley, A. Kheirandish, J. Kim, M. Kim, T. Kintscher, J. Kiryluk, T. Kittler, S. R. Klein, R. Koirala, H. Kolanoski, L. Köpke, C. Kopper, S. Kopper, J. P. Koschinsky, D. J. Koskinen, M. Kowalski, B. Krammer, K. Krings, M. Kroll, G. Krückl, S. Kunwar, N. Kurahashi, T. Kuwabara, A. Kyriacou, M. Labare, J. L. Lanfranchi, M. J. Larson, F. Lauber, K. Leonard, M. Lesiak-Bzdak, M. Leuermann, Q. R. Liu, C. J. Lozano Mariscal, L. Lu, J. Lünemann, W. Luszczak, J. Madsen, G. Maggi, K. B. M. Mahn, S. Mancina, R. Maruyama, K. Mase, R. Maunu, K. Meagher, M. Medici, M. Meier, T. Menne, G. Merino, T. Meures, S. Miarecki, J. Micallef, G. Momenté, T. Montaruli, R. W. Moore, R. Morse, M. Moulai, R. Nahnhauer, P. Nakarmi, U. Naumann, G. Neer, H. Niederhausen, S. C. Nowicki, D. R. Nygren, A. Obertacke Pollmann, A. Olivas, A. O'Murchadha, E. O'Sullivan, P. Padovani, T. Palczewski, H. Pand ya, D. V. Pankova, P. Peiffer, J. A. Pepper, C. Pérez de los Heros, D. Pieloth, E. Pinat, M. Plum, P. B. Price, G. T. Przybylski, C. Raab, L. Rädel, M. Rameez, K. Rawlins, I. C. Rea, R. Reimann, B. Relethford, M. Relich, E. Resconi, W. Rhode, M. Richman, S. Robertson, M. Rongen, C. Rott, T. Ruhe, D. Ryckbosch, D. Rysewyk, I. Safa, N. Sahakyan, T. Sälzer, S. E. Sanchez Herrera, A. Sandrock, J. Sandroos, M. Santander, S. Sarkar, S. Sarkar, K. Satalecka, P. Schlunder, T. Schmidt, A. Schneider,

S. Schoenen, S. Schöneberg, L. Schumacher, S. Sclafani, D. Seckel, S. Seunarine, J. Soedingrekso, D. Soldin, M. Song, G. M. Spiczak, C. Spiering, J. Stachurska, M. Stamatikos, T. Stanev, A. Stasik, J. Stettner, A. Steuer, T. Stezelberger, R. G. Stokstad, A. Stößl, N. L. Strotjohann, T. Stuttard, G. W. Sullivan, M. Sutherland, I. Taboada, J. Tatar, F. Tenholt, S. Ter-Antonyan, A. Terliuk, S. Tilav, P. A. Toale, M. N. Tobin, C. Toennis, S. Toscano, D. Tosi, M. Tselengidou, C. F. Tung, A. Turcati, C. F. Turley, B. Ty, E. Unger, M. Usner, J. Vandenbroucke, W. Van Driessche, D. van Eijk, N. van Eijndhoven, S. Vanheule, J. van Santen, E. Vogel, M. Vraeghe, C. Walck, A. Wallace, M. Wallraff, F. D. Wandler, N. Wand kowsky, A. Waza, C. Weaver, M. J. Weiss, C. Wendt, J. Werthebach, S. Westerhoff, B. J. Whelan, N. Whitehorn, K. Wiebe, C. H. Wiebusch, L. Wille, D. R. Williams, L. Wills, M. Wolf, J. Wood, T. R. Wood, K. Woschnagg, D. L. Xu, X. W. Xu, Y. Xu, J. P. Yanez, G. Yodh, S. Yoshida, and T. Yuan.
Neutrino emission from the direction of the blazar TXS 0506+056 prior to the IceCube-170922A alert.
Science, 361(6398):147–151, July 2018.

[77] H. T. Intema, P. Jagannathan, K. P. Mooley, and D. A. Frail.
The GMRT 150 MHz all-sky radio survey. First alternative data release TGSS ADR1.
A&A, 598:A78, February 2017.

[78] Svetlana G. Jorstad, Alan P. Marscher, Paul S. Smith, Valeri M. Larionov, Iván Agudo, Mark Gurwell, Ann E. Wehrle, Anne Lähteenmäki, Maria G. Nikolashvili, Gary D. Schmidt, Arkady A. Arkharov, Dmitry A. Blinov, Kelly Blumenthal, Carolina Casadio, Revaz A. Chigladze, Natalia V. Efimova, Joseph R. Eggen, José L. Gómez, Dirk Grupe, Vladimir A. Hagen-Thorn, Manasvita Joshi, Givi N. Kimeridze, Tatiana S. Konstantinova, Evgenia N. Kopatskaya, Omar M. Kurtanidze, Sofia O. Kurtanidze, Elena G. Larionova, Liudmilla V. Larionova, Lorand A. Sigua, Nicholas R. MacDonald, Jeremy D. Maune, Ian M. McHardy, H. Richard Miller, Sol N. Molina, Daria A. Morozova, Terri Scott, Brian W. Taylor, Merja Tornikoski, Ivan S. Troitsky, Clemens Thum, Gary Walker, Karen E. Williamson, Stephanie Sallum, Santina Consiglio, and Vladimir Strelnitski.

A Tight Connection between Gamma-Ray Outbursts and Parsec-scale Jet Activity in the Quasar 3C 454.3.
ApJ, 773(2):147, August 2013.

[79] Shi-Ju Kang, Yong-Gang Zheng, Qingwen Wu, Liang Chen, and Yue Yin.
On the origin of GeV spectral break for Fermi blazars: 3C 454.3.
arXiv e-prints, page arXiv:2102.08962, February 2021.

[80] T. Kawase, H. Negoro, S. Ueno, H. Tomida, N. Isobe, M. Ishikawa, Y. Sugawara, T. Mihara, M. Sugizaki, M. Serino, S. Nakahira, W. Iwakiri, M. Shidatsu, K. Makishima, M. Matsuoka, N. Kawai, S. Sugita, T. Yoshii, Y. Tachibana, S. Harita, K. Morita, Y. Muraki, A. Yoshida, T. Sakamoto, Y. Kawakubo, Y. Kitaoka, H. Tsunemi, T. Yoneyama, M. Nakajima, A. Sakamaki, Y. Ueda, T. Hori, A. Tanimoto, S. Oda, Y. Tsuboi, Y. Nakamura, R. Sasaki, M. Yamauchi, C. Hanyu, K. Hidaka, K. Yamaoka, and T. Kawamuro.
MAXI/GSC observations of the gamma-ray/X-ray transient Fermi J1544-0649.
The Astronomer's Telegram, 10495:1, June 2017.

[81] A. Keivani, K. Murase, M. Petropoulou, D. B. Fox, S. B. Cenko, S. Chaty, A. Coleiro, J. J. DeLaunay, S. Dimitrakoudis, P. A. Evans, J. A. Kennea, F. E. Marshall, A. Mastichiadis, J. P. Osborne, M. Santander, A. Tohuvavohu, and C. F. Turley.
A Multimessenger Picture of the Flaring Blazar TXS 0506+056: Implications for High-energy Neutrino Emission and Cosmic-Ray Acceleration.
ApJ, 864:84, September 2018.

[82] J. G. Kirk, F. M. Rieger, and A. Mastichiadis.
Particle acceleration and synchrotron emission in blazar jets.
A&A, 333:452–458, May 1998.

[83] C. S. Kochanek, B. J. Shappee, K. Z. Stanek, T. W. S. Holoien, Todd A. Thompson, J. L. Prieto, Subo Dong, J. V. Shields, D. Will, C. Britt, D. Perzanowski, and G. Pojmański.
The All-Sky Automated Survey for Supernovae (ASAS-SN) Light Curve Server v1.0.
, 129(980):104502, October 2017.

[84] Yi Liu, Dong Rong Jiang, and Min Feng Gu.
The Jet Power, Radio Loudness, and Black Hole Mass in Radio-loud Active Galactic Nuclei.
ApJ, 637(2):669–681, February 2006.

[85] B. Lott, L. Escande, S. Larsson, and J. Ballet.
An adaptive-binning method for generating constant-uncertainty/constant-significance light curves with Fermi-LAT data.
A&A, 544:A6, August 2012.

[86] B. Lott, D. Gasparrini, and S. Ciprini.
The Fourth Catalog of Active Galactic Nuclei Detected by the Fermi Large Area Telescope – Data Release 2.
arXiv e-prints, page arXiv:2010.08406, October 2020.

[87] K. Mannheim.
The proton blazar.
A&A, 269:67–76, March 1993.

[88] K. Mannheim and P. L. Biermann.
Photomeson production in active galactic nuclei.
A&A, 221:211–220, September 1989.

[89] L. Maraschi, G. Ghisellini, and A. Celotti.
A Jet Model for the Gamma-Ray–emitting Blazar 3C 279.
ApJL, 397:L5, September 1992.

[90] L. Maraschi, G. Ghisellini, and A. Celotti.
A jet model for the gamma-ray emitting blazar 3C 279.
ApJL, 397:L5–L9, September 1992.

[91] E. Massaro, A. Tramacere, M. Perri, P. Giommi, and G. Tosti.
Log-parabolic spectra and particle acceleration in blazars. III. SSC emission in the TeV band from Mkn501.
A&A, 448(3):861–871, March 2006.

[92] F. Massaro, R. D'Abrusco, G. Tosti, M. Ajello, A. Paggi, and D. Gasparrini.
Unidentified γ-Ray Sources: Hunting γ-Ray Blazars.
ApJ, 752(1):61, June 2012.

[93] F. Massaro, E. J. Marchesini, R. D'Abrusco, N. Masetti, I. Andruchow, and Howard A. Smith.
Radio-weak BL Lac Objects in the Fermi Era.
ApJ, 834(2):113, January 2017.

[94] Apostolos Mastichiadis and Maria Petropoulou.
Hadronic X-ray Flares from Blazars.
arXiv e-prints, page arXiv:2009.12158, September 2020.

[95] Masaru Matsuoka, Kazuyoshi Kawasaki, Shiro Ueno, Hiroshi Tomida, Mitsuhiro Kohama, Motoko Suzuki, Yasuki Adachi, Masaki Ishikawa, Tatehiro Mihara, Mutsumi Sugizaki, Naoki Isobe, Yujin Nakagawa, Hiroshi Tsunemi, Emi Miyata, Nobuyuki Kawai, Jun Kataoka, Mikio Morii, Atsumasa Yoshida, Hitoshi Negoro, Motoki Nakajima, Yoshihiro Ueda, Hirotaka Chujo, Kazutaka Yamaoka, Osamu Yamazaki, Satoshi Nakahira, Tetsuya You, Ryoji Ishiwata, Sho Miyoshi, Satoshi Eguchi, Kazuo Hiroi, Haruyoshi Katayama, and Ken Ebisawa.
The MAXI Mission on the ISS: Science and Instruments for Monitoring All-Sky X-Ray Images.
PASJ, 61:999, October 2009.

[96] J. R. Mattox, D. L. Bertsch, J. Chiang, B. L. Dingus, S. W. Digel, J. A. Esposito, J. M. Fierro, R. C. Hartman, S. D. Hunter, G. Kanbach, D. A. Kniffen, Y. C. Lin, D. J. Macomb, H. A. Mayer-Hasselwander, P. F. Michelson, C. von Montigny, R. Mukherjee, P. L. Nolan, P. V. Ramanamurthy, E. Schneid, P. Sreekumar, D. J. Thompson, and T. D. Willis.
The Likelihood Analysis of EGRET Data.
ApJ, 461:396, April 1996.

[97] A. Mücke and R. J. Protheroe.
A proton synchrotron blazar model for flaring in Markarian 501.
Astroparticle Physics, 15(1):121–136, March 2001.

[98] A. Mücke, R. J. Protheroe, R. Engel, J. P. Rachen, and T. Stanev.
BL Lac objects in the synchrotron proton blazar model.
Astroparticle Physics, 18:593–613, March 2003.

[99] K. Murase, F. Oikonomou, and M. Petropoulou.

Blazar Flares as an Origin of High-energy Cosmic Neutrinos?
ApJ, 865:124, October 2018.

[100] K. Nalewajko.
The brightest gamma-ray flares of blazars.
MNRAS, 430:1324–1333, April 2013.

[101] L. Pacciani, F. Tavecchio, I. Donnarumma, A. Stamerra, L. Carrasco, E. Recillas, A. Porras, and M. Uemura.
Exploring the Blazar Zone in High-energy Flares of FSRQs.
ApJ, 790(1):45, August 2014.

[102] L. Pacciani, V. Vittorini, M. Tavani, M. T. Fiocchi, S. Vercellone, F. D'Ammando, T. Sakamoto, E. Pian, C. M. Raiteri, M. Villata, M. Sasada, R. Itoh, M. Yamanaka, M. Uemura, E. Striani, D. Fugazza, A. Tiengo, H. A. Krimm, M. C. Stroh, A. D. Falcone, P. A. Curran, A. C. Sadun, A. Lahteenmaki, M. Tornikoski, H. D. Aller, M. F. Aller, C. S. Lin, V. M. Larionov, P. Leto, L. O. Takalo, A. Berdyugin, M. A. Gurwell, A. Bulgarelli, A. W. Chen, I. Donnarumma, A. Giuliani, F. Longo, G. Pucella, A. Argan, G. Barbiellini, P. Caraveo, P. W. Cattaneo, E. Costa, G. De Paris, E. Del Monte, G. Di Cocco, Y. Evangelista, A. Ferrari, M. Feroci, M. Fiorini, F. Fuschino, M. Galli, F. Gianotti, C. Labanti, I. Lapshov, F. Lazzarotto, P. Lipari, M. Marisaldi, S. Mereghetti, E. Morelli, E. Moretti, A. Morselli, A. Pellizzoni, F. Perotti, G. Piano, P. Picozza, M. Pilia, M. Prest, M. Rapisarda, A. Rappoldi, A. Rubini, S. Sabatini, P. Soffitta, M. Trifoglio, A. Trois, E. Vallazza, D. Zanello, S. Colafrancesco, C. Pittori, F. Verrecchia, P. Santolamazza, F. Lucarelli, P. Giommi, and L. Salotti.
The 2009 December Gamma-ray Flare of 3C 454.3: The Multifrequency Campaign.
ApJL, 716(2):L170–L175, June 2010.

[103] P. Padovani, D. M. Alexander, R. J. Assef, B. De Marco, P. Giommi, R. C. Hickox, G. T. Richards, V. Smolčić, E. Hatziminaoglou, V. Mainieri, and M. Salvato.
Active galactic nuclei: what's in a name?
A&AR, 25:2, August 2017.

[104] P. Padovani, D. M. Alexander, R. J. Assef, B. De Marco, P. Giommi, R. C. Hickox, G. T. Richards, V. Smolčić, E. Hatziminaoglou, V. Mainieri, and M. Salvato.
Active galactic nuclei: what's in a name?
A&AR, 25(1):2, August 2017.

[105] P. Padovani, P. Giommi, E. Resconi, T. Glauch, B. Arsioli, N. Sahakyan, and M. Huber.
Dissecting the region around IceCube-170922A: the blazar TXS 0506+056 as the first cosmic neutrino source.
MNRAS, 480(1):192–203, October 2018.

[106] P. Padovani, E. Resconi, P. Giommi, B. Arsioli, and Y. L. Chang.
Extreme blazars as counterparts of IceCube astrophysical neutrinos.
MNRAS, 457(4):3582–3592, April 2016.

[107] Paolo Padovani and Paolo Giommi.
The connection between x-ray- and radio-selected BL Lacertae objects.
ApJ, 444:567–581, 1995.

[108] A. Paggi, A. Cavaliere, V. Vittorini, F. D'Ammando, and M. Tavani.
Flaring Patterns in Blazars.
ApJ, 736(2):128, August 2011.

[109] Vaidehi S. Paliya, M. Ajello, R. Ojha, R. Angioni, C. C. Cheung, K. Tanada, T. Pursimo, P. Galindo, I. R. Losada, L. Siltala, A. A. Djupvik, L. Marcotulli, and D. Hartmann.
Detection of a Gamma-Ray Flare from the High-redshift Blazar DA 193.
ApJ, 871(2):211, February 2019.

[110] Elena Pian, Giuseppe Vacanti, Gianpiero Tagliaferri, Gabriele Ghisellini, Laura Maraschi, Aldo Treves, C. Megan Urry, Fabrizio Fiore, Paolo Giommi, Eliana Palazzi, Lucio Chiappetti, and Rita M. Sambruna.
BeppoSAX Observations of Unprecedented Synchrotron Activity in the BL Lacertae Object Markarian 501.
ApJL, 492(1):L17–L20, January 1998.

[111] T. S. Poole, A. A. Breeveld, M. J. Page, W. Landsman, S. T. Holland, P. Roming, N. P. M. Kuin, P. J. Brown, C. Gronwall, S. Hunsberger,

S. Koch, K. O. Mason, P. Schady, D. vanden Berk, A. J. Blustin, P. Boyd, P. Broos, M. Carter, M. M. Chester, A. Cucchiara, B. Hancock, H. Huckle, S. Immler, M. Ivanushkina, T. Kennedy, F. Marshall, A. Morgan, S. B. Pandey, M. de Pasquale, P. J. Smith, and M. Still.
Photometric calibration of the Swift ultraviolet/optical telescope.
MNRAS, 383(2):627–645, January 2008.

[112] Juri Poutanen and Boris Stern.
GeV Breaks in Blazars as a Result of Gamma-ray Absorption Within the Broad-line Region.
ApJL, 717(2):L118–L121, July 2010.

[113] C. M. Raiteri, M. Villata, J. A. Acosta-Pulido, I. Agudo, A. A. Arkharov, R. Bachev, G. V. Baida, E. Benítez, G. A. Borman, W. Boschin, V. Bozhilov, M. S. Butuzova, P. Calcidese, M. I. Carnerero, D. Carosati, C. Casadio, N. Castro-Segura, W. P. Chen, G. Damljanovic, F. D'Ammando, A. di Paola, J. Echevarría, N. V. Efimova, Sh. A. Ehgamberdiev, C. Espinosa, A. Fuentes, A. Giunta, J. L. Gómez, T. S. Grishina, M. A. Gurwell, D. Hiriart, H. Jermak, B. Jordan, S. G. Jorstad, M. Joshi, E. N. Kopatskaya, K. Kuratov, O. M. Kurtanidze, S. O. Kurtanidze, A. Lähteenmäki, V. M. Larionov, E. G. Larionova, L. V. Larionova, C. Lázaro, C. S. Lin, M. P. Malmrose, A. P. Marscher, K. Matsumoto, B. McBreen, R. Michel, B. Mihov, M. Minev, D. O. Mirzaqulov, A. A. Mokrushina, S. N. Molina, J. W. Moody, D. A. Morozova, S. V. Nazarov, M. G. Nikolashvili, J. M. Ohlert, D. N. Okhmat, E. Ovcharov, F. Pinna, T. A. Polakis, C. Protasio, T. Pursimo, F. J. Redondo-Lorenzo, N. Rizzi, G. Rodriguez-Coira, K. Sadakane, A. C. Sadun, M. R. Samal, S. S. Savchenko, E. Semkov, B. A. Skiff, L. Slavcheva-Mihova, P. S. Smith, I. A. Steele, A. Strigachev, J. Tammi, C. Thum, M. Tornikoski, Yu. V. Troitskaya, I. S. Troitsky, A. A. Vasilyev, and O. Vince.
Blazar spectral variability as explained by a twisted inhomogeneous jet.
Nature, 552(7685):374–377, December 2017.

[114] C. M. Raiteri, M. Villata, M. F. Aller, M. A. Gurwell, O. M. Kurtanidze, A. Lähteenmäki, V. M. Larionov, P. Romano, S. Vercellone, I. Agudo, H. D. Aller, A. A. Arkharov, U. Bach, E. Benítez, A. Berdyugin, D. A.

Blinov, E. V. Borisova, M. Böttcher, O. J. A. Bravo Calle, C. S. Buemi, P. Calcidese, D. Carosati, R. Casas, W. P. Chen, N. V. Efimova, J. L. Gómez, C. Gusbar, K. Hawkins, J. Heidt, D. Hiriart, H. Y. Hsiao, B. Jordan, S. G. Jorstad, M. Joshi, G. N. Kimeridze, E. Koptelova, T. S. Konstantinova, E. N. Kopatskaya, S. O. Kurtanidze, E. G. Larionova, L. V. Larionova, P. Leto, Y. Li, R. Ligustri, E. Lindfors, M. Lister, A. P. Marscher, S. N. Molina, D. A. Morozova, E. Nieppola, M. G. Nikolashvili, K. Nilsson, N. Palma, M. Pasanen, R. Reinthal, V. Roberts, J. A. Ros, P. Roustazadeh, A. C. Sadun, T. Sakamoto, R. D. Schwartz, L. A. Sigua, A. Sillanpää, L. O. Takalo, J. Tammi, B. Taylor, M. Tornikoski, C. Trigilio, I. S. Troitsky, G. Umana, A. Volvach, and T. A. Yuldasheva.

The long-lasting activity of ¡ASTROBJ¿3C 454.3¡/ASTROBJ¿. GASP-WEBT and satellite observations in 2008-2010.

A&A, 534:A87, October 2011.

[115] C. M. Raiteri, M. Villata, V. M. Larionov, M. A. Gurwell, W. P. Chen, O. M. Kurtanidze, M. F. Aller, M. Böttcher, P. Calcidese, F. Hroch, A. Lähteenmäki, C. U. Lee, K. Nilsson, J. Ohlert, I. E. Papadakis, I. Agudo, H. D. Aller, E. Angelakis, A. A. Arkharov, U. Bach, R. Bachev, A. Berdyugin, C. S. Buemi, D. Carosati, P. Charlot, E. Chatzopoulos, E. Forné, A. Frasca, L. Fuhrmann, J. L. Gómez, A. C. Gupta, V. A. Hagen-Thorn, W. S. Hsiao, B. Jordan, S. G. Jorstad, T. S. Konstantinova, E. N. Kopatskaya, T. P. Krichbaum, L. Lanteri, L. V. Larionova, G. Latev, J. F. Le Campion, P. Leto, H. C. Lin, N. Marchili, E. Marilli, A. P. Marscher, B. McBreen, B. Mihov, R. Nesci, F. Nicastro, M. G. Nikolashvili, R. Novak, E. Ovcharov, E. Pian, D. Principe, T. Pursimo, B. Ragozzine, J. A. Ros, A. C. Sadun, R. Sagar, E. Semkov, R. L. Smart, N. Smith, A. Strigachev, L. O. Takalo, M. Tavani, M. Tornikoski, C. Trigilio, K. Uckert, G. Umana, A. Valcheva, S. Vercellone, A. Volvach, and H. Wiesemeyer.

A new activity phase of the blazar ¡ASTROBJ¿3C 454.3¡/ASTROBJ¿. Multifrequency observations by the WEBT and XMM-Newton in 2007-2008.

A&A, 491(3):755–766, December 2008.

[116] B. Rani, B. Lott, T. P. Krichbaum, L. Fuhrmann, and J. A. Zensus.

Constraining the location of rapid gamma-ray flares in the flat spectrum radio quasar 3C 273.
A&A, 557:A71, September 2013.

[117] B. Rani, B. Lott, T. P. Krichbaum, L. Fuhrmann, and J. A. Zensus.
Constraining the location of rapid gamma-ray flares in the flat spectrum radio quasar 3C 273.
A&A, 557:A71, September 2013.

[118] E. Resconi, S. Coenders, P. Padovani, P. Giommi, and L. Caccianiga.
Connecting blazars with ultrahigh-energy cosmic rays and astrophysical neutrinos.
MNRAS, 468(1):597–606, June 2017.

[119] Stephen P. Reynolds.
Synchrotron-Loss Spectral Breaks in Pulsar-Wind Nebulae and Extragalactic Jets.
ApJ, 703(1):662–670, September 2009.

[120] C. Righi, F. Tavecchio, and L. Pacciani.
A multiwavelength view of BL Lac neutrino candidates.
MNRAS, 484(2):2067–2077, April 2019.

[121] Peter W. A. Roming, Thomas E. Kennedy, Keith O. Mason, John A. Nousek, Lindy Ahr, Richard E. Bingham, Patrick S. Broos, Mary J. Carter, Barry K. Hancock, Howard E. Huckle, S. D. Hunsberger, Hajime Kawakami, Ronnie Killough, T. Scott Koch, Michael K. McLelland, Kelly Smith, Philip J. Smith, Juan Carlos Soto, Patricia T. Boyd, Alice A. Breeveld, Stephen T. Holland, Mariya Ivanushkina, Michael S. Pryzby, Martin D. Still, and Joseph Stock.
The Swift Ultra-Violet/Optical Telescope.
Space Science Reviews, 120(3-4):95–142, October 2005.

[122] N. Sahakyan.
Lepto-hadronic γ-Ray and Neutrino Emission from the Jet of TXS 0506+056.
ApJ, 866:109, October 2018.

[123] N. Sahakyan.
Origin of the multiwavelength emission of PKS 0502+049.

A&A, 622:A144, February 2019.

[124] N. Sahakyan.
Broad-band study of high-synchrotron-peaked BL Lac object 1ES 1218+304.
MNRAS, 496(4):5518–5527, July 2020.

[125] N. Sahakyan.
Investigation of the γ-ray spectrum of CTA 102 during the exceptional flaring state in 2016-2017.
A&A, 635:A25, March 2020.

[126] N. Sahakyan, V. Baghmanyan, and D. Zargaryan.
Fermi-LAT observation of nonblazar AGNs.
A&A, 614:A6, June 2018.

[127] N. Sahakyan and S. Gasparyan.
High energy gamma-ray emission from PKS 1441+25.
MNRAS, 470(3):2861–2869, September 2017.

[128] N. Sahakyan and P. Giommi.
The strange case of the transient HBL blazar 4FGL J1544.3-0649.
MNRAS, 502(1):836–844, March 2021.

[129] N. Sahakyan, D. Israyelyan, G. Harutyunyan, M. Khachatryan, and S. Gasparyan.
Multiwavelength study of high-redshift blazars.
MNRAS, 498(2):2594–2613, August 2020.

[130] S. Saito, Ł. Stawarz, and et al.
Very Rapid High-amplitude Gamma-Ray Variability in Luminous Blazar PKS 1510-089 Studied with Fermi-LAT.
ApJL, 766:L11, March 2013.

[131] T. Sbarrato, G. Ghisellini, L. Maraschi, and M. Colpi.
The relation between broad lines and γ-ray luminosities in Fermi blazars.
MNRAS, 421(2):1764–1778, April 2012.

[132] T. Sbarrato, G. Ghisellini, L. Maraschi, and M. Colpi.

The relation between broad lines and γ-ray luminosities in Fermi blazars.
MNRAS, 421:1764–1778, April 2012.

[133] Jeffrey D. Scargle, Jay P. Norris, Brad Jackson, and James Chiang.
Studies in Astronomical Time Series Analysis. VI. Bayesian Block Representations.
ApJ, 764(2):167, February 2013.

[134] Edward F. Schlafly and Douglas P. Finkbeiner.
Measuring Reddening with Sloan Digital Sky Survey Stellar Spectra and Recalibrating SFD.
ApJ, 737(2):103, August 2011.

[135] A. Shukla, K. Mannheim, S. R. Patel, J. Roy, V. R. Chitnis, D. Dorner, A. R. Rao, G. C. Anupama, and C. Wendel.
Short-timescale γ-Ray Variability in CTA 102.
ApJL, 854(2):L26, February 2018.

[136] M. Sikora, M. C. Begelman, and M. J. Rees.
Comptonization of diffuse ambient radiation by a relativistic jet: The source of gamma rays from blazars?
ApJ, 421:153–162, January 1994.

[137] Marek Sikora, Łukasz Stawarz, Rafał Moderski, Krzysztof Nalewajko, and Greg M. Madejski.
Constraining Emission Models of Luminous Blazar Sources.
ApJ, 704(1):38–50, October 2009.

[138] Lorenzo Sironi and Anatoly Spitkovsky.
Relativistic Reconnection: An Efficient Source of Non-thermal Particles.
ApJL, 783(1):L21, March 2014.

[139] Andrei Sokolov, Alan P. Marscher, and Ian M. McHardy.
Synchrotron Self-Compton Model for Rapid Nonthermal Flares in Blazars with Frequency-dependent Time Lags.
ApJ, 613(2):725–746, October 2004.

[140] Errol J. Summerlin and Matthew G. Baring.

Diffusive Acceleration of Particles at Oblique, Relativistic, Magnetohydrodynamic Shocks.
ApJ, 745(1):63, January 2012.

[141] F. Tavecchio, G. Ghisellini, G. Bonnoli, and L. Foschini.
Extreme TeV blazars and the intergalactic magnetic field.
MNRAS, 414(4):3566–3576, July 2011.

[142] A. Tramacere, P. Giommi, M. Perri, F. Verrecchia, and G. Tosti.
Swift observations of the very intense flaring activity of Mrk 421 during 2006. I. Phenomenological picture of electron acceleration and predictions for MeV/GeV emission.
A&A, 501(3):879–898, July 2009.

[143] A. Tramacere, E. Massaro, and A. M. Taylor.
Stochastic Acceleration and the Evolution of Spectral Distributions in Synchro-Self-Compton Sources: A Self-consistent Modeling of Blazars' Flares.
ApJ, 739(2):66, October 2011.

[144] C. Megan Urry and Paolo Padovani.
Unified Schemes for Radio-Loud Active Galactic Nuclei.
, 107:803, September 1995.

[145] C Megan Urry and Paolo Padovani.
Unified Schemes for Radio-Loud Active Galactic Nuclei.
PASP, 107:803–845, 1995.

[146] F. Ursini, L. Bassani, F. Panessa, E. Pian, G. Bruni, A. Bazzano, N. Masetti, K. Sokolovsky, and P. Ubertini.
An XMM-Newton look at the strongly variable radio-weak BL Lac Fermi J1544-0639.
A&A, 622:A116, February 2019.

[147] S. Vercellone, F. D'Ammando, V. Vittorini, I. Donnarumma, G. Pucella, M. Tavani, A. Ferrari, C. M. Raiteri, M. Villata, P. Romano, H. Krimm, A. Tiengo, A. W. Chen, G. Giovannini, T. Venturi, M. Giroletti, Y. Y. Kovalev, K. Sokolovsky, A. B. Pushkarev, M. L. Lister, A. Argan, G. Barbiellini, A. Bulgarelli, P. Caraveo, P. W. Cattaneo, V. Cocco, E. Costa, E. Del Monte, G. De Paris, G. Di

Cocco, Y. Evangelista, M. Feroci, M. Fiorini, F. Fornari, T. Froysland, F. Fuschino, M. Galli, F. Gianotti, C. Labanti, I. Lapshov, F. Lazzarotto, P. Lipari, F. Longo, A. Giuliani, M. Marisaldi, S. Mereghetti, A. Morselli, A. Pellizzoni, L. Pacciani, F. Perotti, G. Piano, P. Picozza, M. Pilia, M. Prest, M. Rapisarda, A. Rappoldi, S. Sabatini, P. Soffitta, E. Striani, M. Trifoglio, A. Trois, E. Vallazza, A. Zambra, D. Zanello, C. Pittori, F. Verrecchia, P. Santolamazza, P. Giommi, S. Colafrancesco, L. Salotti, I. Agudo, H. D. Aller, M. F. Aller, A. A. Arkharov, U. Bach, R. Bachev, P. Beltrame, E. Benítez, M. Böttcher, C. S. Buemi, P. Calcidese, D. Capezzali, D. Carosati, W. P. Chen, D. Da Rio, A. Di Paola, M. Dolci, D. Dultzin, E. Forné, J. L. Gómez, M. A. Gurwell, V. A. Hagen-Thorn, A. Halkola, J. Heidt, D. Hiriart, T. Hovatta, H. Y. Hsiao, S. G. Jorstad, G. Kimeridze, T. S. Konstantinova, E. N. Kopatskaya, E. Koptelova, O. Kurtanidze, A. Lähteenmäki, V. M. Larionov, P. Leto, R. Ligustri, E. Lindfors, J. M. Lopez, A. P. Marscher, R. Mujica, M. Nikolashvili, K. Nilsson, M. Mommert, N. Palma, M. Pasanen, M. Roca-Sogorb, J. A. Ros, P. Roustazadeh, A. C. Sadun, J. Saino, L. Sigua, M. Sorcia, L. O. Takalo, M. Tornikoski, C. Trigilio, R. Turchetti, and G. Umana.
Multiwavelength Observations of 3C 454.3. III. Eighteen Months of Agile Monitoring of the "Crazy Diamond".
ApJ, 712(1):405–420, March 2010.

[148] S. Vercellone, E. Striani, V. Vittorini, I. Donnarumma, L. Pacciani, G. Pucella, M. Tavani, C. M. Raiteri, M. Villata, P. Romano, M. Fiocchi, A. Bazzano, V. Bianchin, C. Ferrigno, L. Maraschi, E. Pian, M. Türler, P. Ubertini, A. Bulgarelli, A. W. Chen, A. Giuliani, F. Longo, G. Barbiellini, M. Cardillo, P. W. Cattaneo, E. Del Monte, Y. Evangelista, M. Feroci, A. Ferrari, F. Fuschino, F. Gianotti, M. Giusti, F. Lazzarotto, A. Pellizzoni, G. Piano, M. Pilia, M. Rapisarda, A. Rappoldi, S. Sabatini, P. Soffitta, M. Trifoglio, A. Trois, P. Giommi, F. Lucarelli, C. Pittori, P. Santolamazza, F. Verrecchia, I. Agudo, H. D. Aller, M. F. Aller, A. A. Arkharov, U. Bach, A. Berdyugin, G. A. Borman, R. Chigladze, Yu. S. Efimov, N. V. Efimova, J. L. Gómez, M. A. Gurwell, I. M. McHardy, M. Joshi, G. N. Kimeridze, T. Krajci, O. M. Kurtanidze, S. O. Kurtanidze, V. M. Larionov, E. Lindfors, S. N. Molina, D. A. Morozova, S. V. Nazarov, M. G. Nikolashvili, K. Nilsson, M. Pasanen, R. Reinthal, J. A. Ros, A. C. Sadun, T. Sakamoto,

S. Sallum, S. G. Sergeev, R. D. Schwartz, L. A. Sigua, A. Sillanpää, K. V. Sokolovsky, V. Strelnitski, L. Takalo, B. Taylor, and G. Walker.
The Brightest Gamma-Ray Flaring Blazar in the Sky: AGILE and Multi-wavelength Observations of 3C 454.3 During 2010 November.
ApJL, 736(2):L38, August 2011.

[149] M. Villata, C. M. Raiteri, T. J. Balonek, M. F. Aller, S. G. Jorstad, O. M. Kurtanidze, F. Nicastro, K. Nilsson, H. D. Aller, A. Arai, A. Arkharov, U. Bach, E. Benítez, A. Berdyugin, C. S. Buemi, M. Böttcher, D. Carosati, R. Casas, A. Caulet, W. P. Chen, P. S. Chiang, Y. Chou, S. Ciprini, J. M. Coloma, G. di Rico, C. Díaz, N. V. Efimova, C. Forsyth, A. Frasca, L. Fuhrmann, B. Gadway, S. Gupta, V. A. Hagen-Thorn, J. Harvey, J. Heidt, H. Hernandez-Toledo, F. Hroch, C. P. Hu, R. Hudec, M. A. Ibrahimov, A. Imada, M. Kamata, T. Kato, M. Katsuura, T. Konstantinova, E. Kopatskaya, D. Kotaka, Y. Y. Kovalev, Yu. A. Kovalev, T. P. Krichbaum, K. Kubota, M. Kurosaki, L. Lanteri, V. M. Larionov, L. Larionova, E. Laurikainen, C. U. Lee, P. Leto, A. Lähteenmäki, O. López-Cruz, E. Marilli, A. P. Marscher, I. M. McHardy, S. Mondal, B. Mullan, N. Napoleone, M. G. Nikolashvili, J. M. Ohlert, S. Postnikov, T. Pursimo, M. Ragni, J. A. Ros, K. Sadakane, A. C. Sadun, T. Savolainen, E. A. Sergeeva, L. A. Sigua, A. Sillanpää, L. Sixtova, N. Sumitomo, L. O. Takalo, H. Teräsranta, M. Tornikoski, C. Trigilio, G. Umana, A. Volvach, B. Voss, and S. Wortel.
The unprecedented optical outburst of the quasar ¡ASTROBJ¿3C 454.3¡/ASTROBJ¿. The WEBT campaign of 2004-2005.
A&A, 453(3):817–822, July 2006.

[150] W. Voges, B. Aschenbach, Th. Boller, H. Bräuninger, U. Briel, W. Burkert, K. Dennerl, J. Englhauser, R. Gruber, F. Haberl, G. Hartner, G. Hasinger, M. Kürster, E. Pfeffermann, W. Pietsch, P. Predehl, C. Rosso, J. H. M. M. Schmitt, J. Trümper, and H. U. Zimmermann.
The ROSAT all-sky survey bright source catalogue.
A&A, 349:389–405, 1999.

[151] G. R. Werner, D. A. Uzdensky, B. Cerutti, K. Nalewajko, and M. C. Begelman.
The Extent of Power-law Energy Spectra in Collisionless Relativistic Magnetic Reconnection in Pair Plasmas.

ApJL, 816(1):L8, January 2016.

[152] Jong-Hak Woo and C. Megan Urry.
Active Galactic Nucleus Black Hole Masses and Bolometric Luminosities.
ApJ, 579(2):530–544, November 2002.

[153] D. Zargaryan, S. Gasparyan, V. Baghmanyan, and N. Sahakyan.
Comparing 3C 120 jet emission at small and large scales.
A&A, 608:A37, December 2017.

[154] S. Zenitani and M. Hoshino.
The Generation of Nonthermal Particles in the Relativistic Magnetic Reconnection of Pair Plasmas.
ApJL, 562(1):L63–L66, November 2001.